Title
Gap-junctional coupling of mammalian rods and its effect on visual detection thresholds

Author
Li, Peter Hawley

Publication Date
2008

Peer reviewed|Thesis/dissertation

Gap-junctional coupling of mammalian rods and its effect on visual detection thresholds

by

Peter H. Li

DISSERTATION

Submitted in partial satisfaction of the requirements for the degree of

DOCTOR OF PHILOSOPHY

in

Neuroscience

in the

GRADUATE DIVISION

of the

UNIVERSITY OF CALIFORNIA, SAN FRANCISCO

For my parents, with love

Acknowledgments

UCSF has proven a wonderful place for my graduate studies. Despite the many typical graduate school frustrations, and some exceptional personal challenges, I can honestly say that thanks to UCSF's great faculty, students, and staff, as well as the support of my friends and family, I have spent some of the most enjoyable years of my life here.

First and foremost I want to thank my advisor, Julie Schnapf, a gifted mentor, teacher, colleague, and friend. Julie taught me virtually everything I know about vision science, and most of what I know about science period. My time with Julie taught me how to approach scientific questions, and gave me the confidence to discuss my ideas with colleagues and to see my projects through. I also feel very privileged that working in the Schnapf lab has offered me so many exceptional opportunities to grow as a scientist, especially by participating in the peer review process, collaborating with other universities, and developing my presentation skills at conferences. More than that though, Julie has really helped me grow as a person over the last 6 years. She created an environment where I could not only learn to become an independent scientist, but where I also felt I could come to for advice on any topic. Her clear, rational thought process, combined with her straightforward but keen empathetic sense really helped guide me during difficult personal situations, and I hope to carry some of that wisdom with me into my future endeavors. Thanks in no small part to Julie, my graduate education has rivaled my undergraduate experience for academic learning, but far exceeded it in terms of personal growth. Most of all, Julie is a good friend. Whether we are discussing upcoming presentations, analytic approaches, color vision (or lack thereof), Mozart, biking, or a recipe for dried persimmons, it's always a pleasure to spend time together.

Jan and Eric, two post-docs in the lab, have also been instrumental in guiding me through my graduate studies. I thank Eric for his warm support when I first joined the

lab. He always had time to discuss some paper or presentation I was struggling with, and made an effort to include me in his own projects. Even after heading on to a new job he has kept in touch, answering my occasional confused math questions and continuing to offer his advice and support. Jan has been another big influence on me over my time in San Francisco. I've learned so much working with him, but probably the biggest thing he taught me is to be kind to myself as well as to others, and to stand up for what I believe in. When discussing scientific quesitons, his intuitive sense often gives him insight directly into the heart of the matter, while I would get lost in details. He inspires me to be more free, alert, and open to the present moment.

Many thanks to my thesis committee for all their time, help, and input. Special thanks to Juan Korenbrot and Loren Frank for their guidance as committee chairs. Although I found Juan a bit brusque at first, that passed quickly and I really valued his insightful advice, critiques, and no-nonsense approach. Loren I first got to know when taking his data analysis course, probably the most educational, practically applicable, and best organized class I took at UCSF. He has been a helpful and insightful mentor for as long as I've known him, and he was an extremely supportive and conscientious commitee chair in the home stretch. Erik Ullian was a natural addition to my committee, with his retinal expertise. He is always fun to talk to, and his enthusiasm for scientific questions really shines through. Jonathan Horton I met when I first interviewed at UCSF, and I appreciate his steadfast support for my scientific efforts. I have always admired his clear thinking, his expansive knowledge of visual science, and his rhetorical panache. Marie Burns was my outside committee member, joining us from UC Davis. Her expertise in photoreceptor signaling made her a natural choice, and working with her I found her to be wonderfully warm, insightful, and considerate. Juan, Loren, Erik, and Julie all sat through numerous presentations of my results and provided invaluable feedback as I progressed through the painstaking process of focusing and refining my experiments. As I prepared the dissertation, Loren, Erik, and Marie pro-

vided much helpful input on the manuscript, especially chapter 3. Jonathan provided input on all areas of the manuscript, and he and Marie also gave much help in organizing and writing the introductory material. Of course, Julie was crucial throughout, and helped me plan, execute, analyze, present, and write-up all my work.

I would also like to thank the UCSF faculty who served on my qualifying exam committee, especially my chair and academic advisor, David Copenhagen. I always felt that David wanted me to succeed, and that motivated me to do better even when things weren't going smoothly. Among the faculty there were also many excellent professors who taught courses in the Neuroscience program, and several professors and post-docs who coached me for presentations, led my rotation projects, and otherwise helped me along. Special thanks to Loren Frank, Jonathan Horton, Jeff Lansman, Pam England, Karen Cusato, Michael Stryker, Flip Sabes, Allison Doupe, Jenny LaVail, Hilary Beggs, Lawrence Sincich, Juliette Johnson, and Rene Renteria.

Outside of UCSF, there have been many important influences on my development as a scientist. First, I would like to thank Harvey McMahon of the MRC Laboratory of Molecular Biology for giving me my start in bench science and for being a great mentor, friend, and steadfast support. Marijn Ford and Yvonne Vallis were also wonderful people to work with and get to know during my time at Cambridge. Jack McMahan led me through another positive experience, this time at Stanford, and put a remarkable effort into teaching three undergraduates the subtleties of electron microscopy. Tecumseh Fitch led my work for my undergraduate research thesis. He taught several of my favorite courses throughout my time at Harvard, and pushed me a good ways in my development towards becoming a responsible researcher. For more recent support, I would like to recognize Dennis Dacey, Orin Packer, Jo Crook, Fred Rieke, and Felice Dunn, for hosting me at the University of Washington; Peter Sterling, Jian Li, Lu Yin, Jonathan Demb, and EJ Chichilnisky, for advice on guinea pig studies; and Joe Carroll and Steve Massey, for their friendship and

encouragement.

In the Neuroscience program we are fortunate to have wonderful and able administrators. Pat Veitch, Deb Rosenberg, and Carrie Huckaba have gotten me through innumerable bureaucratic pitfalls relatively unscathed and were always a pleasure to interact with. Lou Reichardt, the head of our program, has put a lot of work into keeping things running and keeping UCSF Neuroscience at the top of its field. In the ophthalmology department we also have many helpful and friendly staff members. Thelma de Souza, in particular, has guided me through the department ins and outs. Mike Deiner and Matt Feusner have saved me on several occasions when a computer was breaking down and I was desperately trying to save my precious data. Geoffrey Lambright was always ready to assist on confocal imaging requests.

Besides being my colleagues, I have also counted many of these people my friends, and many other friendships have also enriched my time in San Francisco. Certainly I couldn't have gotten through the years without my classmates Marta, Amy, Mel, Hillel, Florian, Mattias, Bhavana, and Matt to commiserate with. It has been a real pleasure to get to know these great people over the years and watching them grow as scientists was truly inspiring. I also want to thank Cara and Joy for listening to my problems and for getting me outdoors where the Bay Area is at its most beautiful. Lucky for me, some of my oldest and dearest friends were also nearby for much of my time here. Austin, David, Bernie, Sara, and Ivor, thanks for your friendship over all these years and for keeping San Francisco fun and familiar. Joe, Dave, Ken, and Rebekah, thank you for your love and support and I hope to see you all again soon. I was also lucky to live with some great guys for my time in San Francisco. Ben, Matthew, Brian, Nikhil, thank you for your friendship and for putting up with all my roommate quirks for so many years. Many thanks also to Courtney for supporting me, encouraging my naturalist tendencies, putting up with me in stressed out graduate student mode, and for all that you taught me over the years that we shared.

My family has of course also been a great support for my whole life, and for their support during my time in graduate school I would especially like to thank Marion, Sharon, Lynn, Tryggve, Patty, Tony, Patrick, Victoria, and Liz. My aunt Jade has been particularly inspiring in my scientific endeavors. She was instumental in some of my early efforts and has always had plenty of good advice along the way. And I am constantly inspired by my grandmother Nancy, who has lived through so much hardship but never misses an opportunity to show her love and support for her grandchildren.

As much as my life has changed over my time at UCSF, the biggest change came just a year and a half ago, when I reconnected with an old college acquaintance. Patty and I started dating a little over a year ago, and I could never have predicted how quickly she would become a vital part of my life. She has shown great faith in me through many difficulties, and this was crucial in me finishing my Ph.D. Her care sustained me when I would otherwise have been lost or lacked the will to continue. Her love gave me the confidence and the inspiration to succeed. We are excited to be starting a new chapter in our lives together this fall in New York City.

Finally, I would like to dedicate my Ph.D. with love and gratitude to my mother, Elaine, and my father, Eric. I owe so much to my parents, especially my joy in learning and exploring. They taught me from an early age to be inquisitive, experimental, skeptical, and intensely bookish. I am inspired by the memory of my father's loyalty to his family, his diligent work ethic, and his bright intelligence and warm humor. So much of what I have accomplished I did to make him proud. Losing him was the hardest thing I ever experienced, but I think he would be very happy to see how far I've come. My mother has always supported me and reminded me to take care of myself, keep things in perspective, and enjoy life. Her artistic, literary, and above all musical talents are a part of me that I will always cherish.

Contributions

Chapter 2, "Gap-junctional coupling and absolute sensitivity of photoreceptors in macaque retina", is reprinted with permission from:

> Eric P. Hornstein, Jan Verweij, Peter H. Li, and Julie L. Schnapf. Gap-junctional coupling and absolute sensitivity of photoreceptors in macaque retina. *Journal of Neuroscience*, 25(48):11201–11209, November 2005.

This work was a collaboration between the coauthors. Peter H. Li collected about 10% of rod electrical recordings, as well as 90% of the rod tracer coupling data. He also performed all the network analysis, 3D anatomical reconstructions, and psychophysical modeling, and contributed to additional anatomical analyses. All authors participated equally in writing the paper.

Gap-junctional coupling of mammalian rods and its effect on visual detection thresholds

Peter H. Li

Abstract

In many non-mammalian vertebrate species, retinal rod photoreceptors have been found to couple extensively to one another via gap junctions. Yet the functional role of coupling remains enigmatic. Coupling could enhance night vision by circumventing saturation at the rod output synapse, but it could also reduce absolute sensitivity by rendering the output synapse less effective at separating photon signals from intrinsic rod noise. Recent results suggest that rodent rods are also coupled, but rod circuitry differs significantly between mammals and other vertebrates, so existing data on non-mammalian coupling may not be applicable to understanding mammalian vision; the rod to rod-bipolar pathway is a mammalian specialization, and mammalian rod networks appear distinctive in their limited extent of coupling, and in the type of connexin proteins underlying the junctions.

Here, I show that primate rods are also coupled, suggesting a role for coupling in human vision. I then present more detailed data on rod coupling from guinea pig retina, showing that guinea pig rod-rod junctional conductance is about 350 pS. By developing a rod network model to analyze the combined primate and guinea pig results, I confirm that the junctional conductance in guinea pig and primate is comparable. Finally, I model the effects of coupling on human visual detection, focusing particularly on the interaction between rod coupling and the nonlinear operations of the rod output synapse. Based on primate data alone, the model confirms that coupling can have competing beneficial and detrimental effects on vision depending on the strength of coupling and the parameters of the rod output synapse, as well as the spatial configuration of the stimulus. Incorporating the guinea pig data reveals that the strength of coupling in mammals is appropriate for mitigating detrimental effects on absolute detection while enhancing benefits for detection of small spots.

Contents

List of Tables

List of Figures

Chapter 1

General Introduction

This dissertation describes studies of night vision in two mammalian species: macaque monkeys and guinea pigs. In both studies, I focus on aspects of retinal circuitry underlying night vision, particularly the direct electrical communication between rod photoreceptors via gap junctions. In the macaque study, I also present data from recordings in cone photoreceptors, which provide context for the rod results. The guinea pig work parallels the results from macaque, but I present additional more detailed data on coupling, and then develop a rod network model to consolidate the guinea pig data and to allow comparison with the results from macaque. Both studies also present psychophysical modeling to clarify how direct electrical communication between rods affects visual performance, particularly detection near absolute threshold. Predicting the effect of coupling on detection thresholds requires consideration of the rod circuitry downstream of the photoreceptor layer, from the rods to the ganglion cell output layer of the retina, and on to the brain where ultimate psychophysical detection takes place.

1.1 Gap junctional coupling

1.1.1 Background

The retinal circuit central to this dissertation is the communication between photoreceptors via gap junctions, direct intercellular channels linking the cytoplasm of two adjacent cells. Far from being simple, non-selective conduits, gap junctions are now recognized as having many of the distinctive properties of other membrane channels, namely pharmacological modulability, voltage gating, molecular selectivity, and some charge selectivity (although small ions still pass freely) (reviewed: [71, 45]). Along with this new perspective has come the recognition that the gap junction channel proteins are a genetically and functionally diverse family [71, 45].

A gap junction is composed of two hemichannels ("connexons"), each bridging the membrane of one cell. When two hemichannels come together, a continuous channel between neighboring cells is formed. Hemichannels are in turn hexamers composed of six individual transmembrane protein subunits. In vertebrates, the primary hemichannel subunits are the connnexin (Cx) family of gap junction channel proteins, of which there are roughly 20 major subtypes in the mammalian genome. These genetically distinct connexins impart functional distinctions to the channels they constitute [71, 45]. Invertebrate hemichannels are composed of subunits from the innexin protein family, which is functionally analogous to the connexin family although the two are not closely genetically related [91, 45]. Recently, it was discovered that innexins are found in the vertebrate genome alongside the vertebrate specific connexins, leading to the recommendation that the innexins be renamed pannexins [9]. Research on pannexins in vertebrates is a relatively new field, but it is already known that one subtype, Panx1, is expressed in the adult mammalian retina [96, 43].

Gap junctions are generally abundant in retinal circuitry, with homogeneous laterally

coupled networks of single retinal cell types documented among photoreceptors, horizontal cells, bipolar cells, amacrine cells, and ganglion cells [135, 29]. Gap junctions are also found at heterologous electrical synapses, where they serve as feed-forward connections from one cell type onto another. Two well-documented heterologous electrical synapses in the retina are the AII amacrine to On-cone bipolar cell junction critical for detection at absolute threshold (see below), and the rod-cone coupling circuit important for extending rod signaling into the twilight ("mesopic") range [135, 29]. The retina thus provides a useful model system for understanding direct electrical communication throughout the nervous system [136]. In considering night vision, we are particularly interested in gap-junctional coupling among rod photoreceptors, the input layer of the night circuitry.

Anatomical evidence for rod coupling has been found in a number of non-mammalian vertebrates [34, 52, 153], as well as in rodents [130]. The anatomical evidence in primates is less clear [132, 95, 27], with the implication that if primate rods are coupled, the coupling may be weak or non-functional. Physiological studies of rod coupling have focused almost exclusively on non-mammalian vertebrates [46, 112, 145, 154], as have modeling efforts [72, 7, 126]. However, there is good reason to believe that coupling in mammals is functionally distinct from other vertebrates. First, the molecular substrate for mammalian rod coupling appears to be distinct; while salamander rods express Cx35 at their junctions [153], in mammals the homologue, Cx36, is reported only in cones [74, 82, 35, 30] (although see [37]). Second, the connectivity of the mammalian rod network appears to be more sparse. While the salamander rod network forms an effectively continuous syncytium of coupled cells [153], mammalian rods are connected in smaller, discrete pools [130]. Finally, as described below, the mammalian retina has evolved a specialized circuit for rod vision, so that there is reason to expect that the effects of coupling on visual performance may be significantly different in mammals, particularly near absolute threshold.

1.1.2 Results presented here

The first aspect of the present work is my extension to the mammalian retina of previous physiological studies of rod coupling in non-mammalian vertebrates. In the first study (chapter 2, [62]), we used tracer injections and electrical recordings from individual primate rods to assess their coupling. Filling primate rods with the tracer neurobiotin, we frequently observed spread of the tracer into neighboring rods, demonstrating that the coupling of primate rods is more substantial than previous anatomical studies have suggested. Although we did not measure rod gap-junctional conductance directly, we found functional evidence for rod coupling in our electrical recordings, based on the statistical variability of responses to dim flashes of light.

Chapter 2 also presents recordings from primate cones, providing important context for the rod recordings. One finding is that rod signals can be recorded directly from cones, due to rod-cone coupling, but the rod signal in a cone is small. This bears significantly on the network modeling in chapter 3. Building further on this finding, it is shown that although rod signals measured in cones are small, the low intrinsic noise of the cone makes them relatively easy to detect. Although not directly relevant to visual performance at absolute threshold, this finding is relevant for rod signaling through alternative pathways at intermediate light levels ([122], figure 1.1 below). Finally, the cone experiments provided an opportunity to compare the amplitude of rod electrical signals in an individual cone with the number of rods tracer coupled to the cone. The significant correlation found between these two measures is an important validation of the tracer coupling technique in the photoreceptor layer, in agreement with studies in other retinal regions [22] (but see [21]).

In the second study presented here, chapter 3, we assessed rod coupling in the guinea pig. Guinea pig tissue is more readily available than primate tissue, so using this system al-

lowed us to study rod coupling in more detail, including measuring coupling conductance directly via simultaneous dual-electrode recording from neighboring rods. We also assessed guinea pig coupling using tracer coupling and statistical analysis of light responses, as in the primate work. By developing a mathematical and computational model for the rod network, I was able to interrelate the three coupling measures from guinea pig and found them to be consistent with the idea of discrete coupled pools [130]. Furthermore, I compared the couping conductance measured in guinea pig rods to the tracer coupling and statistical analysis from primate and found these measures also consistent, suggesting that the conductance values measured in guinea pig could be a fairly general mammalian feature.

1.2 Effect of rod coupling on psychophysical detection

The second part of my analyses was to consider the effect of rod coupling on human visual detection of light stimuli near absolute threshold. To understand how rod coupling ultimately affects detection, we must consider the intervening layers of processing between the rod input layer and the visual cortex, where psychophysical detection ultimately takes place. Previous models of rod coupling have relied on data from non-mammalian vertebrates, and have focused on effects within the coupled rod network itself [72, 7, 126]. However, the modeling I present here demonstrates that the implications of coupling for mammalian visual detection depend not so much on effects within the rod network, but more significantly on the interaction between rod coupling and the synaptic nonlinearities at the rod output onto the rod bipolar cell. Indeed, considering the high degree of convergence in the primary rod pathway, the predicted effects of rod coupling would be entirely negligible were it not for these nonlinearities.

The degree of convergence in the night circuitry between the rod input layer and the

psychophysical detection stage is also an important factor in determining visual sensitivity. We know that convergence in the rod pathways is great, with signals from on the order of thousands of rods combining before reaching the ganglion cell layer. But unfortunately we do not know enough about the night vision circuitry at the ganglion cell layer and beyond to be able to estimate convergence from anatomy alone. Therefore, in my modeling of the night circuit I rely on psychophysical data on spatial summation in visual detection tasks to estimate convergence.

1.2.1 Mammalian night vision circuitry

The mammalian visual system is remarkable for its dynamic range and for its sensitivity. Mammalian vision has evolved for a natural world in which it must operate effectively over an extremely wide range of intensities, roughly 10 log units or 10 billion times difference between the brightest and dimmest possible working conditions [122]. This dynamic range is achieved in part by dividing duties between two major photoreceptor populations: cone photoreceptors for daytime use and rods for night. In considering mammalian night vision ("scotopic" vision), we are primarily concerned with the rod system, which is particularly tuned for extreme sensitivity under the dimmest conditions.

The fact that rods can respond reliably to absorption of a single photon, the smallest indivisible quantum of electromagnetic energy, was first deduced over 60 years ago, based purely on observations of human behavioral performance (i.e. psychophysics) [58]. Eventually, this proposition was confirmed through physiological recordings, first in invertebrate ommatidia [50, 23], and later in vertebrate retinas [46, 13], including in the primate [14]. In the meantime, it was also reported that rod absorption of a single photon (a "photoisomerization", commonly denoted R*) could reliably induce ganglion cells at the output layer of the retina to send 2–3 extra nerve impulses to the brain [12]. These studies clearly

demonstrate that the retina's night circuitry can operate effectively all the way up to the biophysical limits of performance; detection at absolute threshold is ultimately limited by the quantal nature of the light stimulus.

In a discussion of what it means to "understand" the retina, Sterling points out that where physiological performance approaches "ideal" performance calculated from physical limits we have a unique opportunity to understand the requirements and compromises that dictated the evolution of the physiological system [122]. The rod system at absolute threshold is a prime example. While understanding the constraints on natural daytime vision is an important goal, it requires controlling for myriad considerations such as selective attention, adaptational state, psychological influences on chromatic percepts, etc.. By focusing on detection at absolute threshold, we can reduce the problem of vision to pure physical constraints on retinal circuitry.

Rod signals pass through numerous consecutive layers of processing, via several parallel pathways, before reaching the ganglion cell output layer of the retina. Mammals, in particular, have evolved a special pathway to enhance night sensitivity [122]. In non-mammalian vertebrates, both rods and cones synapse onto a largely shared population of retinal bipolar cells. In mammals, in contrast, rods synapse onto a specialized rod bipolar cell, which then synapses onto a specialized AII amacrine cell. Although the mammalian outer retina is believed to employ two additional parallel rod circuits (fig. 1.1), I will focus on the primary pathway via rod bipolar and AII amacrine cells because it underlies highest sensitivity vision [143, 122].

The primary rod pathway is highly convergent, with signals from 10-20 rods converging onto each rod bipolar cell, hundreds of rods converging onto AII amacrines, and numbers into the thousands of rods converging onto the ganglion cell layer [123]. Considering this convergence (as well as the substantial gap-junctional coupling among AIIs themselves [125, 20]) it would seem that for detection at absolute threshold, rod coupling is somewhat

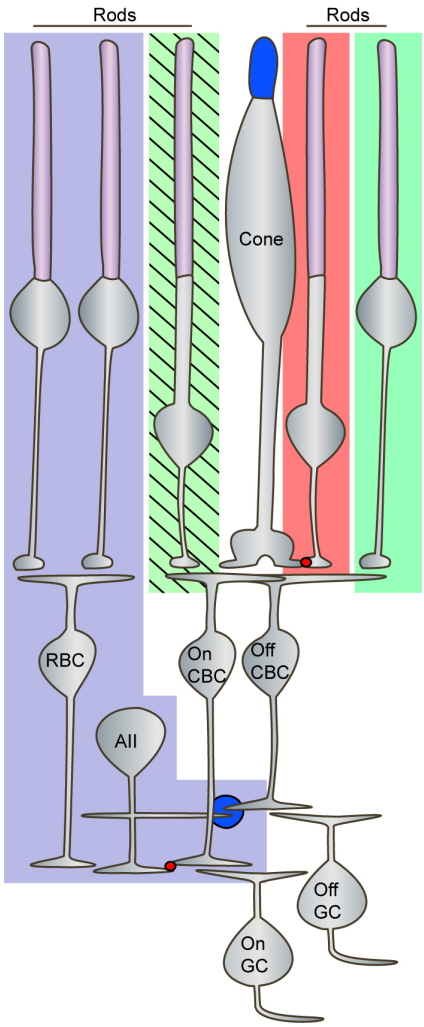

Figure 1.1: Rod pathways of mammalian outer retina

The mammalian outer retina features three putative rod signaling pathways [122]. All three eventually recombine with cone pathways, thus co-opting cone circuitry. The classic, high sensitivity rod pathway (blue background) relies on the specialized rod bipolar cell (RBC), which synapses onto the AII amacrine. The AII amacrine then signals on to both On- and Off-retinal ganglion cells (GCs) via electrical (red dot) and inhibitory chemical (blue circle) synapses at the axon terminals of cone bipolar cells (CBCs). AIIs also appear to contact some GCs directly, particularly the Off-GCs [85]. A second well-documented pathway (red background) relies on direct electrical coupling (red dot) between rod terminals and cone pedicles ([108, 40, 62], chapter 2). Finally, a third recently reported [118, 130] putative pathway relies on direct rod synapses onto a subset of Off-CBCs (green background). Even more recently, tentative evidence has emerged suggesting that rods may also directly contact On-CBCs (green background with diagonal hatching) [129]. Of these three, the classic RBC pathway is the most sensitive [143, 122]. Direct synapses from rods onto CBCs have so far only been found in rodents, while the other two pathways are well-established in primate and other mammals such as rabbit and cat.

superfluous; if the converging signals from rods were summed linearly, signal spreading between neighboring coupled rods at the input layer would be obviated by downstream signal mixing. However, rod signals in the primary rod pathway are not summed linearly; the output synapse from rods onto rod bipolar cells features two important nonlinearities.

The first is a cutoff nonlinearity that selectively passes larger signals while attenuating smaller ones [48]. Through convergence, optimal filtering, and selective amplification of rod signals, the human visual system reaches an absolute sensitivity for detection of around 1 photoisomerization per 1000 rods [113]. At 0.001 R* / rod, this performance is 1000 times better than the absolute physical limit of 1 R* required for detection in an individual rod. A fundamental problem is understanding how this system can reliably transmit its very sparse photon signals. Rods are intrinsically noisy, and although the amplitude of a rod photoresponse to 1 R* is several times larger than typical rod noise, with only 0.001 R* / rod at psychophysical threshold, the vast majority of the rods in the detection pool do not absorb a photon. If the output of all the rods in the detection pool were summed linearly, the noise would completely wash out the sparse signal [14]. The cutoff nonlinearity at the rod output synapse is the mammalian retina's solution to this problem [14, 134]. Using this nonlinearity, the rod selectively passes larger amplitude photoresponses while rejecting the lower amplitude intrinsic rod noise, thus preventing the convergence of noisy detectors from washing out the sparse signal. However, this specialization seems at odds with the effects of rod coupling. By spreading signals among neighboring rods before the rod output synapse can filter out intrinsic noise, rod coupling in effect short circuits the noise filtering of the cutoff nonlinearity. Thus we would expect coupling to confer some disadvantage to detection at absolute threshold.

The second important nonlinearity at the rod output synapse is saturation. Because rods performing at absolute threshold must make the largest possible signal in response to the very sparse R* delivered to the detection pool, the rod output synapse saturates with

absorption of only 1–2 photons [16]. Thus, although the rod is capable of graded signaling up to about 100 R*, its output when adapted for absolute threshold is truncated at only 1–2 R*. This effect leads to one possible advantage of rod coupling in the detection of small, concentrated spots of light: the ability to spread larger photoresponses into neighboring rods and thus circumvent output saturation [5].

1.2.2 Ganglion cell pathways

Downstream of the AII amacrine cell, details of the night circuitry are not well understood. AIIs appear to directly contact some ganglion cells, particularly via inhibitory synapses onto Off-ganglion cells [85]. AIIs can also signal to ganglion cells indirectly via synapses onto the axon terminals of On- and Off-cone bipolar cells, which then synapse onto their respective ganglion cell types. However, neither the direct nor the indirect pathways have been worked out sufficiently to clarify the specific subset of cone bipolar cells or retinal ganglion cells involved in night vision. There is currently only limited anatomical [81, 83, 56, 65] and physiological [139] data on contacts between AIIs and specific cone bipolar cell types. Ganglion cell studies have focused almost exclusively on the midget and parasol ganglion cell classes, the most numerous ganglion cell populations in primate retina. Anatomical [56], physiological [73], and psychophysical [75, 84] evidence suggests that rods do input to midget cells, while physiological recordings [73] suggest greater rod input to parasols. However, the physiological evidence is confusing; within a specific morphological class of ganglion cells, only a fraction of the cells appear to receive rod input, suggesting possible additional subtleties in ganglion cell classification beyond the morphological categories. In any case, to understand the role of ganglion cell pathways in night vision it is probably inadequate to consider only midget and parasol cells.

Retinal ganglion cells come in many types, allowing for parallel streams of processed

visual information in the retinal output. In mammals, about 20 morphologically distinct ganglion cell types are recognized (21 to date in cat, for example [67], and 17 in primate [47]). The most studied primate ganglion cell types are the midget and parasol cells (both On and Off subtypes), primarily because they are the most numerous. The midget and parasol cells are also known to project to the primary visual areas of the brain (the lateral geniculate thalamus and visual cortex), rather than to more accessory areas. However, many of the less well characterized ganglion cell types are now also known to project to the lateral geniculate, particularly its magnocellular and koniocellular layers [59, 47]. Furthermore, it is important to recognize that although midget cells dominate macaque and human retinas, they are only a recent adaptation.

The midget system arose recently within the primate lineage as a parallel pathway specialized for high acuity vision, particularly cone-driven daytime vision in the fovea. The comparative anatomical evidence suggests that this system augments the primate retina, without substantially displacing preexisting ganglion cell pathways [80]. The development of the midget system was accompanied by a huge increase in the total number of ganglion cells: roughly 1,500,000 in macaque compared to 400,000 in rabbit. Of the 1,500,000 macaque ganglion cells, roughly 70% are midgets. Thus the total number of non-midget cells is actually little different between macaque and rabbit. Furthermore, the diversity of bipolar and amacrine cell types is largely conserved between macaques and other mammals [80]. The implication is that despite the major evolutionary shift towards high acuity daytime vision in macaque and human retinas, the preexisting low acuity, high sensitivity night vision pathways inherited from our nocturnal mammalian ancestors rely on conserved non-midget populations. Thus non-midget cells are likely more relevant to understanding vision at absolute threshold, even though some of these cell types may comprise less than 1% of the total human or macaque ganglion cell complement.

1.2.3 Psychophysics of rod vision

Despite the uncertainty as to the specific circuitry of the ganglion cell layer, having some estimate of the convergence of the highest sensitivity rod pathways in humans is useful for modeling psychophysical detection. To estimate convergence, I therefore rely on psychophysical evidence for areas of "complete spatial summation" in detection at absolute threshold [155]. The classic statement of the spatial summation effect is "Ricco's Law" [98]: for spot stimuli up to some critical diameter, the threshold for visual detection is independent of the area of the stimulus, and depends only on the number of photons delivered within that area. This suggests that, up to the critical diameter, all the rods in the stimulus area are converging to the same psychophysical detection unit and contribute equally to detection. The corollary is that rods outside the critical area must converge to different detection units, so that photons delivered outside the critical diameter do not contribute equally to detection, and for stimuli larger than the critical diameter the threshold number of photons required for detection increases with spot size.

Although it is generally recognized that Ricco's Law is a simplified, approximate model of actual visual detection [53], it still provides a useful empirical estimate of rod convergence to the psychophysical detection stage for absolute threshold. Interestingly, the critical diameter for spatial summation does vary gradually with retinal eccentricity [155], but does not follow reported variations in human ganglion cell densities [31] or the consequent expected variation in ganglion cell receptive field sizes. In general, psychophysical critical area ranges from about 1 to 2 degrees diameter [155], while midget receptive field sizes are roughly 100 times smaller, and parasols 10 times smaller. This suggests that either detection at absolute threshold relies on a ganglion cell class that is sparser and has larger receptive fields than parasols, or else ganglion cell outputs must further converge downstream prior to the detection stage.

Using the critical area of about 1 degree diameter as an estimate of rod convergence at 10 degrees eccentricity [155], this corresponds to a critical diameter of about 300 μm [147], or a critical area of about 0.07 mm^2. Given reported human rod densities at this eccentricity [32], this corresponds to about 10^4 rods converging to the detection stage. As described above, absolute human psychophysical threshold is about 10 R* for brief flashes [113], so in my modeling I use a value of 10 R* delivered to a detection pool of 10^4 rods, or 0.001 R* / rod, as a baseline estimate of threshold intensity.

1.2.4 Results presented here

Chapters 2 and 3 both include modeling of the effect of rod coupling on psychophysical detection. In chapter 2, I introduce a model of visual detection that specifically accounts for the interaction between rod coupling and the nonlinearities at the rod output synapse. Since we did not measure macaque rod coupling conductance directly, I use a simplified coupling model, finding as predicted above that coupling is actually detrimental to visual performance due to its mixing of signals among neighboring rods before the output synapse can filter out intrinsic noise. This suggests that there must be some other purpose for rod coupling that outweighs the negative effects for detection at absolute threshold. One possibility explored, as discussed above, is that coupling enhances detection of small spots.

The guinea pig study, chapter 3, provides direct measurements of rod coupling conductance, and a network model indicating that this conductance is applicable to the primate case as well. Therefore, I extend the visual detection model from chapter 2, now using the network model to compute the spread of phototransduction currents through the coupled network. With this more accurate model, the performance of the coupled network is revealed to be significantly improved for all conditions; detriments to detection of full-field stimuli are much reduced, while the benefit for detection of small spots is enhanced,

strengthening the argument that this trade-off could be part of the functional purpose of rod coupling.

Chapter 2

Gap-junctional coupling and absolute sensitivity of photoreceptors in macaque retina

2.1 Abstract

We investigated gap-junctional coupling of rods and cones in macaque retina. Cone voltage responses evoked by light absorption in neighboring rods were briefer and smaller than responses recorded in the rods themselves. Rod detection thresholds, calculated from noise and response amplitude histograms, closely matched the threshold for an ideal detector limited by quantal fluctuations in the stimulus. Surprisingly, cone thresholds were only approximately two times higher. Amplitude fluctuations in cones could be explained by a Poisson distribution of photoisomerizations within a pool of seven or more coupled rods. Neurobiotin coupling between rods and cones was consistent with our electrical recordings, with approximately six rods labeled per injected cone. The spatial distribution of tracer coupled rods matched the light-evoked cone receptive field. The gap junction inhibitor carbenoxolone abolished both electrical and tracer coupling. Amplitude fluctuations in most rods were accounted for by the expected rate of light absorption in their outer segments. The fluctuations in some rods, however, were consistent with a summation pool of up to six rods. When single rods were injected with Neurobiotin, up to 10 rods were labeled. Rod-

rod and rod-cone electrical coupling is expected to extend the range of scotopic vision by circumventing saturation at the rod to rod-bipolar cell synapse; however, because coupling also renders the rod synapse less effective at separating out photon signals from dark noise, coupling is expected to elevate the absolute threshold of dark-adapted observers.

2.2 Introduction

The light-evoked signals of rod photoreceptors in mammalian retina are transmitted via chemical synapses to bipolar cells and via gap junctions to cone photoreceptors [86, 108, 19, 130]. Gap junctions have been observed at the tips of telodendria projecting from cone synaptic terminals to both rod and cone synaptic terminals [95, 128]. In rodent but not primate retina, gap junctions have also been observed between rods [130]. A portion of the light response in a cone can be attributed to photon absorption in coupled rods, as evidenced by its temporal, spectral, and adaptational properties [108, 109]. The importance of rod-cone coupling for vision remains uncertain. Human psychophysical studies suggest that rod signals are processed by two distinct neural pathways [28, 114, 124]. The slower more sensitive pathway was postulated to involve the transmission of rod signals to rod-bipolar cells, and the faster less sensitive pathway was postulated to involve transmission of rod signals through coupled cones to cone-bipolar cells. One goal of this study was to compare in rods and cones the noise, kinetics, and sensitivity of rod photon signals. We found that rod signals are high-pass filtered in cones and that rod and cone detection thresholds are surprisingly similar.

Photon signals in primate rods stand out clearly above the electrical noise in the dark; when "optimally filtered," the peak amplitude of the response to a single photoisomerization is approximately five times larger than the standard deviation (s.d.) of the dark noise [14, 110]. The human visual system, however, integrates signals across a pool of ~10^4

rods [54]. With linear summation, the size of a single photon response relative to the pooled dark noise is expected to be 100 times smaller than the signal-to-noise ratio of a single rod. Thus it is remarkable that human observers can detect stimuli evoking only 10 photoisomerizations [113]; the signal-to-noise ratio for this stimulus would be only ~0.5. Considering the problem of rod summation, Baylor et al. [14] proposed that the rod synapse filters out low-amplitude dark fluctuations and preferentially transmits the larger photon responses. The existence of such a nonlinear filter at the synapse between rods and rod-bipolar cells has been confirmed by electrical recordings in mouse retina [48, 103]. We were surprised, therefore, to discover that macaque rods are electrically coupled to one another by gap junctions; coupling will render synaptic thresholding less effective at separating out signals from noise. We used computer simulation to explore the effects of gap-junctional coupling on visual detection in human observers.

2.3 Methods

2.3.1 Retinal preparation

Membrane voltage was recorded from rod and cone photoreceptors from 11 cynomolgus monkeys (*Macaca fascicularis*) and 4 rhesus monkeys (*Macaca mulatta*). No differences were found in the physiology of the two species. Monkeys were housed and cared for according to guidelines established by the National Institutes of Health. All procedures were approved by the University of California San Francisco Committee on Animal Research, which has approved assurance from the Office of Protection from Research Risks at the National Institutes of Health.

Enucleation was performed under general anesthesia. The eye was hemisected just anterior to the ora serrata. The vitreous was removed, and the eyecup was placed within

a light-tight container in 36 °C bicarbonate-buffered Ames solution (Sigma, St. Louis, MO) equilibrated with 95% O_2/5% CO_2. The retina was dark adapted for a minimum of 1 hour. All subsequent procedures were performed under infrared illumination with the aid of infrared image converters. A 4×4 mm piece of retina was isolated and placed photoreceptor side up in the recording chamber. Photoreceptors were visualized with infrared Nomarski optics through an upright microscope and a 40× water immersion objective. To give recording electrodes clean access to photoreceptor plasma membranes, the retina was incubated for 3–15 minutes in Ames solution containing the following enzymes (in U/ml): 80 collagenase, 300 hyaluronidase, 500 deoxyribonuclease, and 0.2 chondroitin ABC lyase. The enzymes collagenase CLSPA, hyaluronidase HSEP, and deoxyribonuclease I DPFF were obtained from Worthington Biochemical (Lakewood, NJ). Chondroitin ABC lyase 190334 was obtained from ICN Biochemicals (Aurora, OH). After enzyme treatment, the retina was superfused with bicarbonate-buffered Ames medium. The bath temperature was maintained at 36 °C (Cell Micro Controls, Norfolk, VA).

2.3.2 Electrical recording and light stimulation

Membrane potentials of rods and cones were measured with the whole-cell perforated-patch method [61, 108] at retinal eccentricities of 1 cm from the fovea. The electrode solution contained (in mM): 130 K-gluconate, 10 KCl, 4 $MgCl_2$, 10 HEPES, 3 ATP-Na_2, 1 GTP-Na_3, and 0.12 amphotericin B, and was titrated to pH 7.25 with KOH. The chemicals were obtained from Sigma.

The electrical signals were recorded with an Axopatch 2D amplifier (Molecular Devices, Union City, CA). Signals were low-pass filtered by the Axopatch four-pole Bessel analog filter with a cutoff frequency of 2 kHz and by an eight-pole Bessel analog filter (Frequency Devices, Haverhill, MA) with a cutoff frequency of 250 Hz. Additional digital

filtering of signals shown in the figures is indicated in the figure legends. Phase shifts resulting from the filtering were corrected. Membrane voltage was corrected for the electrode junction potential. Data acquisition, analysis, and stimulus presentation were performed with a Macintosh G4 computer, an ITC-18 interface (Instrutech, Port Washington, NY), and the program Igor Pro Carbon 4.0 (Wavemetrics, Lake Oswego, OR). Signals were digitized at 2 or 5 kHz.

Photoreceptors were stimulated with unpolarized light incident perpendicular to the retinal surface. Unless indicated otherwise, light flashes were 500 nm and 10 ms in duration. Light intensity was calibrated before each experiment with a radiometer (model 350; UDT Instruments, Baltimore, MD). The expected number of photoisomerizations (R*) evoked per rod was estimated from the product of the measured photon density (i) and an assumed collecting area of photon capture (A_C) of 1.0 μm^2 [108].

Cones were distinguished from rods by their faster light responses (see fig. 2.1) and larger cell bodies as visualized with Nomarski optics (see figs. 2.7–2.9). Photoreceptor types were further distinguished by their relative sensitivities to flashes of 500 and 660 nm light [14, 15].

2.3.3 Data analysis

The amplitude and kinetics of rod photon signals in rods and cones were determined from the ensemble mean response to 50 or more flashes in the linear range. Results were averaged across cells by scaling the ensemble mean responses of individual cells to a normalized peak amplitude and peak time and then averaging across the population of rods or cones. The population average was then rescaled to reflect the average peak amplitude and peak time. The amplitude distributions of the temporal frequency components of the photon responses were characterized from the fast Fourier transform of rod and cone pop-

ulation averages.

A matched filtering method was used to determine the distribution of response amplitudes to dim flashes [13]. In brief, responses to 50–150 flashes of a fixed intensity were recorded, and the ensemble mean response was calculated. The ensemble mean was fit with the impulse response of a third-order low-pass filter to create a response template. The peak amplitude of an individual response r was taken as the peak amplitude of the response template, scaled to minimize the squared differences between the individual response and the template. Response linearity and stability were verified by interleaving flashes of two intensities in blocks of ~50 responses.

For a given flash photon density i, two amplitude histograms were constructed: a signal histogram $p_S(r)$ obtained from flash-evoked responses, and a dark noise histogram $p_N(r)$ obtained from recordings in intervening dark periods. The fit to the mean flash response was used as the scaling template for both the flash-evoked and dark histograms. The dark histograms were fit to Gaussian distributions with s.d. σ_0. The signal histograms were fit to a theoretical function $f_S(r)$, which assumed that the number of photoisomerizations was Poisson distributed within an electrical coupling pool of N rods and that the response amplitudes were dispersed by baseline dark noise and variability in the size of the single photon response. The equation, modified from Baylor et al. [13] is as follows:

$$f_S(r) = \sum_{k=0}^{\infty} \frac{e^{-iA_CN}(iA_CN)^k}{k!} \frac{1}{\sqrt{2\pi\left(\sigma_0^2 + k\sigma_1^2\right)}} \exp\left(-\frac{(r-ka)^2}{2\left(\sigma_0^2 + k\sigma_1^2\right)}\right) \tag{2.1}$$

where a is the average peak amplitude of a single photon response, σ_0 is the s.d. of the dark noise, and σ_1 is the s.d. in the peak amplitude of a single photon response. The value for σ_0 was taken from the fit of $p_N(r)$ to a Gaussian distribution. For the rod histograms, σ_1 was adjusted to minimize the squared differences between the measured and theoretical functions. For cone histograms, σ_1 was fixed to 0 because empirically $\sigma_1 \ll \sigma_0$. On the

assumption that the ensemble variance is dominated by variability in the number of photoisomerizations, the values of a and N were determined from the peak amplitudes μ_E and σ_E^2 of the light-evoked ensemble mean and variance, respectively, from $a = \sigma_E^2/\mu_E$ and $N = \mu_E^2/\left(A_C i \sigma_E^2\right)$ [108]. These calculations make the simplifying assumption that electrical coupling is "perfect," i.e., photon responses are equivalent in all coupled rods. To the extent that a varies within the coupling pool, the value of N can be viewed as the effective pool size, and a can be viewed as the equivalent photon response amplitude.

The probability P_C that the amplitude of the response to a flash exceeded the amplitude measured in the dark was calculated as follows:

$$P_C = \int_{r=-\infty}^{\infty} p_S(r) \left(\int_{R=-\infty}^{r} p_N(R)\, dR \right) dr \tag{2.2}$$

Detection threshold, defined as the value of i where $P_C = 0.73$, was calculated by linear interpolation from the measured values of P_C close to 0.73.

2.3.4 Network modeling

Rod amplitude histograms were used to model the effects of rod-rod coupling on the absolute sensitivity of dark-adapted human observers. The signal and noise amplitude distributions of coupled and uncoupled rods were simulated from equation 2.1 at varying flash strengths (R* / rod $= iA_C$) and pool sizes (N). Assuming perfect coupling, we took the constants in equation 2.1 to be as follows: $a = 1/N$ mV, $\sigma_0 = 0.4/\sqrt{N}$ mV, and $\sigma_1 = 0.4/N$ mV. The effects of spontaneous photopigment isomerizations were included, with an assumed rate of 0.0063 R* / rod / s [14]. We assumed that spontaneous isomerizations occurring within the rod integration time (400 ms) were indistinguishable from flash-evoked isomerizations. The integration time was obtained from the time integral of the normalized flash response. Given that the rod synapse preferentially transmits photon signals while selec-

tively filtering out the lower amplitude dark noise [48], the dark and light histograms were modified by a nonlinear operation like that described in mouse rod synapses (Field and Rieke [48], their eq. 1).

The rod to rod-bipolar cell synapse saturates with stimuli evoking more than ~1 R* / rod [102, 16]. Saturation is insignificant, however, for dark-adapted thresholds when retinal illumination is uniform, because the probability of two or more R* occurring in one rod at the threshold intensity is very small. For spatially restricted stimuli, however, the photon density of the threshold stimulus increases with decreasing stimulus diameter, so saturation needed to be included. To account for saturation, response amplitudes ≥ 2 mV were set to 2 mV.

We assumed that after these nonlinearities, signals were summed linearly across 10^4 rods [54]. The pooled histograms of the 10^4 rod detection pool were derived as sums of Monte-Carlo-simulated data generated from single rod histograms by the transformation method [93]. Equation 2.2 was used to calculate P_C of the pool. For comparison with a human psychophysical two-alternative forced-choice task with a criterion of 73% correct [113], we calculated the total number of flash-evoked R* within the detection pool required to achieve a P_C of 0.73.

2.3.5 Tracer coupling

The tracer coupling of rods and cones in macaque retina was examined by including Neurobiotin (Vector Laboratories, Burlingame, CA) and Lucifer yellow (Sigma) in the patch electrode. Lucifer yellow, which does not diffuse across photoreceptor gap junctions [63], was used to identify the recorded cell. The patch solution contained (in mM): 127 K-gluconate, 4 $MgCl_2$, 10 HEPES, 3 ATP-Na_2, 1 GTP-Na_3, 12.4 Neurobiotin chloride, and 0.58 Lucifer yellow dipotassium. Solutions were titrated to pH 7.25 with KOH. The tracer

was loaded into photoreceptors by recording from cells in whole-cell mode for ~5–10 minutes. Whole-cell recording allowed the tracer to diffuse readily from the electrode solution into a photoreceptor, but it did not support the maintenance of normal cell function much beyond 10 min. This duration was sufficient to allow us to determine the spectral type of the tracer-injected cell, the magnitude of rod input in cones, and the receptive field shape. Determination of the detection threshold and coupling pool size *N* required longer recording times; consequently, these values were obtained with the perforated-patch method in a population of cells separate from those labeled by tracer injection.

Twenty minutes to 1.5 hours after tracer loading, the retina was placed in 4% paraformaldehyde in sodium phosphate buffer (0.1 M) for 0.5–2 hours. The retina was then rinsed in phosphate buffer and incubated overnight in a 1:200 dilution of streptavidin/cyanine 3 (Jackson ImmunoResearch, West Grove, PA) and 0.3% Triton X-100 in phosphate buffer. Finally, the retina was rinsed in phosphate buffer and coverslipped with Vectashield (Vector Laboratories). Cells were imaged with an LSM 5 Pascal confocal microscope (Zeiss, Oberkochen, Germany) or an RT Spot camera (Diagnostic Instruments, Sterling Heights, MI) mounted on a Zeiss Axioskop microscope. Serial reconstructions of rods and cones were made from z-stacks of confocal images with the isosurface routine in MatLab 6.5 (MathWorks, Natick, MA). Neurobiotin was also injected into rods from a single squirrel monkey, *Saimiri sciureus*. The resulting pattern of tracer coupling was indistinguishable from that found with macaque rod injections.

2.4 Results

2.4.1 Rod photoresponses in cones

Rod and cone voltage responses were measured as a function of flash intensity (fig. 2.1A–2.1B). The cone photovoltage is composed of two kinetically distinct components: a fast component with peak amplitudes that can exceed 25 mV and a slow component with peak amplitudes of up to 6 mV, but more typically 1–2 mV (fig. 2.1B). The fast component arises primarily from phototransduction in cone outer segments [108, 109]. The slow component arises from phototransduction in rods that are coupled to the cone through gap junctions [108, 109] and is the subject of this study. Rod signals were evident in 90% of the red and green cones recorded ($n = 144$), with no observed differences between the two cone types. Rod input was not seen in the two recorded blue cones.

The rod component of the cone response was smaller in amplitude but kinetically similar to the photovoltages recorded directly in rods. To compare rod and cone responses in detail, we recorded photovoltages in response to flashes of 500 nm light that evoked on average between 0.25 and 2.0 R* / rod. At these low light levels, the contribution of cone phototransduction to the cone photovoltage is negligible [109]. In part, the trial-to-trial variability in response amplitude reflects fluctuations in the number of photons absorbed [13, 108]. Response variability was smaller in cones than in rods (fig. 2.1C–2.1D), presumably because cones averaged signals within the pool of coupled rods and because the voltage evoked by a rod photoisomerization was smaller in cones than in rods.

In a population of 13 cones and 7 rods from 10 animals, the peak amplitude of the rod photon response recorded in cones was approximately eight times smaller than the response recorded directly in rods: 0.11 ± 0.10 mV rod / R* (mean $\pm$ s.d.) in cones and 0.86 ± 0.35 mV rod / R* in rods (fig. 2.2A). Differences in response amplitude were accompanied by a twofold difference in the time to the peak of the response: 112 ± 25 ms in cones and $215 \pm$

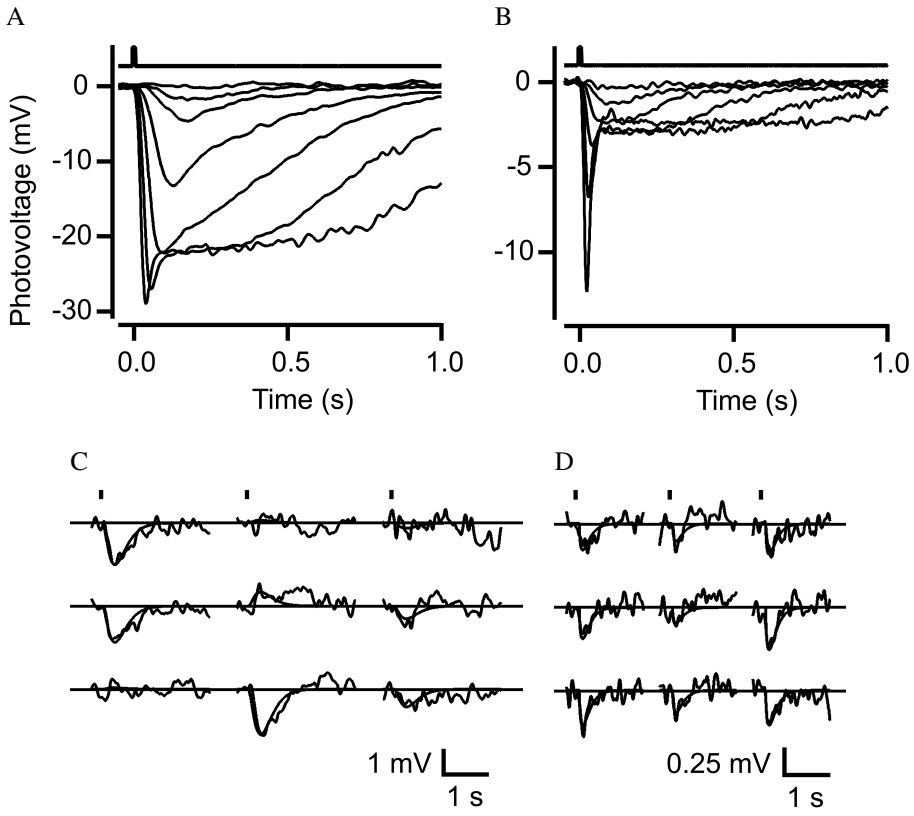

Figure 2.1: Rod signals measured in cones and rods

A, B: Photovoltage responses in a rod (A) or cone (B) to flashes of increasing flash strength ranging from 0.3 to 803 photons / μm^2 in A and 2.0 to 3874 photons / μm^2 in B. Traces are averages of one to four responses. A, Bandwidth, DC–20 Hz. B, Bandwidth, DC–50 Hz. C, D: Response fluctuations to dim flashes in a rod (C) or cone (D). The smooth curves through the noisy measured responses are the scaled response templates from matched filtering. Flash photon densities are 1.0 photon / μm^2 (C) and 2.0 photons / μm^2 (D); bandwidth, DC–5 Hz.

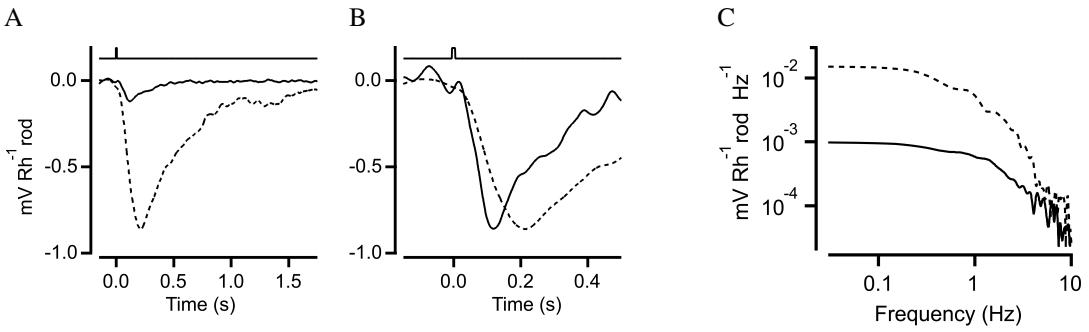

Figure 2.2: High-pass filtering of rod signals in cones
A: Dim flash responses averaged across 7 rods (dashed trace) and 13 cones (solid trace) and normalized by photoisomerizations per rod. See methods for averaging procedure. Bandwidth, DC–10 Hz. B: Same responses as in A on an expanded time scale, with cone response rescaled to match rod response peak. C: Amplitude density of the Fourier components of the flash responses in A.

31 ms in rods (fig. 2.2B). The smaller and faster cone responses indicate high-pass filtering within the rod-cone coupling network. To characterize these filtering properties, the temporal frequency components of the responses were calculated from the Fourier transform of the averages (fig. 2.2C). At the lowest temporal frequencies, the cone response was attenuated by a factor of ~10 compared with the rod response, whereas at higher frequencies the rod and cone functions converged. Highpass filtering has been described previously for electrically coupled rods in salamander, turtle, and frog retinas [39, 6, 127], where it was attributed to voltage-dependent conductances.

2.4.2 Response variation

If responses to single photons were all stereotypic in shape, then the waveform of the ensemble variance would be proportional to the square of the waveform of the ensemble mean. Instead, for both rods and cones, the variance was somewhat longer lasting than the squared mean (fig. 2.3). These differences in waveform might reflect trial-to-trial variation in the duration of light-activated rhodopsin in individual rod outer segments [108, 99, 146]. Alternatively, light responses generated by photon absorption in rods that are distant from

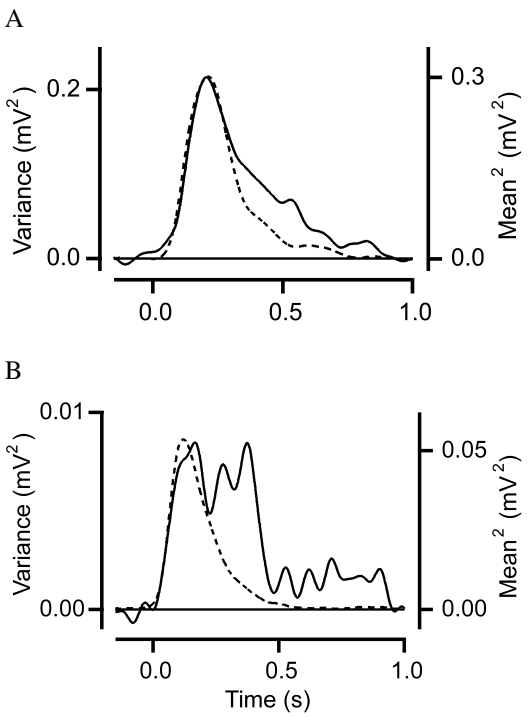

Figure 2.3: Response fluctuations in dim light

Ensemble variance (solid line) and square of ensemble mean (dashed line) recorded in a rod (A) and cone (B) from 100–147 flashes. Flashes = 0.5 photons $/\mu$m^2 (A) and 2.0 photons $/\mu$m^2 (B). Bandwidth, DC–5 Hz.

the recorded cell could have kinetics that are different from those generated in the impaled rod [39]. The positional dependence of the response waveform was not evaluated in this study.

Assuming that the number of photoisomerizations evoked by a flash of fixed intensity is Poisson distributed, the peak amplitude a of the average single photon response can be estimated from σ_E^2/μ_E, the ratio of the peak amplitudes of the ensemble variance and mean. In 9 of 13 cones, the light-evoked variance was too small to resolve. For the remaining four cones in which the variance was large enough to measure, a was 0.051 ± 0.022 mV. In the same population of four cones, the effective number of rods coupled to a cone, calculated from $N = \mu_E^2/\left(A_C\, i\, \sigma_E^2\right)$, was 2.2 ± 1.1. Because we were constrained to analyze cones with variances that were atypically large, these estimates are biased toward large values of

a and small values of N.

2.4.3 Electrical coupling between rods

The value of a calculated in 10 rods was 0.64 $\pm$ 0.48 mV. In eight of these rods, N was close to 1 (1.4 $\pm$ 0.9; mean $\pm$ s.d.), as would be expected for rods that are uncoupled from neighboring rods [108, 130]. Unexpectedly, however, N was considerably larger for two rods: 5.2 and 5.9. The estimate of N was independent of stimulus intensity. As expected for a Poisson process, both the mean and variance increased linearly with flash strength (fig. 2.4); however, the relative slopes of these two functions were inconsistent with photon capture in a single rod outer segment. For an uncoupled rod, the slope of the variance function ($\sigma_E^2/A_C\,i$) should be equal to the square of the slope of the mean function $(\mu_E/A_C\,i)^2$. Instead, for the cell in figure 2.4, ($\sigma_E^2/A_C\,i$) was 5.2 times smaller than $(\mu_E/A_C\,i)^2$, consistent with responses generated by the summation of signals in a pool of approximately five rods.

The calculation of N depends critically on estimates of the photon capture rate and hence on the assumed value of A_C (1.0 μm^2). As an alternative to rod-rod coupling, the unusual intensity dependence of these rods could be explained by an atypically large collecting area. If that were the case, however, flash sensitivity (S_F) would also be five times larger, and the incident photon density that evoked a half-maximal response ($i_{1/2}$) would be five times smaller. Instead, the mean values from these two rods ($S_F = 1.2$ mV photon^{-1} μm^2; $i_{1/2} = 23$ photons / μm^2) were close to average values of the five rods in which N was estimated to be < 2 ($S_F = 0.83$ mV photon^{-1} μm^2; $i_{1/2} = 19$ photons μm^{-2}). Although we cannot rule out the possibility that some rods have both larger collecting areas and correspondingly smaller photon responses, the simplest explanation of the results, also consistent with tracer coupling experiments described below (in rod-rod tracer coupling),

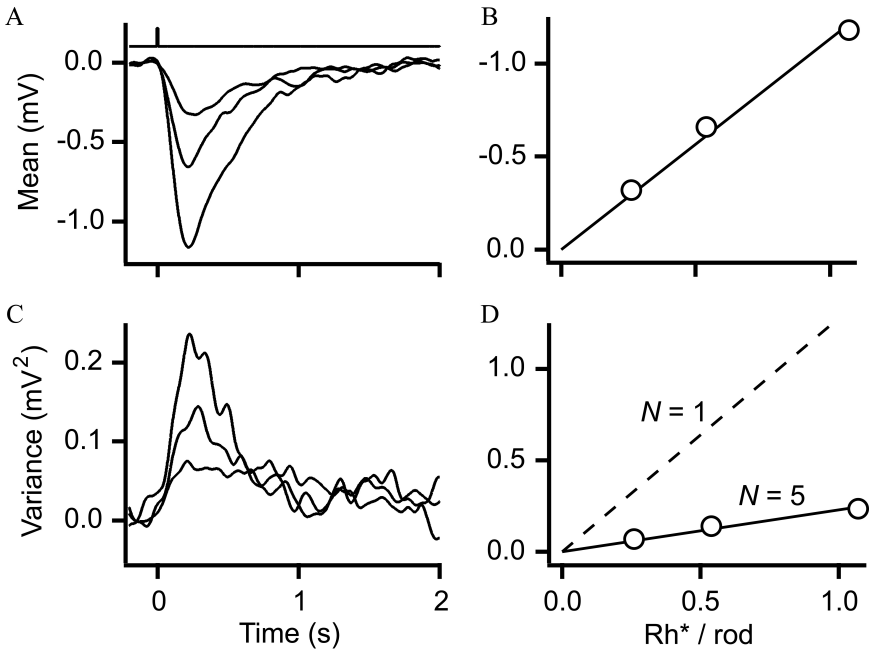

Figure 2.4: Evidence of rod-rod signal coupling

A: Average rod response at three flash strengths. Bandwidth, DC–5 Hz; 142–147 responses per average. B: Circles plot peak amplitude of mean responses in A as a function of flash strength. The line is the least squares fit of the data points to a line intersecting the origin (slope, 1.17 mV per R* / rod). C: Ensemble variance of the same responses as in A. D: Circles plot peak amplitude of the variance in C as a function of flash strength. The solid line is the best linear fit through the origin (slope, 0.265 mV^2 per R* / rod). Dashed line indicates the expected function of an uncoupled rod. From the slopes in B and D, $a = 0.23$ mV and $N = 5.2$ rods.

is that some rods are coupled by gap junctions to other rods.

2.4.4 Detection threshold

Reliable detection of dim light is limited both by variations in the number of photons absorbed and by neural noise [36, 104, 10, 11]. Detection limitations in 10 rods and 16 cones were evaluated from dark and flash-evoked amplitude histograms. The cone responses evoked by the dim 500 nm flashes were generated by their rod inputs. Response amplitudes were measured by using a matched-filter technique (see methods), on the basis of the idea that photoreceptor outputs are "optimally" filtered by the visual system to extract photon signals from the underlying noise [13, 106, 17]. The histograms measured in the dark were well fit by Gaussian distributions with s.d. of 0.46 ± 0.14 mV (rods) (fig. 2.5A) and 0.14 ± 0.08 mV (cones) (fig. 2.5B). The larger dark noise in rods is caused in part by the larger input impedance of rods (1.2 GΩ) as compared with cones (0.1 GΩ).

In some rods, the flash-evoked histograms were multimodal [108], reflecting the quantal nature of photon absorption of uncoupled rods [13]; however, in other rods and all cones (fig. 2.5C–2.5D), multiple peaks in the flash histograms were not evident. These histograms could be accounted for by a Poisson distribution of photoisomerizations in a pool of coupled rods (equation 2.1).

The noise and signal histograms were used to calculate the fraction of trials in which the amplitude of the response to a flash exceeded the amplitude in the dark (equation 2.2). This fraction P_C is equivalent to the probability of making a correct choice in a two alternative forced-choice psychophysical detection paradigm [55]. For a given cell, P_C increased with increasing flash strength in a manner expected from the Poisson distribution of response amplitudes (equations 2.1–2.2). Detection threshold was defined as the flash strength (in R* / rod) at which $P_C = 0.73$. Surprisingly, despite the eightfold difference in rod and

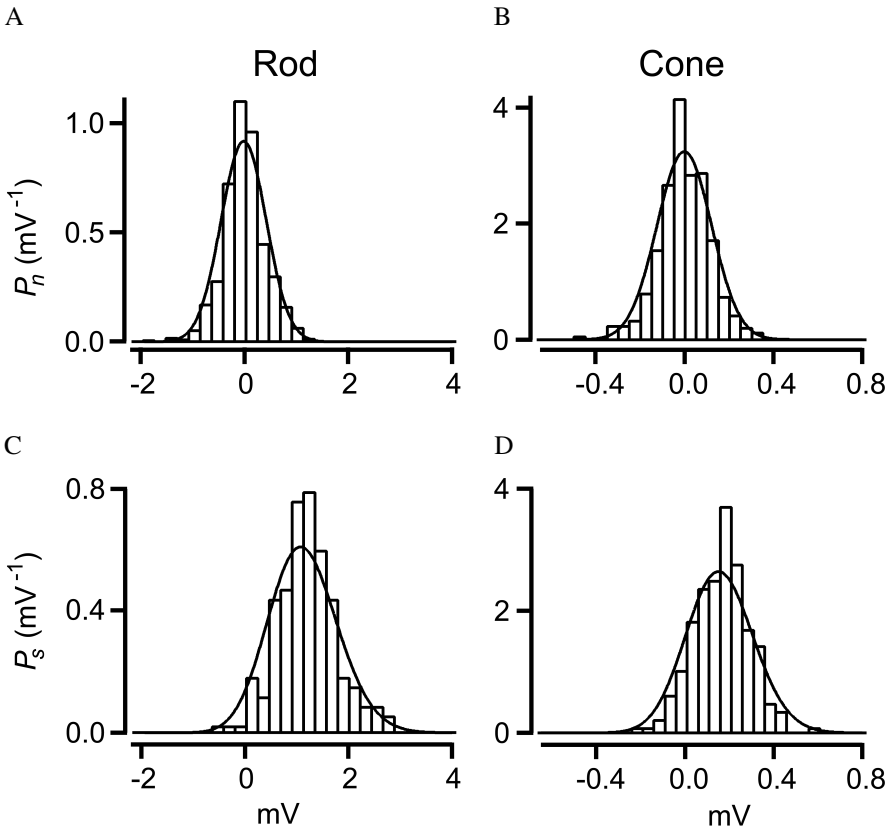

Figure 2.5: Probability density distribution of response amplitudes

Dark noise histograms p_N (A, B) and signal histograms p_S (C, D), obtained from matched filtering, are plotted by the bars. Number of trials = 675–805 (A, B) and 143–149 (C, D). Flash strength = 1.0 photons / μm^2. Smooth curves drawn through noise histograms are Gaussian distributions with s.d. $\sigma_0 = 0.43$ mV (A) and 0.12 mV (B). Smooth curves through signal histograms are from equation 2.1, with the constants in C and D, respectively: $i = 1.0$, 1.0 photons / μm^2; $a = 0.23$, 0.049 mV; $N = 5.2$, 3.1 rods; $\sigma_0 = 0.43$, 0.12 mV; and $\sigma_1 = 0.03$, 0 mV. $P_C = 0.95$ (A, C), and $P_C = 0.82$ (B, D).

cone flash sensitivities, the distribution of rod and cone thresholds largely overlapped (fig. 2.6A). The average thresholds in 10 rods (0.62 $\pm$ 0.25 R* / rod) and 16 cones (1.36 $\pm$ 0.69 R* / rod) differed by only a factor of ~2.

The detection limitation imposed on cones by their lower flash sensitivity was partially offset both by lower cone dark noise and by signal averaging across multiple rods. The expected threshold at a criterion of $P_C = 0.73$ for an ideal noiseless detector (limited only by the Poisson statistics of light) is $-[\ln(0.54)]\ N^{-1}$ R* / rod. A comparison of the estimated values of threshold and N are roughly consistent with this relationship (fig. 2.6B). That most of the points lie above the ideal line is expected from the added variability associated with the phototransduction noise and dark noise of "nonideal" photoreceptors.

2.4.5 Rod-cone tracer coupling

Tracer-coupling between rods and cones was assessed by injecting single cones with Neurobiotin. Neurobiotin was detected in the injected cone as well as in neighboring rods and cones (fig. 2.7A, 2.7D). Of the 33 cone injections, 3 cones were found to be tracer coupled to both rods and cones, 18 to rods only, and 2 to cones only; 10 were uncoupled. The number of labeled rods per injected cone varied from 0 to 28, with a mean of 5.7 $\pm$ 6.7. The size of the maximal rod response in an injected cone correlated with the number of rods to which the cone was tracer coupled, with a Spearman rank-order correlation coefficient [152] of 0.59 $\pm$ 0.20 ($p < 0.0015$ by permutation test; $n = 28$).

To test whether the spread of Neurobiotin into neighboring photoreceptors was mediated by gap junctions, cones were injected with Neurobiotin in the presence of the gap junction inhibitor carbenoxolone (100 μM). Under these conditions, only the recorded cone was labeled (fig. 2.7B) ($n = 4$). Carbenoxolone also abolished the rod component of the cone light response (fig. 2.7C) ($n = 4$). The abolition of the rod component further supports

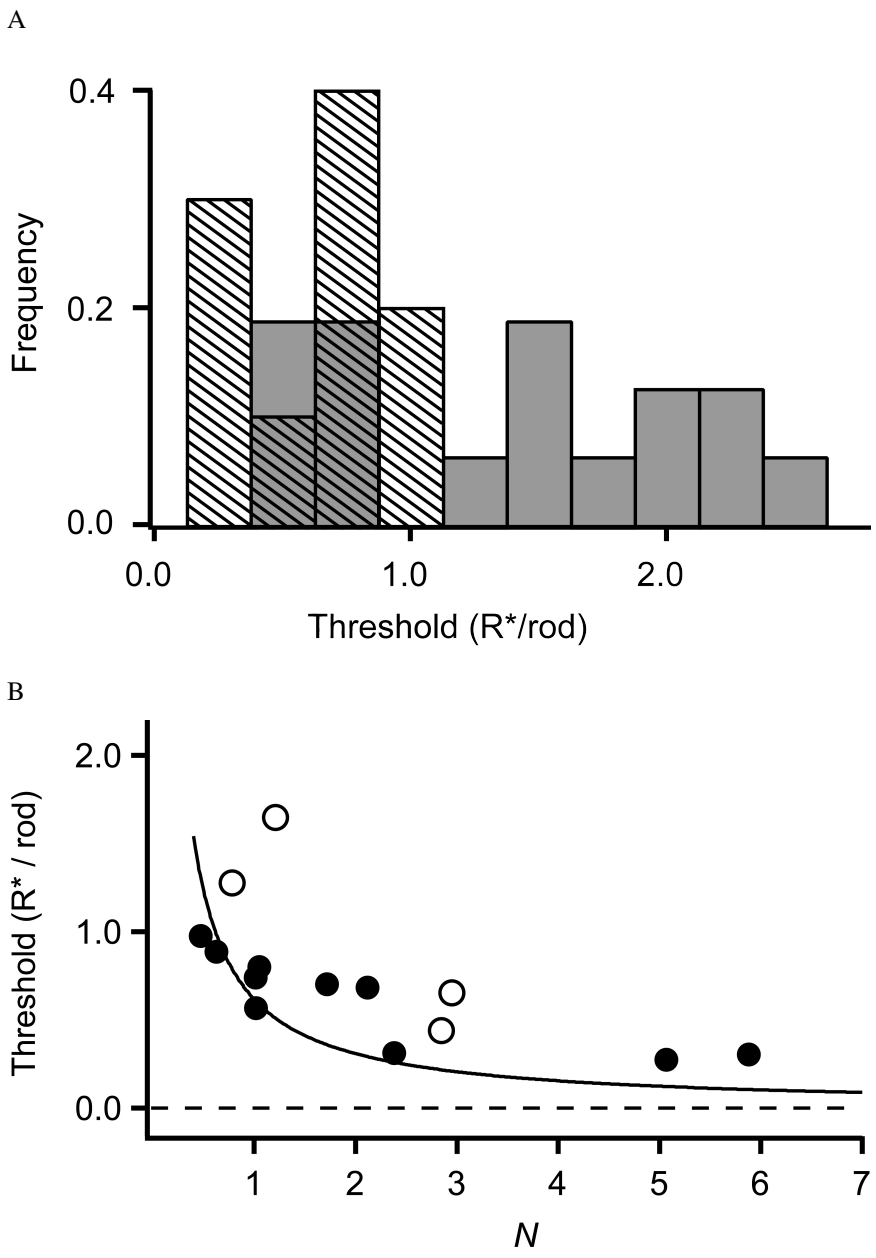

Figure 2.6: Detection thresholds of rods and cones

A: Frequency distribution of thresholds (at $P_C = 0.73$) from 10 rods (striped bars) and 16 cones (shaded bars). B: Electrical coupling reduces detection threshold. Thresholds versus rod pool size N in 10 rods (F) and 4 cones (E). N was obtained from variance and means analysis (see methods). Smooth curve is for an ideal (noiseless) detector, given by $-[\ln(0.54)]\, N^{-1}$ R* / rod.

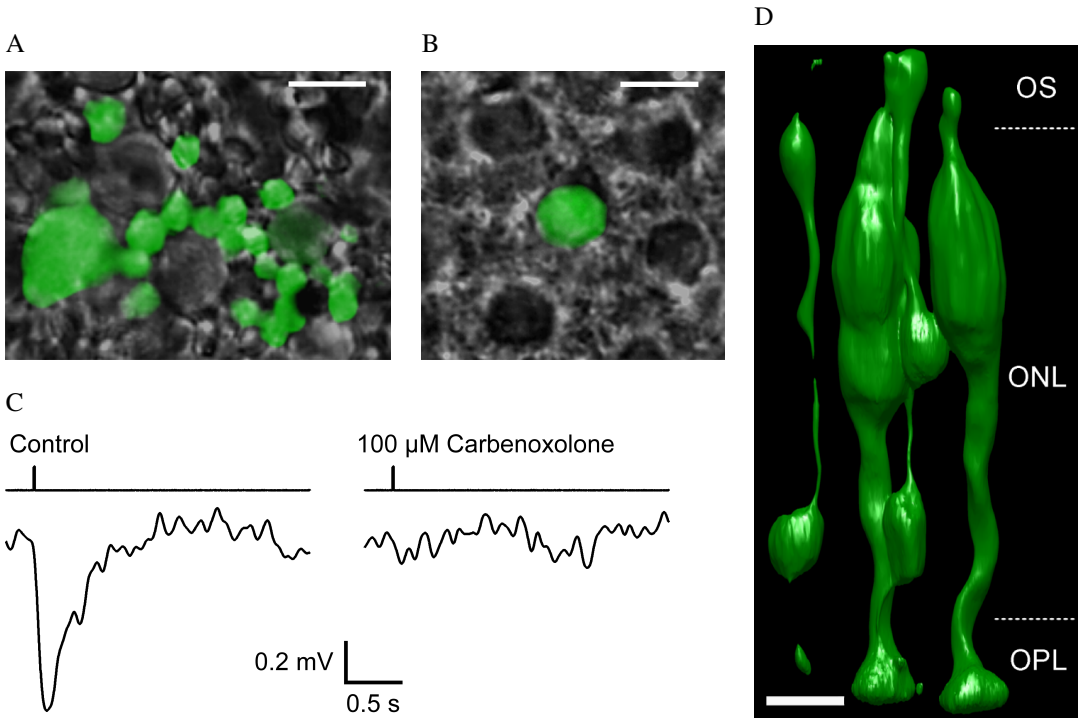

Figure 2.7: Rod and cone coupling is blocked by carbenoxolone

A, B: Combined confocal and Nomarski contrast images of the outer nuclear layer after cone injection of Neurobiotin (green). The cone in A, injected in control solution, is coupled to neighboring rods. The cone in B, injected in the presence of 100 μM carbenoxolone, was not tracer coupled to other cells. C: Rod responses measured in a cone in control solution (left) and again after application of 100 μM carbenoxolone (right). Flashes = 28 photons / μm^2. Traces are averages of four to six responses. Bandwidth, DC–5 Hz. D: Three-dimensional reconstruction of Neurobiotin-labeled rods and cones after injection in a cone. OS, Outer segment; ONL, outer nuclear layer; OPL, outer plexiform layer. Scale bars: A, B, D, 10 μm. Results in A–D were obtained from four separate cone recordings.

the tracer-coupling result, although a direct inhibitory effect of carbenoxolone on rod phototransduction [140] or other photoreceptor conductances [148, 142] has not been ruled out.

Close contacts between colabeled rods and cones (fig. 2.7D) were observed at their synaptic terminals, the location of rod-cone gap junctions described previously from electronmicroscopic studies in primate retina [95, 128]. Unexpectedly, the pattern of labeled rods was often not symmetrical around the recorded cone. Instead, the pattern tended to be skewed toward one side of the cone (figs. 2.7A, 2.8A). By means of hemicircular light stimuli to map out the spatial distribution of rod inputs in the cone, the skewed distribution of tracer coupling was found to match the skewed receptive field (fig. 2.8B) ($n = 4$). The anatomical basis of the spatial distribution is unclear. There was no relationship between the orientation of the skew and retinal eccentricity, the direction of the fovea, or left versus right eye. There was a tendency for tracer-filled rods to lie in the direction of the recording electrode; that is, labeled rods were found preferentially on the electrode side of the cone in 54% of cone injections, on the side opposite the electrode in 23% of injections, and on both sides in the remaining 23%. This observation suggests that the electrode might alter the coupling efficiency of the rod-cone junctions by mechanical disturbance. Whatever the mechanism responsible for the skewed field, it appears not to involve tracer uptake via an extracellular route, as evidenced by the correspondence in the patterns of tracer and electrical coupling and the suppression of tracer coupling by carbenoxolone.

2.4.6 Rod-rod tracer coupling

Of the 35 rods injected with Neurobiotin, 11 (31%) were not tracer coupled to neighboring photoreceptors (fig. 2.9A). The remaining 69% were coupled to one or more additional rods (fig. 2.9B). Sites of close contact between colabeled rods were often found in regions

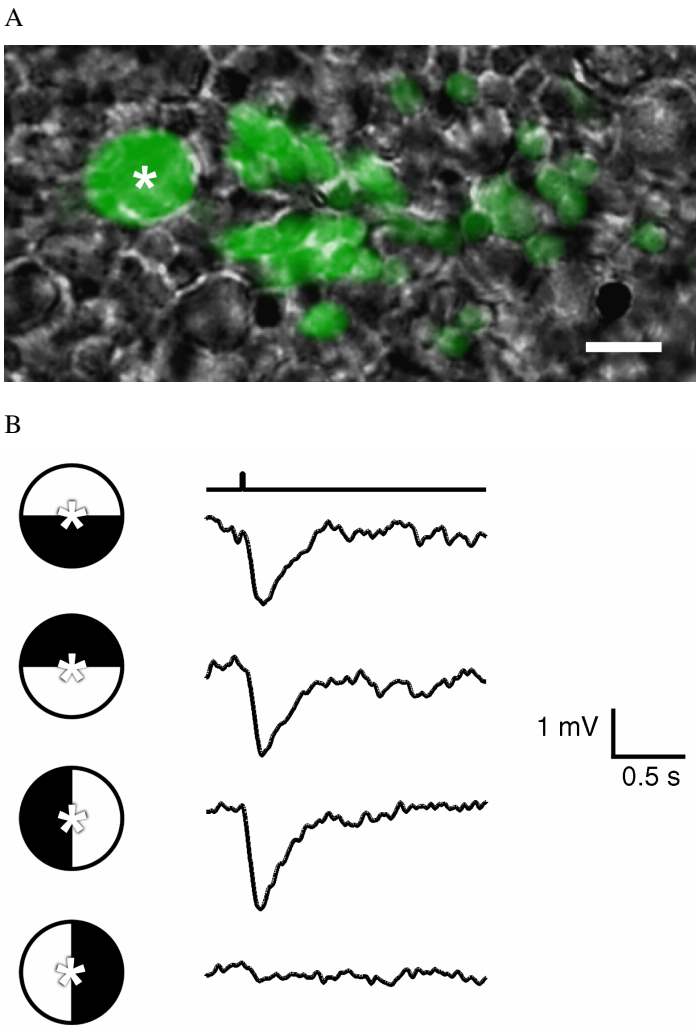

Figure 2.8: Correspondence of tracer coupling and receptive field

A: Neurobiotin labeling (green) of rods coupled to injected cone (asterisk). Scale bar, 10 μm. B: Rod responses in the cone shown in A to flashes of light covering a hemifield rotated around the recorded cone. Traces are averages of 6–12 responses to flashes of 16 photons / μm^2. Bandwidth, DC–5 Hz. Cone membrane potential was recorded in whole-cell mode. Symbols to left of traces denote orientation of the stimulus hemifield relative to the recorded cone.

containing rod cell bodies, inner segments, and passing rod axons (fig. 2.9C), the region described in mouse retina where rod-rod gap junctions are located [130]. Some labeled rods had no apparent sites of physical contact with labeled neighboring rods (fig. 2.9C), although the occasional presence of faintly labeled "ghost" cells suggests that intervening labeled cells may have been lost during tissue processing.

The total number of rods labeled with rod injection of Neurobiotin ranged from 1 to 10, with an average of 3.4 ± 2.6 ($n = 35$). The distribution in the number of tracer-coupled rods overlapped with the distribution of N, the effective number of electrically coupled rods calculated from the mean and variance analysis (fig. 2.9D). The spread of Neurobiotin from rods to cones was rare. Rod-cone tracer coupling was observed in only 2 (6%) of 35 rod injections as compared with 64% of cone injections.

2.4.7 The effects of rod-rod coupling on detection

The rod to rod-bipolar cell synapse is highly nonlinear, transmitting signals over a narrow range of rod membrane potentials. The synapse attenuates fluctuations in membrane potential close to the dark potential, and it saturates with light-evoked hyperpolarizations of only a few millivolts [102, 48, 16]. Thus the synapse effectively transmits single photon responses at high gain and attenuates both dark noise and multiple photoisomerizations within single rods. Electrical coupling of rods will affect photon signaling at both ends of the transmission range. Coupling will reduce the size of the single photon response relative to the dark noise in a single rod, thus rendering the rod synapse less effective at separating dark noise from single photon responses [116, 48]. At the same time, the spread of photon signals within the pool of coupled rods reduces the effects of synaptic saturation [126]. To investigate the effects of rod-rod coupling on the detection of dim light, the sensitivity of dark-adapted observers was modeled from the signal and noise histograms of single rods

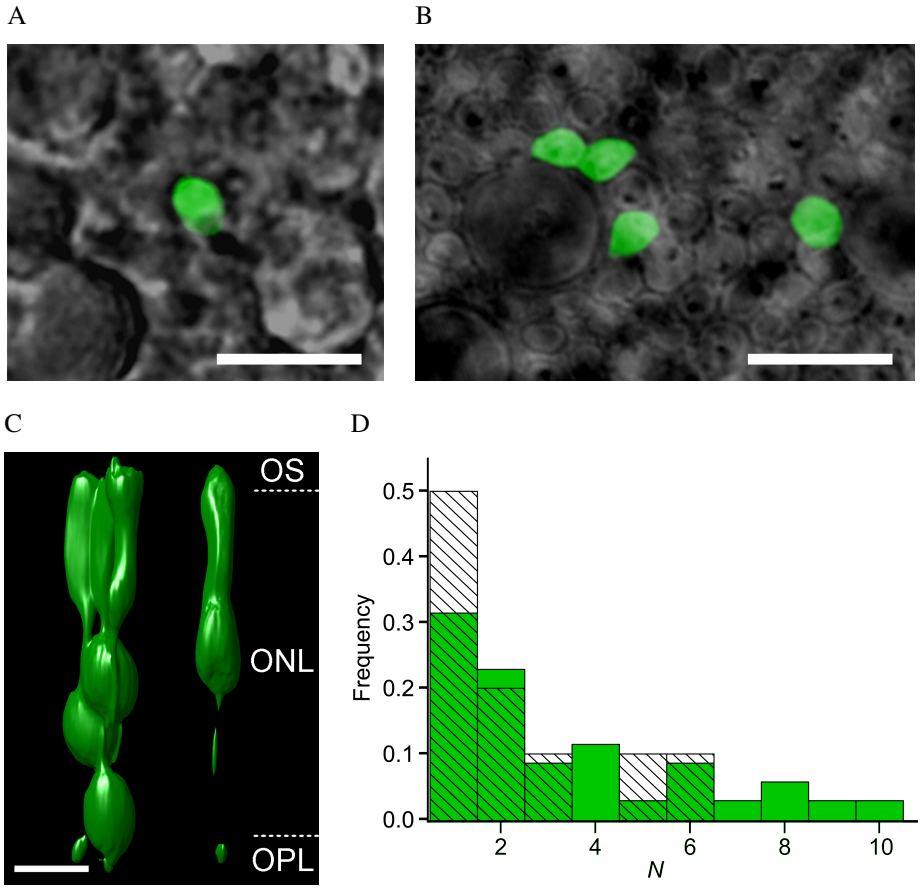

Figure 2.9: Tracer and signal coupling between rods

A, B: Combined confocal and Nomarski contrast images after Neurobiotin injection of single rods. Only the injected rod is labeled in A; four rods were labeled in B. C: Three-dimensional reconstruction of rods in B. OS, Outer segment; ONL, outer nuclear layer; OPL, outer plexiform layer. Scale bars: A–C, 10 μm. D: Frequency distribution of rod pool size (N). Tracer coupling is indicated by green bars. Signal coupling, determined from mean and variance analysis of dim flash responses, is indicated by striped bars. $N = 1$ indicates an uncoupled rod.

and a theoretical detection pool of 10^4 rods (see methods). For uniform illumination of a detection pool of uncoupled rods, the model estimated a threshold (at $P_C = 0.73$) of 9 R*, a value nearly identical to the 10 R* estimated in human psychophysical tests at a criterion of 73% correct [113]. Electrical coupling of rods increased threshold. For an assumed coupling pool size of two rods, close to our measured average of N, threshold increased to 15 R*. With more extensive coupling, the threshold continued to increase, asymptotically approaching 35 R* (fig. 2.10A), the threshold expected for uncoupled rods that lack a dark noise synaptic filter.

Including synaptic saturation in the model did not affect thresholds for uniform illumination because the likelihood of two or more R* occurring in the same rod at the dark-adapted threshold intensity was minuscule. Saturation became a significant factor, however, as the stimulus diameter was reduced and photon density increased. Consequently, although detection thresholds for diffuse light were elevated by electrical coupling, thresholds for small-diameter stimuli were actually reduced by electrical coupling (fig. 2.10B). For an assumed saturation level of 2 mV and a pool size of two rods, electrical coupling lowered dark-adapted thresholds relative to that of uncoupled rods for stimulus diameters < 0.066 ° visual angle. This critical diameter was largely insensitive to the assumed degree of coupling (N) but depended on the assumed level of saturation. With lower saturation levels, electrical coupling became beneficial with larger stimulus diameters. The critical diameter also increases with background illumination (data not shown) because backgrounds elevate the threshold intensity of the test flash and hence increase the likelihood of multiple R* / rod.

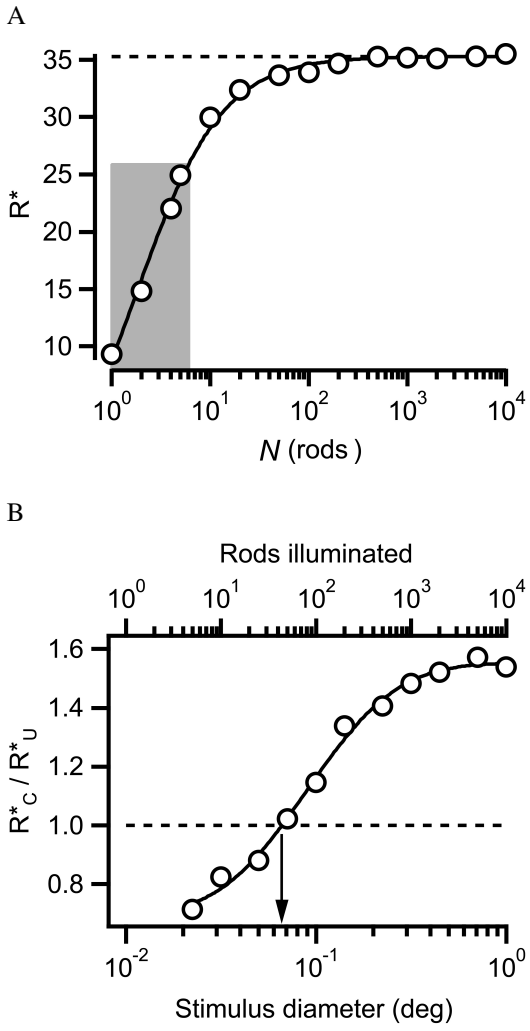

Figure 2.10: Effect of rod-rod coupling on psychophysical thresholds
A: Psychophysical threshold (R*) in a two-alternative forced-choice experiment, calculated from model simulations, as a function of rod pool size N (for details of the model, see methods). The shaded region represents the range of experimentally determined electrical pool sizes of macaque rods (N =1–6). The dashed line indicates the expected threshold in the absence of synaptic nonlinearities. B: Psychophysical threshold intensity of coupled rods (R_C*) relative to uncoupled rods (R_U*) as a function of stimulus diameter, with $N = 2$. Coupling lowered threshold (R_C* / R_U* < 1) for stimulus diameters < 0.066 ° (arrow).

2.5 Discussion

2.5.1 Temporal properties of rod-cone coupling

By using dim flashes to assess the temporal properties of coupling, we found that rod signals were high-pass filtered in cones: the low-frequency components of the signals were preferentially attenuated. Because the energy of the dim flash response is limited to frequencies < 10 Hz, the transfer of higher-frequency signals could not be assessed by this method. A previous study in macaque retina showed that higher frequency signals (> 10 Hz) were also attenuated [109]. Together, these results indicate that the rod-cone coupling network in primates, like the cone-cone network [63], is bandpass in character. These temporal properties are reminiscent of the bandpass characteristics of the so-called π_0' mechanism of human vision [115], a psychophysically defined rod signaling mechanism thought to depend on rod-cone coupling.

2.5.2 Pattern of tracer coupling

Rod-cone tracer coupling was observed 10 times more frequently in Neurobiotin injections of cones as compared with rods. An asymmetry of tracer spread across gap junctions has been described previously in other heterologously coupled cells [49, 101, 151] in which it was speculated to reflect an asymmetry in the free-energy barrier for permeation [49]. An asymmetric barrier between rods and cones can arise if the rod and cone hemichannels are composed of different connexins. Consistent with this idea, immunohistochemical studies in guinea pig and mouse retina [74, 35] showed that connexin Cx36 was expressed in cones but not rods. Alternatively, the observed asymmetry in rod-cone tracer flux might be caused by differences in the convergence of rod and cone contacts. In mouse retina, each rod makes gap-junctional contacts with only approximately one cone, whereas each cone

contacts 30 rods [130].

The distributions of pool sizes for rod-rod tracer and electrical coupling were similar to one another (fig. 2.9D); however, if coupling forms a continuous network of rods across the retina, the precise meaning of these two measures of pool size is unclear. If, on the other hand, rods were coupled into small local syncytia as was observed in mouse retina [130], then the correspondence of tracer and electrical coupling is more straightforward. The pattern and number of tracer-coupled rods observed here is reminiscent of the radial clusters of labeled rods in rat retina derived from common progenitor cells during late retinal development [131]. This similarity suggests the possibility that the clusters of tracer-coupled rods observed here may reflect discrete pools of rods of common clonal lineage.

2.5.3 Importance of photoreceptor coupling for low-light detection

Light responses of primate rods increase in amplitude with increasing stimulus intensity up to ~100 R* / rod [14, 69, 108]; however, the response in rod-bipolar cells reaches maximal size with only one or a few R* / rod [102, 48, 16]. Thus, in the range of ~2–100 R* / rod where the rod-bipolar synapses are saturated and phototransduction within cone outer segments is minimal [107, 108], intensity encoding within the retina depends on the transmission of rod signals via pathways other than rod-bipolar cells.

Two alternative pathways have been described. One alternative is the rod-cone coupling pathway studied here. Measurements in cat and primate cones [86, 109] show that rods transmit signals to coupled cones up to rod-saturating intensities. Our results show that in the dark-adapted retina, lights evoking fewer than two R* / rod can be reliably detected in the cone membrane potential. On the basis of theoretical considerations, Smith et al. [116] proposed that rod-cone gap junctions are closed in dark-adapted retina. Our present

measurements conflict with this hypothesis.

The second alternative pathway for rod signaling described in mouse retina [118, 130] uses a chemical synapse to connect rods to cone Off-bipolar cells. If this connection is also present in primates, the relative contributions of this pathway and the rod-cone coupling pathway for signaling in the mesopic range need to be examined.

Applying our measurements of rod photon signals and noise to a simplified model of coupled rods, we calculated that rod-rod coupling could raise human detection thresholds for large-diameter stimuli by as much as a factor of 3.5. The deleterious impact of coupling on detection is expected to diminish with decreasing stimulus diameter, and, in fact, coupling would actually lower the detection threshold for very small stimuli. Our model yields only an approximate account of the impact of coupling on signal detection. A more complete model would include further evaluation of the temporal requirements for detection, the falloff of signal and noise amplitude with distance across of the rod network [126], the effects of rod-cone coupling, and additional noise contributions such as the quantal noise of synaptic transmission. The development of a more realistic model of signals and noise within a distributed network of coupled rods and cones will first require direct measurements of rod-rod and rod-cone coupling conductances. The effects of light adaptation and circadian rhythm on coupling strength also need to be examined further.

Chapter 3

Gap-junctional coupling of mammalian rods and its effect on visual detection thresholds

3.1 Abstract

Confirmation of gap-junctional coupling between rods in primate retina suggests a role for coupling in human vision (chapter 2). But although coupling is known to reduce the variability of light responses within the rod network, downstream effects on visual performance are not well understood. Here, we assess rod coupling in the guinea pig retina using three techniques: 1) direct measurement of junctional conductance between neighboring rods, 2) measurement of tracer coupling between Neurobiotin-filled rods and neighbors, and 3) statistical analysis of the variability of dim flash responses. We then present a framework for modeling coupled rod networks as resistive circuits, and use this network model to consolidate our three different coupling measurements. Together, the data suggest a retina composed of discrete, local networks of from 1 to 20 hexagonally packed rods, with junctional conductances of about 350 pS. Furthermore, we find that the junctional conductance measured here in guinea pig is consistent with tracer coupling and dim flash variability measured previously in primate. Consequently, we incorporate this junctional conductance into a model of human psychophysical detection. Under this analysis, we find that the ben-

efits of coupling for detection of small spots of light are greater than previously supposed, while detrimental effects are mitigated. Our analysis thus clarifies the interactions between rod coupling and the psychophysical trade-offs governing mammalian night vision.

3.2 Introduction

Gap junctions are direct intercellular channels that allow electrical currents and small molecules to pass between coupled cells. In the retinal photoreceptor layer, electrical coupling of rods has been confirmed by rod recordings in several cold-blooded vertebrate species [46, 112, 145, 154] and is predicted in other species based on electron micrograph (EM) evidence. In mammals, there appear to be two possible sites for rod gap-junctional connection. Most attention has been focused at the rod synaptic level, where rod spherules, ellipsoids, and passing axons form gap junctions in mouse and guinea pig [130], and perhaps also in primate [95]. Two EM studies have also reported apparent gap junctions in primate and human retina at the rod inner segment level [132, 27], where rod junctions are generally found in cold-blooded vertebrates [34, 52, 153].

In chapter 2, we confirmed the presence of rod coupling in primate using the tracer Neurobiotin; in a majority of cases, tracer spread from a single filled rod into a discrete pool of neighbors. In the same preparation, we also recorded rod voltage responses to dim light flashes. Statistical analysis of these recordings further confirmed functional coupling of primate rods by demonstrating the effect of coupling to reduce the variability of dim flash responses due to signal averaging within the coupled network.

Although this effect on response variability within the rod layer is well established [46, 112], downstream effects of coupling on visual performance are not well understood. Previous efforts to model rod coupling [72, 7, 126] have focused on effects within the rod layer, and have focused on cold-blooded vertebrates, whose post-receptoral circuitry

is quite different from that in mammals. The mammalian retina features a specialized rod bipolar cell pathway optimized for detection at absolute threshold [122].

In chapter 2, we endeavored to model the effect of rod coupling on psychophysical detection through this pathway. Because there was no previous measurement of mammalian rod-rod junctional conductance, we based our model on the simplifying assumption of perfect coupling, i.e. that rods were coupled with zero junctional resistance so that two coupled rods acted essentially as a single receptor with twice the normal rod collecting area and half the normal input resistance. Under this analysis, we found coupling to be detrimental to detection of full-field stimuli (~50% increase in detection threshold), but beneficial (~30% reduction in threshold) for detection of very small spots of light. However, the perfect coupling assumption is known to underestimate the signal:noise ratio within the rod layer [126], so we expected that the model might likewise be underestimating the benefits of coupling for downstream processing and psychophysical detection.

Here, we present results from guinea pig retina, where we were able to measure rod-rod junctional conductance directly, a first for mammalian retina. We develop a computational method for analyzing rod networks as resistive circuits and use this network model to compare the present results with previous assessments of mammalian rod coupling. Finally, we update the psychophysical model, replacing the perfect coupling assumption with a more realistic coupling conductance based on our measurements. The updated model yields new insights into the effect of coupling on visual detection thresholds.

3.3 Methods

3.3.1 Retinal preparation

Recordings were made from rod photoreceptors in isolated retinal preparations from pigmented guinea pigs (*Cavia porcellus*, Elm Hill, Chelmsford, MA) aged between 4 and 30 weeks. Guinea pigs were housed and cared for according to guidelines established by the National Institutes of Health. All procedures were approved by the University of California San Francisco Committee on Animal Research, which has approved assurance from the Office of Protection from Research Risks at the National Institutes of Health.

In most cases, the guinea pig was dark adapted for one hour before euthanasia, after which euthanasia and dissection proceeded in darkness, assisted by infrared goggles (Litton Electro-Optical Systems, Tempe, AZ). Following euthanasia and enucleation, the front of the eye was removed just anterior to the ora serrata, the vitreous was removed, and the eyecup was placed within a light-tight container in 36 °C bicarbonate-buffered Ames medium (Sigma, St. Louis, MO) equilibrated with 95% O_2 / 5% CO_2. If the guinea pig was not dark adapted prior to euthanasia, then at this stage the eyecup was left to dark adapt in Ames for 1 hour. Otherwise mounting of retina proceeded directly with a 6 x 6 mm piece of retina isolated and mounted photoreceptor side up in the recording chamber on a coverslip coated with poly-L-lysine (2 mg / mL, 150–300 kDa, Sigma).

Photoreceptors were visualized with an upright microscope (Zeiss, Oberkochen, Germany) with infrared Nomarski optics through a 40x water immersion objective. To give recording electrodes clean access to photoreceptor plasma membranes, the retina was incubated for 3–15 min in Ames solution containing the following enzymes (in U/ml): 80 collagenase, 300 hyaluronidase, 500 deoxyribonuclease, and 0.2 chondroitin ABC lyase. The enzymes collagenase CLSPA, hyaluronidase HSEP, and deoxyribonuclease I DPFF were obtained from Worthington Biochemical (Lakewood, NJ). Chondroitin ABC lyase 190334

was obtained from ICN Biochemicals (Aurora, OH). In some cases, the enzyme treatment was simplified to 3–5 minutes in 2500 Deoxyribonuclease 1 (Sigma) with comparable results. After enzyme treatment, the retina was superfused with bicarbonate-buffered Ames medium with bath temperature maintained at 36 °C (Cell Micro Controls, Norfolk, VA).

3.3.2 Electrical recording and light stimulation

Rod membrane voltages and currents were recorded using the whole-cell or perforated-patch method [108]. In dual-electrode experiments, which focused on the electrical properties of intercellular coupling, whole-cell was used exclusively. Glass electrodes were pulled on a P-87 micropipette puller (Sutter Instruments, Novato, California). The electrode solution contained (in mM): 130 K-gluconate, 10 KCl, 4 $MgCl_2$, 10 HEPES, 3 ATP-Na_2, 1 GTP-Na_2, and was titrated to pH 7.25 with KOH (all chemicals from Sigma). With this internal solution and Ames external, electrode resistances were between 4 and 12 MΩ. In recordings from single rods focusing on robust characterization of light responses, an additional 0.12 amphotericin B (Sigma) was added to allow perforated-patch recording.

Electrical signals were recorded with an Axopatch 1D amplifier (Molecular Devices, Union City, CA). Signals were low-pass filtered by the Axopatch four-pole Bessel analog filter and by an eight-pole Bessel analog filter (Frequency Devices, Haverhill, MA). For recording photoresponses in current clamp mode, filter low-pass cutoff frequencies were 200 Hz and 500 Hz respectively. For voltage step protocols, cutoffs were 2000 Hz and 5000 Hz. Any additional digital filtering of signal is indicated in the figure legends. Group delays resulting from the filtering were corrected. Stimulus presentation and data acquisition were performed by a Macintosh computer, an ITC-18 interface (Instrutech, Port Washington, NY), and the program Igor Pro (Wavemetrics, Lake Oswego, OR). Signals were digitized at 1–5 kHz.

Photoreceptors were stimulated with unpolarized, monochromatic (wavelength half-width ~10 nm, interference filters) light incident perpendicular to the retinal surface. The light intensity was calibrated before each experiment with a radiometer (model 350; UDT Instruments, Baltimore, MD). Stimulus intensity was controlled using a set of calibrated ND filters. The expected number of photoisomerizations (R*) evoked per rod was calculated as the product of: the calculated photon density (i), a scaling factor to account for relative spectral sensitivity, and the effective collecting area of photon capture (A_c). Based on estimated guinea pig rod dimensions [150], and pigment density [90], A_c was taken to be 1 μm^2 at the wavelength of maximum sensitivity (~500 nm; figure 3.1). Unless otherwise indicated, light flashes had a wavelength of 500 nm and were 10 ms in duration.

3.3.3 Tracer coupling

The tracer coupling of rods and cones in macaque retina was examined by including Neurobiotin (Vector Laboratories, Burlingame, CA) in whole-cell patch electrodes. The patch solution contained (in mM): 127 K-gluconate, 4 $MgCl_2$, 10 HEPES, 3 ATP-Na_2, 1 GTP-Na_3, 12.4 Neurobiotin chloride. Solutions were titrated to pH 7.25 with KOH. The tracer was loaded into photoreceptors by recording in whole-cell mode for 5–10 min.

20–90 minutes after tracer loading, the retina was placed in 4% paraformaldehyde in sodium phosphate buffer (0.1 M) for 45–60 min. The retina was then rinsed in phosphate buffer and incubated overnight in a 1:200 dilution of streptavidin/cyanine 3 (Jackson ImmunoResearch,West Grove, PA) and 0.3% Triton X-100 in phosphate buffer. Finally, the retina was rinsed in phosphate buffer and coverslipped with Vectashield (Vector Laboratories). Cells were imaged with an LSM 5 Pascal confocal microscope (Zeiss, Oberkochen, Germany).

3.3.4 Data analysis

Whole-cell junctional currents and voltages were corrected for series resistance and membrane leak errors [133, 137]. In perforated patch experiments, voltage responses to 50–100 flashes of a fixed intensity were recorded, and the mean and ensemble variance were calculated. On the assumption that the ensemble variance is dominated by Poisson variability in the number of photoisomerizations, the peak of the ensemble mean and variance for an isolated rod should follow the relation:

$$\mathrm{E}(V) = a\,m$$

$$\mathrm{Var}(V) = a^2 m$$

where a is the average single photon voltage response peak amplitude and m is the mean number of R* / rod / flash.

Coupling lowers ensemble variance relative to the mean [46, 112, 62]. In order to quantify this reduction in variance, it is useful to make the simplifying assumption that coupling is perfect, i.e. that the gap junctions have zero resistance, so that two coupled rods act together as a single photoreceptor with twice the collecting area and half the membrane resistance. Coupling can thus be quantified in terms of the number of perfectly coupled rods that would yield the observed variance reduction. This effective number of perfectly coupled rods, N_{eff}, was calculated from the measured mean and ensemble variance at given flash intensities:

$$\mathrm{E}(V) = \frac{a}{N_{\mathrm{eff}}}\, m N_{\mathrm{eff}} = a\,m \tag{3.1}$$

$$\mathrm{Var}(V) = \left(\frac{a}{N_{\mathrm{eff}}}\right)^2 m N_{\mathrm{eff}} = \frac{a^2 m}{N_{\mathrm{eff}}} \tag{3.2}$$

$$N_{\mathrm{eff}} = \frac{[\mathrm{E}(V)/m]^2}{\mathrm{Var}(V)/m} \tag{3.3}$$

3.3.5 Network modeling

The pool of coupled photoreceptors was modeled as a resistive circuit network. Photoreceptors were modeled as nodes with resistances to ground, R_m. Gap junctions were modeled as resistances, R_j, between a subset of geometrically neighboring nodes. Phototransduction in the resistive network was modeled as an independent current source at each photoreceptor node. Capacitative effects were found to be negligible (see supplemental material), so membrane capacitances were excluded from further modeling.

For a pure resistive network, the voltage at any node, r, under a given combination of current inputs, $\vec{i}$, is simply the superposition of the voltages that would be generated by each current input treated independently:

$$V_r = \sum_{s \in B} i_s v_{r|s} \tag{3.4}$$

where B is the set of all nodes in the network (including r) and $v_{r|s}$ denotes the current-voltage transfer ratio. This transfer ratio incorporates both the membrane resistance at r, and a scaling factor accounting for the proportion of current input at s that eventually crosses the membrane resistance at r. Therefore, although dimensionally a resistance, $v_{r|s}$ can be thought of as equivalent to the voltage that would be generated independently at node r given unit current injected at node s. In addition to $v_{r|s}$, it is useful to define a voltage-voltage transfer ratio, $w_{r|s}$, equivalent to the voltage generated at r by any current input at s, normalized to the voltage that would have been generated at s in the uncoupled case:

$$w_{r|s} = \frac{v_{r|s}}{R_m} \tag{3.5}$$

For both v and w, the nodes r and s are interchangeable, i.e. $v_{r|s} = v_{s|r}$ and $w_{r|s} = w_{s|r}$.

Analytic solutions for the transfer ratios v and w are possible for trivial networks, as well as a few relevant special cases [72], but in practice these values were obtained computa-

tionally. Circuit simulation software, such as the Gnu Circuit Analysis Package (GnuCAP, http://www.gnucap.org/), provided the most flexible method for computing transfer ratios. GnuCAP netlists representing arbitrarily large geometric networks of rods were generated algorithmically via a context-sensitive L-system [77] [51] implemented in Perl. However, for most networks modeled here, R_m and R_j were assumed to be uniform throughout the network, and a more direct computation was used as follows.

For networks with fixed R_m and R_j, circuit analysis shows that at each node r,

$$V_r = \left[\beta i_r R_m + \left(\sum_{n \in C_r} V_n \right) \right] (\beta + |C_r|)^{-1} \tag{3.6}$$

where $\beta \equiv {}^{R_j}/_{R_m}$, C_r is the set of all nodes directly connected to r (not including r itself), and $|C_r|$ denotes the number of elements in C_r. To calculate $v_{r|s}$ for every s, we assume unit current input at r and calculate the resulting voltage throughout the network. For this situation, the voltage at r is:

$$V_r = v_{r|r} = \left[\beta R_m + \left(\sum_{n \in C_r} V_n \right) \right] (\beta + |C_r|)^{-1} \tag{3.7}$$

while for every other node it is simply:

$$V_s = v_{s|r} = v_{r|s} = \left(\sum_{n \in C_s} V_n \right) (\beta + |C_s|)^{-1}, \quad s \neq r \tag{3.8}$$

For any given network of connectivity C and connection strength β, equations 3.7 and 3.8 define a system of simultaneous linear equations in v. A parallel system of equations is defined in w:

$$w_{r|r} = \left[\beta + \left(\sum_{n \in C_r} w_{r|n} \right) \right] (\beta + |C_r|)^{-1} \tag{3.9}$$

$$w_{r|s} = \left(\sum_{n \in C_s} w_{r|n} \right) (\beta + |C_s|)^{-1}, \quad s \neq r \tag{3.10}$$

The systems of equations defined by equations 3.7–3.10 can be easily solved with a variety of software (e.g. see cellnet.m), once the matrices representing the systems are specified. Connectivity matrices representing simple rod networks were generated by hand, while more complicated network representations were generated algorithmically (see hexconnect.m).

To compare the network model to the results from dim flash variance analysis experiments, the current associated with a single photoisomerization was defined as j and each photoreceptor node was assigned an input current jX, where X was Poisson distributed with average m. Over many iterations, the voltage at node r has expected value:

$$\mathrm{E}(V_r) = jm\sum_{s\in B} v_{r|s}$$

and variance:

$$\mathrm{Var}(V_r) = j^2 m\sum_{s\in B}\left(v_{r|s}^2\right)$$

For N_{eff} as defined in the dim flash variance analysis above, the network model yields N_{eff} at node r:

$$N_{\mathrm{eff}} = \frac{[\mathrm{E}(V_r)/m]^2}{\mathrm{Var}(V_r)/m} = \frac{\left(\sum_s v_{r|s}\right)^2}{\sum_s v_{r|s}^2} = \frac{\left(\sum_s w_{r|s}\right)^2}{\sum_s w_{r|s}^2} \tag{3.11}$$

In their rod network modeling, Tessier-Lavigne and Attwell [126] also present a number of effectively coupled rods, which is not, however, equal to our N_{eff}. Their N'_{eff} is defined as the network resistance measured from node r, divided by the membrane resistance R_m, i.e. $N'_{\mathrm{eff}} = {}^1/_{w_{r|r}}$. The precise relationship between our N_{eff} and their N'_{eff} depends on the network connectivity, although the two quantities both generally increase with lower β or greater connectivity $|C|$.

Arbitrarily large geometric networks of cells were used as approximate representations of infinite networks. In practice, for a hexagonally connected network with $\beta = 2$ (see results) and 4 concentric layers of cells (61 cells total), the N_{eff} calculated (9.1) did not

change significantly (< 0.25%) with additional layers (figure 3.8). Lamb and Simon [72] give an analytic solution for the value $w_{s|s}$ of every node in an infinite square network:

$$w_{s|s} = \frac{2}{\pi}\left(\frac{\beta}{\beta+4}\right) \mathrm{K}\left(\left[\frac{4}{\beta+4}\right]^2\right) \tag{3.12}$$

where $\mathrm{K}(x)$ is the complete elliptical integral of the first kind. Using equations 3.9–3.10 to model moderate sized finite square networks effectively approximates the results of equation 3.12. For a square network with $\beta = 2$ and only 13 cells total, the percent difference between the computed $w_{r|r}$ for central node r and the value given by equation 3.12 for an infinite network is already < 0.5%.

3.3.6 Psychophysical threshold detection modeling

Psychophysical detection threshold was modeled as described in chapter 2, but expanded to replace the simplified perfect coupling model with the resistive network model described above. Following the treatment of Baylor et al. [13], the probability distribution of response amplitudes in an isolated rod, $p(A)$, was modeled as Poisson distributed photovoltages, overlaid with Gaussian spread representing continuous photoreceptor noise (s.d. σ_0) and noise associated with phototransduction (s.d. σ_1):

$$p(A) = \sum_{k=0}^{\infty} \frac{e^{-m}m^k}{k!} \frac{1}{\sqrt{2\pi\left(\sigma_0^2 + k\sigma_1^2\right)}} \exp\left(-\frac{(A-ka)^2}{2\left(\sigma_0^2 + k\sigma_1^2\right)}\right) \tag{3.13}$$

where m is the average R* / rod for the stimulus delivered. In the dark condition, $m = 0$, equation 3.13 reduces to a Gaussian distribution centered around zero with s.d. σ_0. The parameters $\sigma_0 = 0.4$ mV, $\sigma_1 = 0.4$ mV, $a = 1$ mV were chosen according to the values estimated and used previously in chapter 2.

Equation 3.13 describes the distribution of responses that would occur in an isolated rod, s. If s is coupled to its neighbors, its responses will leak through the resistive network; as the responses travel from node s to node r their amplitudes will be systematically

attenuated:

$$p_{r|s}\left(A \cdot w_{r|s}\right) = p\left(A\right) \tag{3.14}$$

where $p_{r|s}(A)$ is the distribution of voltages obtained in r due to phototransduction in s. The responses in s itself are also attenuated, by a factor $w_{s|s}$, due to the leak of signal through the network.

The total voltage distribution for node r can be calculated by convolving the $p_{r|s}$ for every $s \in B$ together. However, the resulting distributions, p_r, for each node are then no longer statistically independent. Although this issue is easily overcome in the case of linearly summed rod outputs, it becomes problematic once nonlinearities are assumed at the rod output synapse (see below). Determining the voltage distribution for the output of the entire rod network then becomes a problem of determining the distribution of a sum of dependent random variables. Theoretically this can be computed (e.g. [44]), using the joint probability distribution for the $|B|$ random variables. For networks of size $|B|$ greater than a few nodes, however, specifying the $|B|$-dimensional joint distribution with any resolution is impractical even on a powerful computer. Therefore, determining the distributions of summed voltages for entire coupled networks required Monte Carlo simulation.

Voltages for rods within a coupled network were simulated by first generating a phototransduction voltage for each rod (equation 3.13), then linearly transferring the voltages between rods according to the network voltage-voltage transfer ratios, w. The resulting simulated rod voltages were then passed through two nonlinear stages representing the rod output synapse. The first stage was a cutoff nonlinearity that selectively attenuated low-amplitude noise while passing higher-amplitude signal [48]. The shape of the input-output relation for the cutoff stage was modeled as a cumulative Gaussian distribution function whose mean and s.d. were optimized by fitting to Field and Rieke's equation 1 [48]. The mean and s.d. for the cutoff were recalculated for different rods, so that the nonlinearity was optimized for each possible coupling condition. In all cases, the cutoff was assumed

to be optimized for discriminating between a stimulus of intensity $m = 0.001$ R* / rod and the dark condition. This intensity was chosen because 10 R* delivered to the pool of 10^4 rods is the psychophysically reported absolute detection threshold [113].

The second stage of the rod output synapse was a saturating nonlinearity, such that all amplitudes ≥ 2 mV were set back to 2 mV [102, 16]. For full-field flashes at absolute threshold ($m \approx 0.001$) the photon delivery is very sparse and the likelihood of amplitudes ≥ 2 mV in individual rods is very small, so that the effect of the saturating nonlinearity is negligible. However, for more concentrated spots of light delivered to a subregion of the entire detection pool (see results), the saturating nonlinearity can affect detection threshold. Recent evidence suggests that the amplitude at which the rod output synapse saturates is modulable (see discussion), but we assume that both cutoff and saturating nonlinearities are stationary for the illumination regime modeled, i.e. near absolute threshold.

Downstream of coupling and the rod output synapse nonlinearities, signals across a pool of 10^4 rods [155] were summed linearly to model the detection stage. Distributions of summed voltages from independent discrete coupling networks were convolved via frequency space multiplication to arrive at the distribution of summed voltages for the entire detection pool. Psychophysical detection was modeled as a two alternative forced choice test. In this test, a subject is presented with two test epochs, one containing a flash and one without, and must identify which epoch contained the flash. The test was modeled by creating one amplitude distribution for the entire detection pool under the flash condition, $p_F(A)$, and one for the dark, $p_D(A)$. It was assumed that the subject always picks the epoch with the larger amplitude as the flash epoch, so that the subject picks correctly as long as the flash amplitude is in fact the larger. Therefore, percent correct performance, P_C, was

calculated as the probability that an amplitude from $p_F(A)$ will exceed one from $p_D(A)$:

$$P_C = \int_{A=-\infty}^{\infty} p_F(A) \left(\int_{A'=-\infty}^{A} p_D(A')\, dA' \right) dA \tag{3.15}$$

Detection threshold was defined as the value of m where $P_C = 0.73$, as calculated by interpolating between modeled values of m that yielded P_C close to 0.73. The value 0.73 was chosen to match the 73% correct criterion level typically used in two alternative forced choice tests [113].

To account for dark thermal isomerization events, we assumed an effective illumination for the dark condition:

$$m = T_i I_D \tag{3.16}$$

where $T_i = 400$ ms is the integration time of the rod [62], and $I_D = 0.0063$ R* / rod / s is the dark event rate [14].

3.4 Results

3.4.1 Guinea pig rod photoresponses

We recorded from dark adapted guinea pig rods, targeting them based on their smaller inner segment diameter relative to cones [150], and confirming our identification functionally by measuring their spectral sensitivities (fig. 3.1). Responses to 430, 500, 570, and 660 nm wavelength stimuli was tested in 9 guinea pig rods, and relative sensitivity was calculated as the inverse of the intensity evoking a half-saturating response amplitude. The mean log sensitivity points were fit with a standard Baylor nomogram [15], taking into account self-screening with an assumed axial optical density of 0.168 calculated from estimates of transverse optical density [90] and rod dimensions [150]. The best fit nomogram for

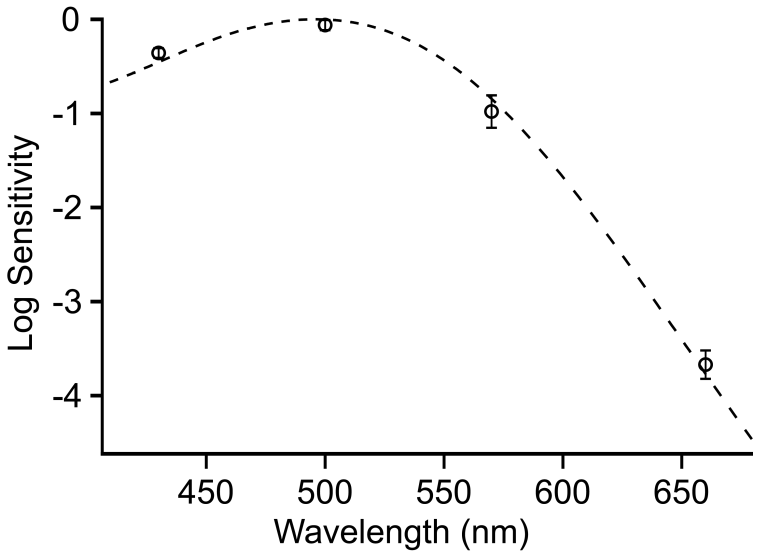

Figure 3.1: Guinea pig rod spectral sensitivity
Mean sensitivity of 9 rods (error bars = s.d.) for 430, 500, 570, and 660 nm wavelength stimuli. The dotted line is the calculated fit with a standard Baylor nomogram [15] through the mean points, peak 496 nm.

the mean sensitivity points peaked at 496 nm, in agreement with previous results from microspectrophotometry [64] as well as estimates derived from recordings in downstream retinal cells [150]. The average single photon response amplitude measured from 12 rods in perforated patch configuration was 0.61 $\pm$ 0.16 mV (mean $\pm$ s.d.).

3.4.2 Gap junctional coupling conductance

To measure gap-junctional coupling conductance, we made paired whole-cell voltage-clamp recordings from neighboring rods. Holding one rod at constant voltage, we measured changes in its membrane current due to a series of brief voltage steps applied to its neighbor (fig. 3.2A). Plotting the change in membrane current in the first rod versus the voltage change applied to its neighbor we find a linear relationship (fig. 3.2B), reflecting the ohmic behavior of the gap junction for brief steps. The slope of the current-voltage relationship gives the junctional conductance. Of 22 paired rod recordings, 11 showed

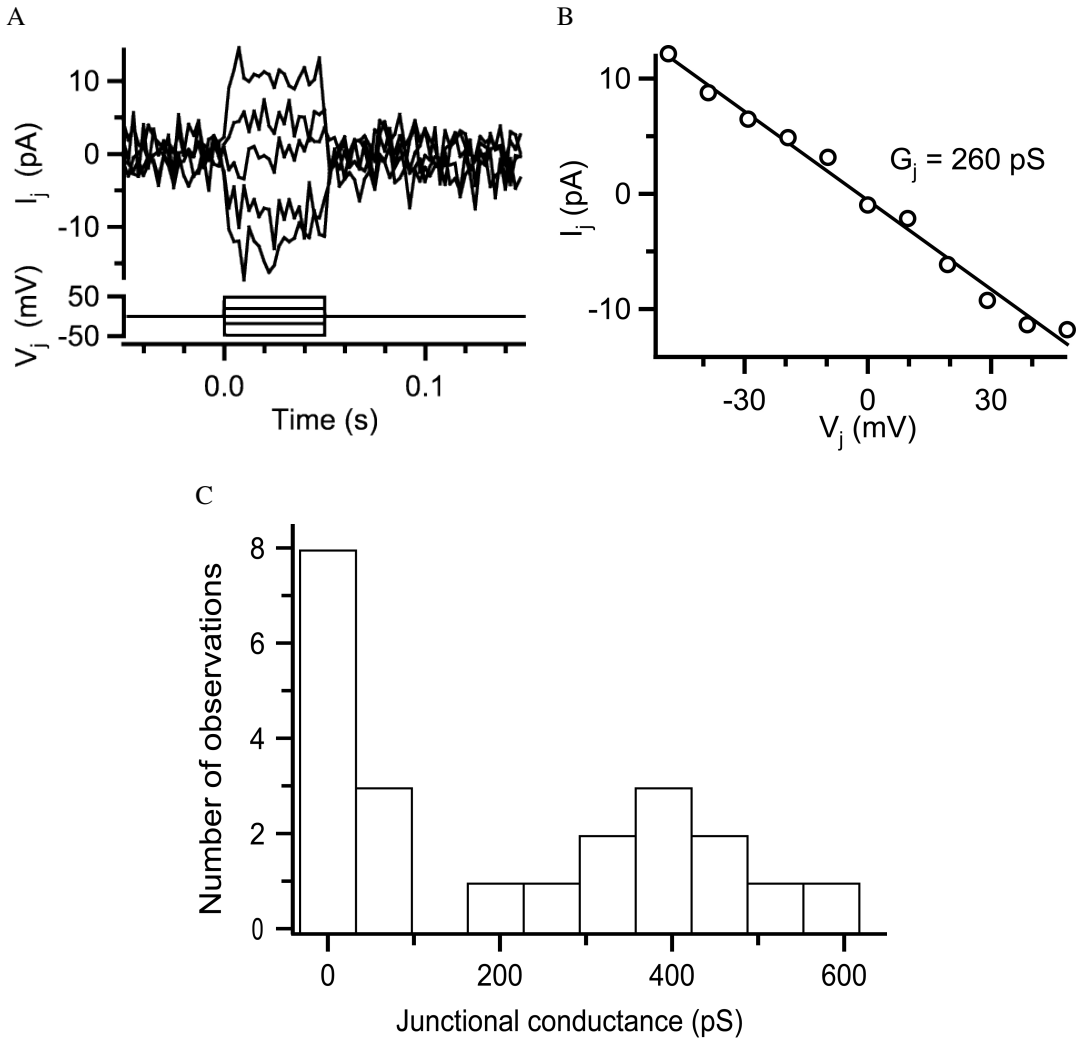

Figure 3.2: Paired rod gap-junctional conductance

A: Change in junctional current (I_j) in one voltage clamped rod in response to voltage steps (V_j) applied to its neighbor. Bandwidth, DC–10 Hz. B: The average I_j from A, plotted (○) against V_j. The solid line is a linear fit whose slope gives the conductance of the junction. C: Junctional conductances measured in 22 rod pairs.

negligible junctional conductance (< 100 pS). The remaining 11 rod pairs had junctional conductances ranging from 195–580 pS, and averaging 386 ± 112 pS (mean ± s.d., fig. 3.2C).

Junctional conductances were symmetric (< 10% difference in conductance when stepping rod 1 compared to stepping rod 2), as expected for junctions between homologous cell types. Unfortunately dual rod recordings were not generally stable enough for more extensive analysis of junctional properties such as pharmacological modulation. One property we considered was the voltage dependent gating of the junction. While instantaneous currents through gap junctions are ohmic, longer voltage steps can evoke a slow gating closed of a portion of the junctional conductance [119]. Thus, the conductance at the end of a long voltage step is typically less than the conductance at the beginning of the step (figures 3.3A–3.3B). This effect is also voltage dependent, with larger voltage steps usually evoking greater reductions in conductance. Voltage gating effects can be summarized by plotting the conductance at steady-state, normalized to the initial, maximal conductance, as a function of voltage step amplitude (figure 3.3C) and fitting the data to a Boltzmann relation [119].

Interestingly, connexin 35/36, the junctional channel protein localized to rods in amphibians [153] is one of the least voltage dependent of the connexin family. Expressed in mammalian cell lines, Cx36 was found to have a half-maximal reduction in conductance at transjunctional voltages of 75 mV [121], compared to 15 mV for the connexins in amphibian blastomere junctions [119]. To test the voltage gating of putative Cx35/36 junctions in an intact vertebrate system, we recorded from pairs of salamander rods and applied long voltage steps to determine steady-state conductances (fig. 3.3A). The Boltzmann plot (fig. 3.3C red circles) confirms a low voltage dependence with half-maximal reduction at 72 mV. In contrast, we found that for a guinea pig rod junction, half-maximal reduction in conductance occurred at 21 mV (fig. 3.3B, fig. 3.3C black circles), consistent with the

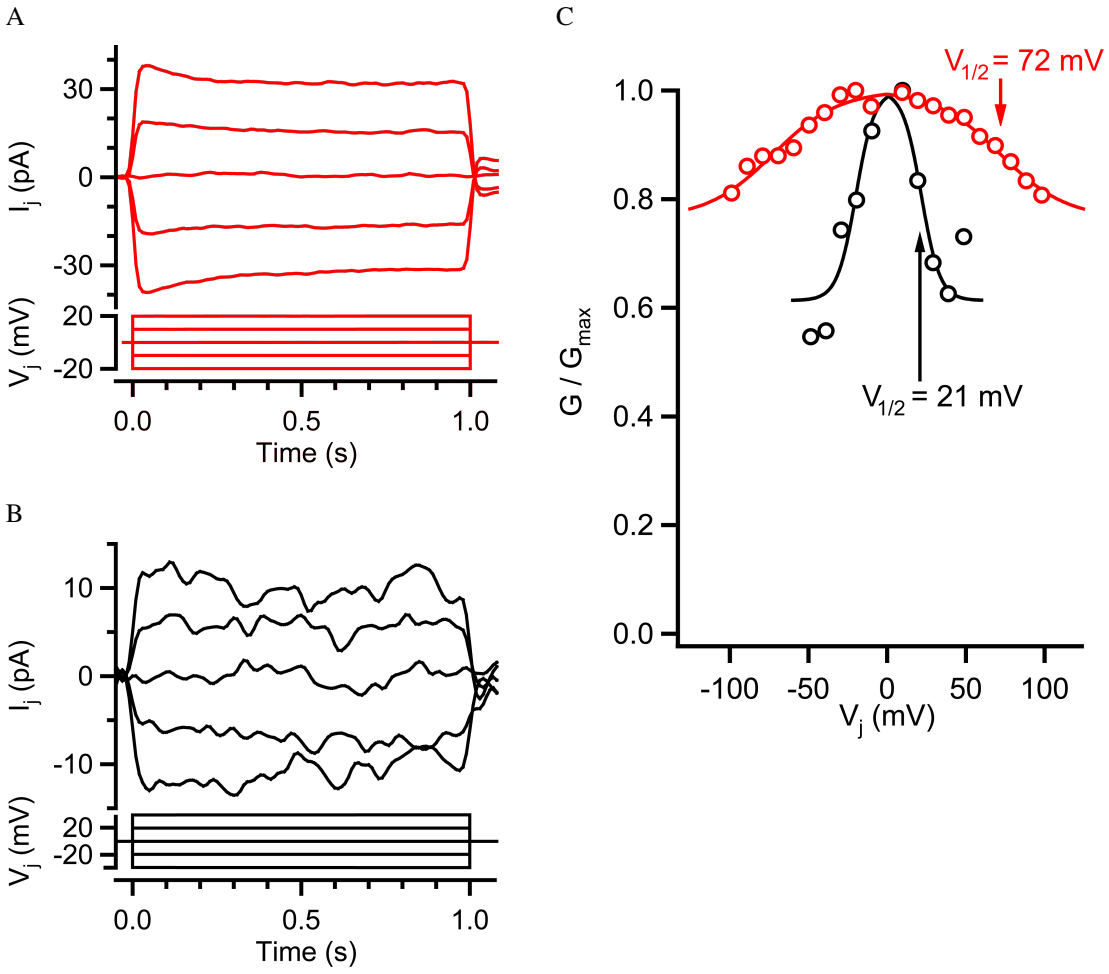

Figure 3.3: Voltage gating of rod junctions

A: Transjunctional currents (I_j) evoked by transjunctional voltage steps (V_j) 1 second in length, in paired salamander rods. The initial currents reflect roughly ohmic conductance, but the currents relax over the course of the step, approaching a reduced steady-state current that reflects a gating closed of some of the junctional conductance. B: I_j and V_j for paired guinea pig rods. C: Data from A (○, red) and B (○, black), plotted as steady-state conductance normalized to initial, maximal conductance as a function of V_j. The solid lines are Boltzmann fits [119]. The low voltage dependence of the salamander junction, with a half-maximal reduction in conductance ($V_{1/2}$) only at high V_j, is characteristic of the Cx35/36 protein putatively constituting those junctions [121, 153]. The guinea pig rod junction, in contrast, is much more strongly voltage dependent than is typical for Cx35/36.

anatomical evidence that mammalian rod junctions are not composed of Cx36 [74, 30].

3.4.3 Tracer coupling

We also assessed the spatial extent of coupling by including the tracer Neurobiotin in one recording electrode and observing any tracer spread from the recorded rod into neighbors. Out of 26 rods thus tracer filled, 4 (15%) showed no tracer coupling (e.g. fig. 3.4A) while the remaining 85% were coupled to one or more neighbors (e.g. fig. 3.4B). The total number of rods in a tracer coupled pool ranged from 1–15, averaging 5.2 $\pm$ 4.2 (mean $\pm$ s.d., fig. 3.4C).

In general, we could not discern specifically where tracer coupled rods contacted each other; many pairs made multiple apparent contacts. Sites of apparent contact included spherules, cell bodies, and passing axons, as well as at the inner segments. Consistent with our previous finding in primate, we rarely observed tracer flow from guinea pig rods into cones. Out of 29 rods filled, only 3 showed tracer coupling to cones. As we were primarily interested in tracer flow directly between rods, we excluded these three cases from further analysis.

3.4.4 Variance analysis

By averaging the membrane voltages among neighboring rods, coupling reduces the variability of photoresponses [46, 112, 62]. We studied this effect in guinea pig by recording rod voltage responses to brief, dim flashes ($\sim$ 0.5–4 R* / rod / flash) in perforated patch mode. For an isolated rod, the dim flash responses exhibited Poisson variability due to quantal variation in the number of photons caught per flash (fig. 3.5A). Coupling averages out this quantal variability, resulting in more uniform responses in a putatively coupled rod (fig. 3.5B). However, coupling is not expected to alter the mean single photon response

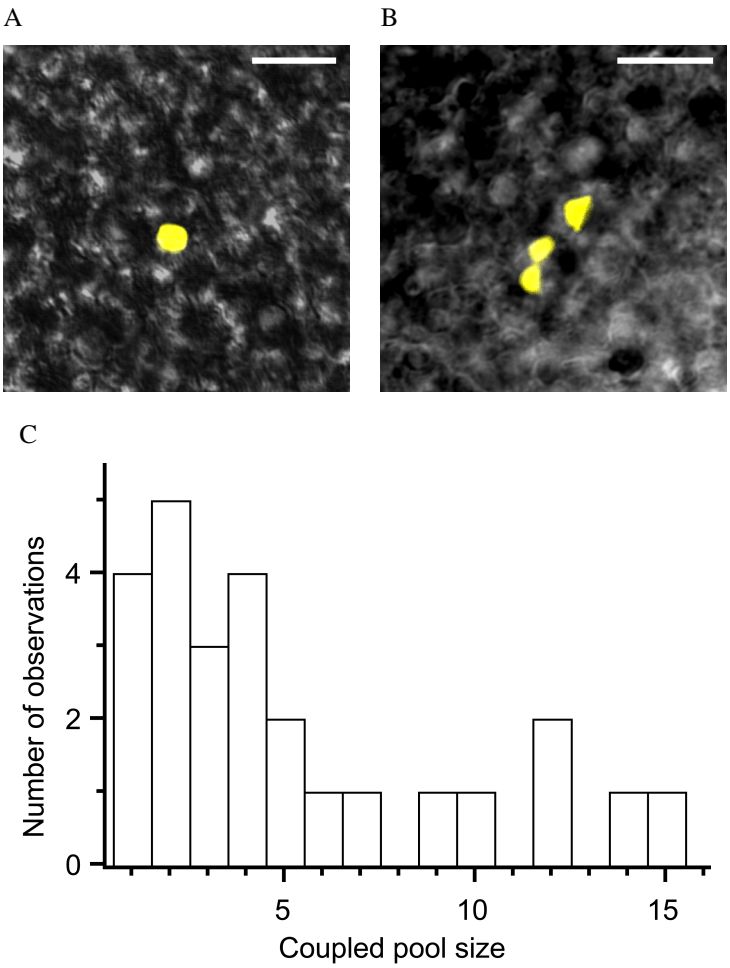

Figure 3.4: Rod tracer coupling

A: Example of a filled rod with no tracer coupling to neighbors. B: Three neighboring tracer coupled rods, imaged at the inner segment level. Scale bars: A–B, 10 μm. C: Tracer coupled pool sizes in 26 filled rods.

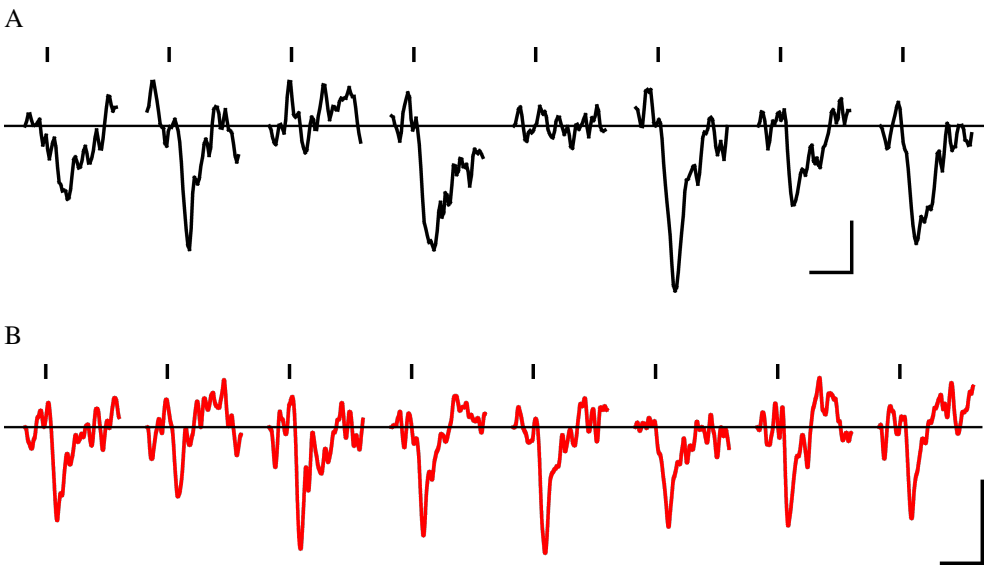

Figure 3.5: Coupling reduces the variability of dim flash responses
A: Rod voltage responses to a series of dim flashes (~ 1 R* / rod / flash). Tick marks indicate flash times. Bandwidth, DC–5 Hz. Scale bars, 0.5 mV, 500 ms. B: Another rod, similar conditions as in A, but in this rod the quantal variability of the flashes has been averaged out due to putative coupling. Bandwidth, DC–10 Hz.

amplitude over many iterations (equation 3.1).

To further analyze the effect of coupling on response variability, we calculated the ensemble variance and mean response over 50–100 flashes at several intensities (figs. 3.6A–3.6B). We quantified the degree of coupling (N_{eff}) by comparing the peak of the mean response to the peak of the ensemble variance, both divided by the flash intensity (equation 3.3). Graphically, this is equivalent to plotting the peak mean and variance versus the flash intensity and comparing the slopes (figs. 3.6C–3.6D).

For an isolated rod ($N_{\text{eff}} = 1$), the variance versus intensity should equal the square of the mean versus intensity, as indicated by the dashed line in fig. 3.6D. The putatively isolated rod from fig. 3.5A, matches this prediction well, while the rod from fig. 3.5B shows reduced variance, which we interpret as being due to the averaging of voltages within a network of coupled rods. Based on this analysis, we can determine the magnitude of the averaging effect for the recorded rod, but we cannot determine the size of the rod network

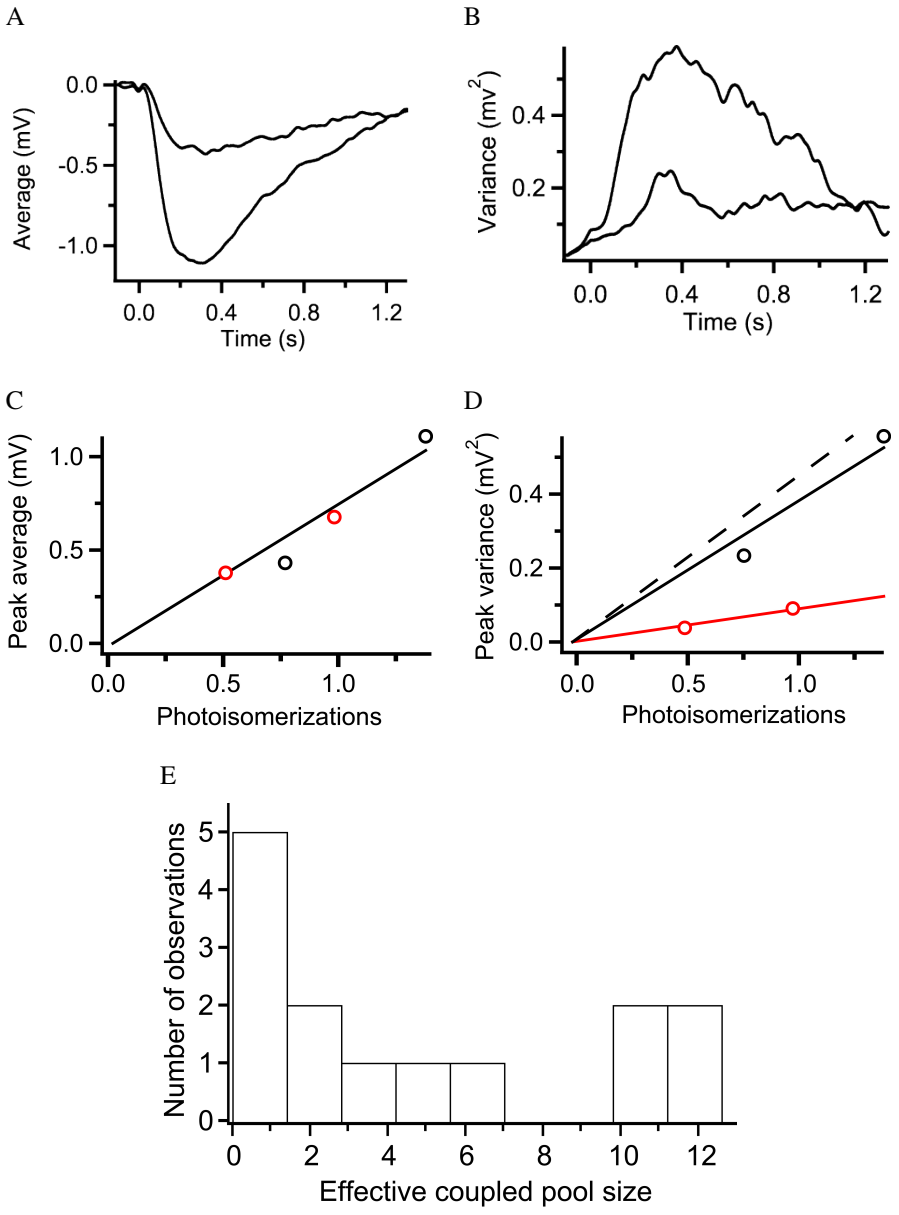

Figure 3.6: Analysis of mean response and ensemble variance

A: Mean voltage response to 50–100 flashes at two intensities. Same rod as figure 3.5A. Bandwidth, DC–10 Hz. B: The ensemble variance from the same set of flashes as A. C: The peaks of the mean responses plotted (○) versus flash intensity. Peaks from mean responses in A are in black. In red are the peaks from the mean responses (not shown) for the coupled rod in figure 3.5B. D: The peaks of the ensemble variances plotted (○) versus flash intensity. Again, peaks from B are in black, and in red are peaks from ensemble variances (not shown) for the rod in figure 3.5B. The dashed line is the prediction for an uncoupled rod based on the mean responses in C.

responsible for the averaging without making assumptions about the connectivity of the network and the junctional conductance (see below). Therefore, we use N_{eff} as a simplified quantification of the degree of coupling: it equals the number of perfectly coupled rods (i.e. rods coupled with zero junctional resistance) that would yield a reduction in variance equivalent to the effect we observed. We analyzed response variance in 14 rods and found N_{eff} ranging from 0.7–11.6, with an average of 4.8 ± 4.5 (fig. 3.6E).

3.4.5 Network model

Having assessed coupling in the rod network via the three methods described above, we constructed a resistive circuit model of the rod network to consolidate the three data sets and to allow further psychophysical modeling. We began by assuming a hexagonal packing of rods across the retina, reflecting the roughly hexagonal packing of the rod inner and outer segment layers (fig. 3.7A). For the purposes of modeling, we ignored rod-cone coupling under the assumption that it would contribute negligibly to rod network behavior (see discussion). As described in the methods, we modeled rods as nodes with membrane resistances to ground and current sources representing phototransduction. We connected some of the rods with lateral junctional resistances to represent coupling (fig. 3.7B). The electrical behavior of such a network depends on three parameters: the connectivity of the network, the membrane resistance, R_m, and the junctional resistance, R_j (equation 3.6).

For R_m, we chose a value of 1.5 GΩ based on input resistances measured in our whole cell recordings. The input resistance measured in a coupled rod would be lower than the true individual rod membrane resistance due to leak through coupled neighbors, so we based R_m on the higher end of our measured input resistances. For comparison, previously reported R_m measured in dark adapted primate rods averaged 1.2 GΩ [108]. Previously reported R_m for guinea pig rods under bright light conditions averaged 2.5 GΩ [38].

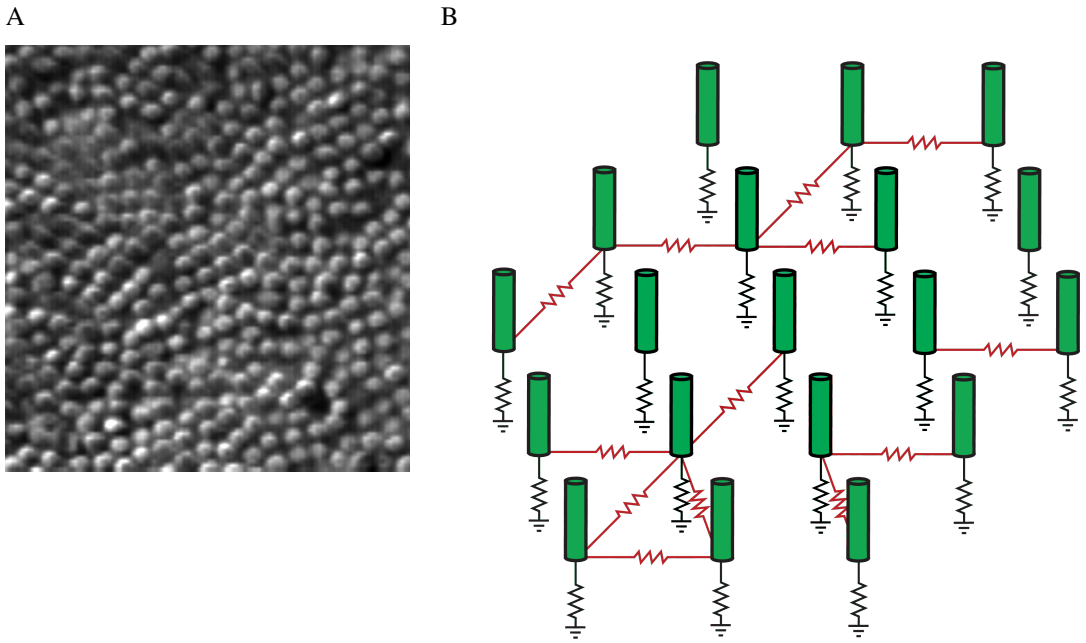

Figure 3.7: Hexagonal network modeling

A: Differential interference contrast photomicrograph illustrating the roughly hexagonal packing of the guinea pig rod mosaic. B: Schematic of the rod network model: hexagonally packed rods subdivided into several coupled networks with different connectivities. A few of the rods are uncoupled. The membrane resistance for each rod (R_m) is shown in black. The junctional resistance (R_j) in red connects rods into separate networks.

We based the value for R_j on our dual electrode results (fig. 3.2), where we found an average junctional conductance of 386 pS. We take this value as an upper limit because the junctional conductance measured in paired rod recordings may not be entirely due to direct coupling; if the rods in the pair are mutually coupled to additional neighbors, some of the conductance measured between the pair will be due to indirect current flow through these additional paths. However, circuit analysis shows for a hexagonal network that even in a highly coupled case the majority of the conductance measured between a rod pair is due to direct coupling (see supplemental material). Therefore in our modeling we used the somewhat conservative value of 3 GΩ for R_j, equivalent to a conductance of 333 pS.

In our circuit analysis of the resistive network, we found that for a given network connectivity, the signal averaging behavior of the network depends only on the ratio $\beta = {}^{R_j}/_{R_m}$ (equations 3.9–3.10), which for the resistances chosen above gives $\beta = 2$. Knowing this value, we can calculate signal transfer ratios, and thus the predicted N_{eff}, for any given network connectivity (equations 3.7–3.11).

Since gap-junctional coupling requires close membrane apposition, and rods are not thought to send processes out to form distant contacts, we assumed that hexagonal packing limits rod network connectivity to a maximum of each rod contacting at most six neighbors. To determine the signal averaging effect expected for this maximal connectivity, we computed the signal transfer for an infinite rod network with full hexagonal connectivity and $\beta = 2$, yielding a predicted $N_{\text{eff}} = 9.1$. This value agrees well with the maximal N_{eff} we measured in our variance analysis experiments. However, given the limited extent of observed tracer coupling ($\leq$ 15 rods coupled), we believe smaller, discrete networks to be more physiological. In fact, for a hexagonally connected network with $\beta = 2$, the great majority of signal transfer comes from just the first two layers of surrounding rods, so that modeling only two surrounding layers (19 rods total) already yields, for the central rod, $N_{\text{eff}} = 8.2$. Figure 3.8 shows the N_{eff} calculated for hexagonal networks with different

A

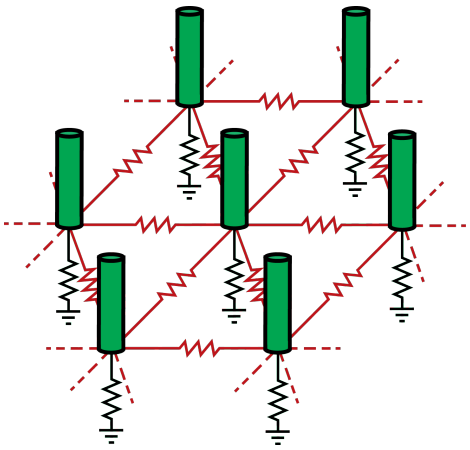

B

# of surrounding layers	# of cells	N_{eff}
0	1	1
1	7	5.4
2	19	8.239
3	37	8.943
4	61	9.070
5	91	9.091
6	127	9.094
7	169	9.095
∞	∞	9.095

Figure 3.8: Networks with full hexagonal connectivity
A: A fully connected hexagonal network: every rod coupled to all 6 immediate neighbors. One surrounding layer is shown, with additional layers implied. B: N_{eff} calculated for fully connected hexagonal networks with $\beta = 2$ and different numbers of surrounding layers.

numbers of surrounding layers.

Overall, the modeling indicates that for a network with $\beta = 2$, as derived from our dual-electrode measurements, the maximal signal averaging observed in our variance analysis experiments is consistent with hexagonal packing, and roughly consistent with the maximal number of rods observed to be tracer coupled. We conclude that our observed values of N_{eff}, from ~1–10, can be explained as resulting from small, discrete networks of rods coupled with junctional resistance 3 GΩ, with the total number of rods in a coupling pool ranging from single isolated rods to about 20, and with each rod connected to between 1 and 6 neighbors.

3.4.6 Primate network model

In chapter 2, we modeled the effect of rod coupling on human psychophysical detection based on the signal averaging (i.e. measurements of N_{eff}) observed in primate rod recordings. Because we were not able to measure R_j directly for primate rods, we based the

psychophysical modeling on the simplifying assumption of perfect coupling, i.e. $R_j = 0$. However, it is known that the perfect coupling assumption tends to underestimate the signal:noise ratio within the rod network [126]. With the aim of improving the psychophysical model, we considered whether an R_j like what we measured in guinea pig could be consistent with the tracer coupling and signal averaging found in primate.

Primate rods have average $R_m = 1.2$ GΩ [108]. Assuming $R_j = 3$ GΩ as in guinea pig, we thus determined $\beta = 2.5$. In our primate study, we found N_{eff} ranging from 1–5.9, and tracer pool sizes ranging from 1–10 rods. Using the network model as described above, we find that for a hexagonally connected network of 10 rods with $\beta = 2.5$, the predicted $N_{\text{eff}} = 5.6$. Thus, in primate as well as in guinea pig, given $R_j = 3$ GΩ, and assuming that each rod connects to between one and six neighbors, we can successfully use the tracer coupling data to account for the observed range of signal averaging.

3.4.7 Psychophysical model

We extended the model of psychophysical detection from chapter 2 by including the junctional resistance $R_j = 3$ GΩ, based on our guinea pig dual electrode measurements and the indication from network modeling that this resistance is also consistent with coupling measurements in primate. Given a particular intensity and spatial pattern of rod illumination, the psychophysical model computes 1) Poisson statistics of photon catch and resulting phototransduction in individual rods, 2) the spread of voltage from phototransducing rods into neighbors due to a given coupling connectivity, 3) the output from the rods onto rod-bipolar cells, accounting for nonlinearities at the rod output synapse, and 4) psychophysical detection performance, assuming that detection depends on comparing the linearly summed output of many rod bipolar cells for a flash condition to the output of the same pool in the dark (see methods).

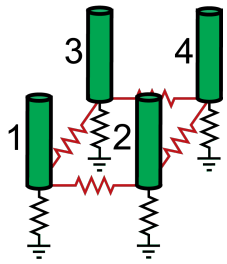

$w_{1\|1}$	$w_{1\|2}$	$w_{1\|3}$	$w_{1\|4}$
0.624	0.154	0.154	0.068

Figure 3.9: The four rod cycle network

Schematic of the four rod cycle network used in psychophysical modeling. The voltage transfer ratios relative to rod 1 are listed, thus of the phototransduction voltage generated in outer segment 1, only 62.4% remains in rod 1, while the rest leaks into the other rods. 15.4% of phototransduction voltage generated in outer segment 1 leaks into rod 2, and vice versa. Etc.

In primate rods, we found an average N_{eff} of 2.3. To model this under the perfect coupling assumption, we would assume networks of exactly two rods coupled together with zero resistance, corresponding to voltage transfer ratios: $w_{1|1} = w_{1|2} = w_{2|1} = w_{2|2} = 0.5$. To replace the perfect coupling assumption with the more physiological junctional resistance of 3 GΩ, we postulated an arrangement of four rods linked in a cycle (fig. 3.9). With $\beta = 2.5$, this network yields $N_{\text{eff}} = 2.3$, precisely the average value found experimentally. The four-rod network is also a better match for the primate tracer coupling data, where we found an average coupled pool size of 3.4 rods.

Consistent with our previous modeling, we found here that a detection pool of 10,000 uncoupled rods yields a detection threshold of 9.7 R* delivered to the pool, very close to the psychophysically measured threshold of about 10 R* [113]. Under the perfect coupling assumption, the detection pool is divided into 5000 pairs of perfectly coupled rods, resulting in an increase in detection threshold to 15.2 R* (44% difference). However, assuming a detection pool divided into 2500 discrete four-rod networks with realistic junctional resistance (fig. 3.9), the detection threshold is calculated to be 11.0 R*, only a 13% difference

from the uncoupled case. Thus, replacing the perfect coupling assumption with a more physiological junctional resistance mitigates most of coupling's detrimental effect on detection.

Furthermore, replacing perfect coupling with resistive coupling enhances the benefits for detection of small spots of light (fig. 3.10). As illumination area shrinks, detection threshold improves for all three modeled conditions, due to improved performance of the noise filtering cutoff nonlinearity at the rod output synapse (see methods and [48]). However, performance improves more sharply for the coupled conditions than the uncoupled one, reflecting the additional advantage of coupling for circumventing the competing effect of rod output synapse saturation.

As expected, the improvement with shrinking spots is most pronounced for the perfectly coupled network. However, resistive coupling performs better than perfect coupling for every spot size, and surpasses the performance of the uncoupled model for spots smaller than 0.11 retinal degrees diameter, while perfect coupling only surpasses the uncoupled model for spots smaller than 0.06 degrees. At the smallest spot sizes modeled, the perfect coupling model yields a detection threshold of 5.1 R*, or a 30% difference improvement over the uncoupled case. The resitively coupled model performs better still, with a threshold of 3.9 R*.

3.5 Discussion

3.5.1 Strength of rod coupling

The results presented here are the first report of directly measured rod junctional conductance in mammals. Furthermore, network modeling indicated that the measured conductance is consistent not only with other coupling measures in guinea pig, but also with

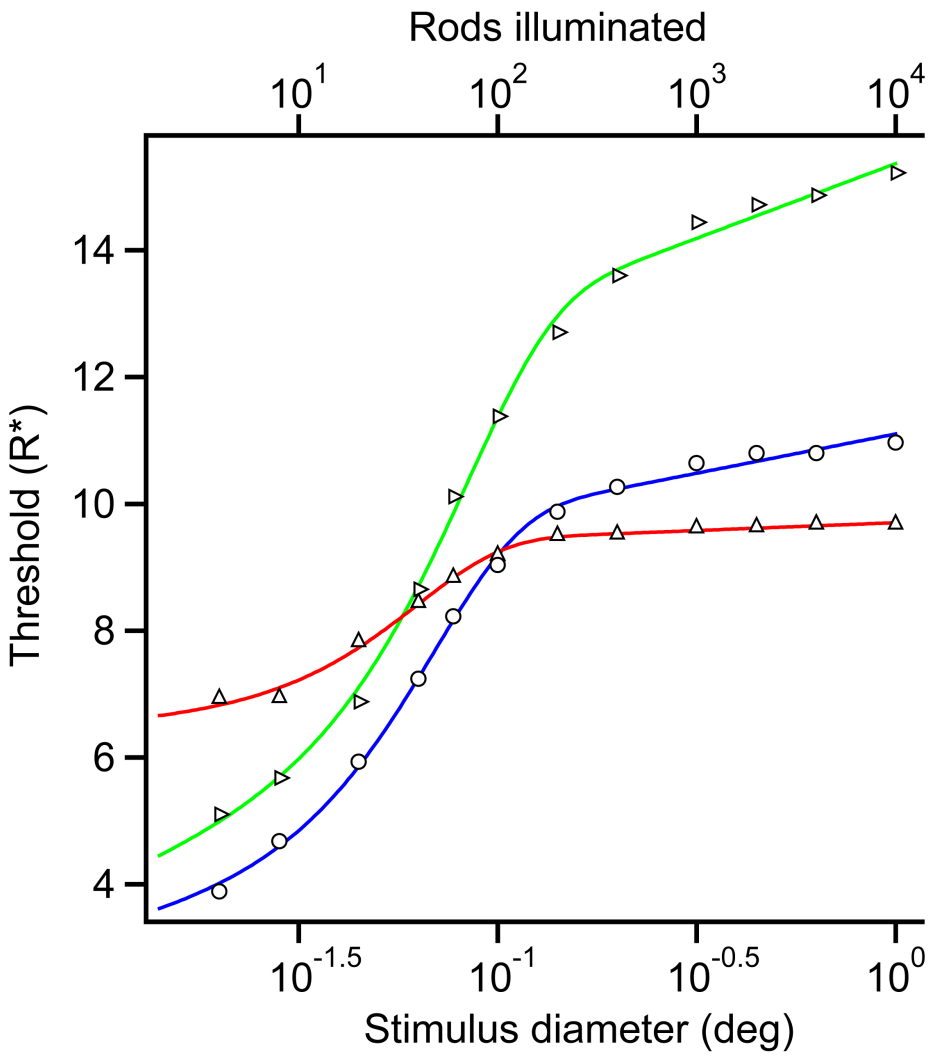

Figure 3.10: Coupling effects on visual detection thresholds

Threshold illumination (in photoisomerizations within the illuminated pool) necessary to reach 73% correct detection performance, plotted versus size of the illuminated pool. Uncoupled model: △, red. Perfectly coupled model: ▷, green. Resistively coupled four rod cycle model: ○, blue. When the entire summation pool is lit (1 retinal degree diameter stimulus or 10^4 rods illuminated), the uncoupled model performs best. With only a subregion of the total pool lit, performance improves. At about 0.11 degrees diameter (120 rods illuminated) the resistively coupled model surpasses the uncoupled performance. Solid lines are empirical smooth fit functions composed of a baseline offset, an exponential, and a log-linear element.

coupling measures from primate (chapter 2), suggesting the possibility that a conductance on this order could be a general feature of mammalian retinas. As noted above, and further discussed in the supplemental material, it is possible that some fraction of the conductance we measured between neighboring rods was actually due to indirect current flow through additional coupled neighbors. However, for a network whose maximum connectivity is hexagonal, even in the worst case the majority of the measured conductance is still direct. In fact, we only expect the network to approach full hexagonal connectivity in the most highly coupled cases, while in general there would be significantly fewer indirect paths between the recorded rods.

It is also worth considering whether some of the apparent junctional resistance we measured could derive not from the gap junction channel itself, but from the cellular structures in between the recording site and the junction. We recorded from the rod inner segment, which connects to the spherule via a narrow axon process. Assuming that junctions occur at the spherule (although see below), we would like to know how much signal is lost between the inner segment, where we recorded, and the junction. In a cable analysis based on the anatomical dimensions of the rod, Smith et al. [116] found that the voltage loss between the inner segment and the spherule is only about 10%. Therefore we conclude that, irrespective of where the junctions reside, our measurements are not seriously impacted by intervening cellular architecture.

The roughly 350 pS conductance between guinea pig rods is towards the low end of reported gap junction conductances. For comparison, guinea pig cardiac cells, whose strong coupling is critical for synchronization of heart rhythms, can have junctional conductances approaching 4 μS [66], more than 4 orders of magnitude greater than reported here. With $\beta \approx 0.14$, the cardiac network behaves very much like a perfectly coupled syncytium. Even in retina, some junctions, such as between fish horizontal cells, have conductances reaching 10–100 nS [94, 78], 2 to 3 orders of magnitude greater than found here. However, as

System	Average coupling conductance (pS)	Reference
Guinea pig rods	386	here
Primate cones	631	[63]
Ground squirrel cones	320	[41]
Ground squirrel cones	217	[76]
Salamander rods	500	[154]

Table 3.1: Photoreceptor network junctional conductances

shown by our circuit analysis, the relatively high membrane resistance of rods means that significant signal transfer occurs even for coupling of only 350 pS. Indeed, the psychophysical modeling indicates that stronger coupling would actually be undesirable for purposes of absolute detection. The bias towards weaker coupling seems to be a general feature of photoreceptor networks (table 3.1).

The relatively weak coupling of mammalian rods is also roughly consistent with their junctional anatomy. In EM of rod junctions, at both the synaptic and inner segment levels, the junctional areas are some of the smallest reported, about 0.01 μm^2 [132, 95, 27, 130]. We do not know other parameters of the rod junction, but if we assume channel density of 1000–5000 μm^{-2}, open probability of 0.5–0.8, and single channel conductance of 15–100 pS [88], then we would expect junctional conductances ranging from 75–4000 pS. The open probability, single channel conductance, and other properties of gap junction channels depend on the molecular subunits constituting the junctions. Vertebrate connexin gap junction channel proteins are a diverse family, with about 20 different connexin subtypes identified so far. Unfortunately, no connexin has yet been associated with mammalian rods. In cold-blooded vertebrates the rod-rod junction appears to include Cx35/36 [153]. Cx35/36 is also localized to contacts between rods and cones in mammal, but it appears to reside only on the cone side of these junctions [74, 82, 35, 30].

3.5.2 Rod network connectivity

We concluded from our network modeling that the values calculated for N_{eff} in both guinea pig and primate are generally consistent with the observed tracer coupled pool sizes, given the junctional conductance measured in guinea pig. However, to account for the highest N_{eff} values, we had to assume that the network was coupled with full hexagonal connectivity, i.e. that every rod in the network, excepting those at the outer border, contacted all 6 immediate neighbors. There is some question as to whether this degree of connectivity is realistic. In EM serial reconstructions from mouse retina, Tsukamoto et al. [130] traced rod junctions within the synaptic layer. This revealed discrete rod networks of from 1–11 coupled rods with an average pool size of 3, somewhat less than our result here of tracer coupled pools ranging from 1–15 rods with average 5.2. More strikingly, the networks found in mouse EM were connected much more sparsely than would be required for full hexagonal connectivity.

Mouse and guinea pig rod networks may simply have different connectivities. However, considering other explanations for the inconsistency brings up several interesting possibilities. Most straightforward, Tsukamoto et al. could have missed some junctions in their reconstruction of the synaptic layer. As noted above, the rod-rod junctional area is only about 0.01 μm^2, and as Smith et al. [116] remark of rod-cone junctions in cat (also about 0.01 μm^2), "gap junctions of this size could easily be missed," and therefore "present counts must be considered a minimum estimate". More intriguing is the possibility that rods are coupled not only in the synaptic region reconstructed by Tsukamoto et al., but also more distally, at their inner segments. In fact, junctions are found at the inner segment level in cold-blooded vertebrates [34, 52, 153], and in macaques [27] and humans [132, 27]. Unfortunately, we were not able to definitively localize the sites of rod contact that mediated the guinea pig tracer coupling we observed. Because the gap junction proteins mediating

mammalian rod coupling have not been identified, antibody studies also have not much clarified this issue, although it does seem suggestive that the mammalian cone gap junction protein Cx36 forms puncta at the inner segment level in ground squirrel, a rodent whose cone mosaic is dense enough for cones to contact each other at that level [30]. Recently, the pannexin family of proteins, usually thought of as an invertebrate gap junction family [9], have also been found in the mammalian retina [96, 43]. Intriguingly, one study [96] has localized Panx1 to the "outer border of the outer nuclear layer", in other words: essentially at the base of the inner segments, precisely where primate rod gap junctions were found [132, 27]. Additional EM and histochemical scrutiny at the inner segment level of mammalian retina seems desirable.

We also considered whether we could have overestimated rod connectivity. In our modeling we assumed that the contribution of the rod-cone coupling pathway to the signal averaging of the rod network is negligible. If rods did influence each other significantly via intervening cones, this would increase the measured N_{eff} and could cause us to overestimate rod connectivity. Although we do not have complete data on rod-cone coupling, the available data lead us to reject this possibility. From a purely theoretical perspective, it has been argued [116] that rod-cone coupling should be maximal under mesopic conditions, and minimal under complete dark adaptation. There does seem to be some indirect physiological support for this idea ([149, 70], reviewed in [135], but see [97]). More significantly, our own recordings from dark adapted primate and guinea pig retina confirm that rod-cone coupling is weak. In primate (chapter 2), we recorded rod single photon responses whose average peak amplitude was 0.86 mV. Due to rod-cone coupling, we could also record rod signals from cones. However, the average rod-derived single photon response measured in the cone had a peak amplitude of only 0.11 mV, almost an order of magnitude smaller than in the rod itself. Similar experiments in blue cones [141] have yielded rod in cone amplitudes averaging 0.1 mV (unpublished). Similarly, in guinea pig the average rod sin-

gle photon response amplitude was 0.61 mV, while in two guinea pig cones the rod signal was only 0.06 mV. GnuCAP network simulation confirmed that with rod signals already attenuated by an order of magnitude upon reaching the cones, any signaling from rod to rod via the cone would be negligible.

3.5.3 Psychophysical significance of coupling

We modeled the effects of coupling from an electrophysiological and psychophysical perspective to address how coupling could affect the performance of retinal circuits and thus ultimately affect visual performance. It remains a possibility that mammalian rod coupling serves other non-electrical purposes, such as conduction of metabolites or intercellular adhesion, or that it plays some role in visual detection under brighter conditions than considered here. From this perspective, the most important finding of the present study would be that, for the junctional conductances measured, modeling indicates at worst only modest detriments to visual performance at absolute threshold due to coupling. The proximal effect of coupling is to average voltages in neighboring rods before the rod output synapse can selectively filter out noise, which increases threshold for full-field stimuli by about 10%.

However, our modeling further suggests that rod coupling can serve to circumvent the saturation of the rod output synapse, thus proving beneficial for detection of small, concentrated spot stimuli. For the conditions we modeled, 73% detection at absolute threshold, coupling was beneficial for spots smaller than 0.11 retinal degrees diameter. Estimates of the optical quality of the human preretinal visual apparatus indicate that even for a point source stimulus, the retinal image has a half maximal diameter of 0.03–0.08 retinal degrees (see supplemental material). A cursory conclusion would therefore be that coupling is only slightly beneficial even for point light sources. However, we should further consider the effect of coupling for other detection paradigms.

We modeled 73% detection accuracy because this is a standard detection threshold used in psychophysical experiments. However, we expect that detection at higher levels of accuracy would also be behaviorally relevant. If detection threshold is set to 90% accuracy, the threshold stimulus for large spots increases from 11.0 R* to 24.7 R*. With this brighter stimulus, the relative benefit of coupling occurs at larger spot sizes, starting at about 0.15 degrees diameter. An even more general extension of the model would consider the effects of coupling on increment thresholds for detection of a stimulus against an ambient background illumination as would happen, for example, on a moonlit night with bright skyshine. With an ambient background, the rods could be imagined to sit at a resting potential closer to the saturation point of the output synapse, so that the benefits of coupling for circumventing saturation would arise for even larger spot sizes. However, in considering conditions including background illumination we must then be concerned with the possibility of dynamic modulation of the visual circuitry.

At the rod output synapse, the parameters for both the noise filtering cutoff nonlinearity and output saturation could be dynamically modulated to optimize for different ambient light conditions. In fact, the history of measurements of the noise filtering cutoff [48, 103] and the saturation point [102, 48, 16, 2] show considerable spread, suggesting that these processes can indeed be modulated, although no mechanism for modulation has yet been determined. In our modeling, we used static parameters under the assumption that at a given ambient light level (in our case, near absolute darkness) the parameters would not change. This reflects the idea that behaviorally the visual system must be able to detect large and small stimuli simultaneously at a given ambient illumination, so that we do not consider instantaneous optimization for every possible stimulus realistic. However, we do not expect that these parameters necessarily remain static under different ambient light levels.

Modulation of coupling itself is also a possible complication. In general, macroscopic

gap-junctional conductances are known to be modulable, either through changes in single channel conductance, channel open probability, or the number of channels at the junction. Modulation of rod-cone coupling in response to changes in ambient illumination has been documented in cold-blooded vertebrates [149, 144, 97], with some recent evidence that this also occurs in mammals [97]. However, in physiological studies of homologous cone-cone and rod-rod networks, modulation has been looked for but no effects have yet been reported [8, 41, 76]. In one study, dopaminergic drugs were found to selectively modulate rod-cone coupling without appearing to affect rod-rod coupling [70]. As with the rod output synapse parameters, coupling conductance in our modeling was constant, under the assumption that, even if modulation of rod coupling occurs, it would not occur at a constant low level of ambient background illumination.

According to our model, rod coupling leads to a system whose absolute performance is better for small spots than for large ones. In figure 3.10, we show that detection threshold decreases steadily with shrinking spot sizes in the coupled case, while in the uncoupled case the threshold stays much more constant. Psychophysical studies of spatial summation suggest that both conditions may exist in the same retina, but at different eccentricities. The classic result on spatial summation is that there is a maximal spot size past which added light no longer adds linearly into the detection threshold [111]. This reflects the total area of summation into the visual detection stage, i.e. the ~10,000 rod detection pool. More recent results [155] indicate that at different retinal eccentricities, summation within the detection pool is either fairly flat for different spot sizes (as predicted by our modeling for uncoupled rods) or detection threshold continues to decrease for smaller spots (as predicted for coupled rod networks). Unfortunately, psychophysical experiments have not produced many clear data specifically at the smallest spot sizes considered here, where the differences between the uncoupled and coupled predictions are most pronounced.

The above discussion suggests several important areas for future attention: 1) continued

search for the protein underlying mammalian rod junctions including consideration of the recently discovered pannexin gene family, 2) EM investigation of possible mammalian rod inner segment junctions 3) investigation of possible modulation of the rod output synapse behavior, 4) further investigation of adaptational or circadian modulation of photoreceptor coupling and 5) consideration of possible variations in coupling over different topographical areas of the retina. The current results yield new insights into the strength of mammalian rod coupling, the electrical behavior of the coupled rod network, the interaction between coupling and downstream synaptic nonlinearities, and the effects of coupling on visual detection near absolute threshold. The apparent trade-off between detection of full-field stimuli versus small spots suggests one functional reason for rod coupling. The results also have more general relevance; imperfect resistive lateral coupling among roughly homogeneous networks of similar cell types is a common feature of retinal circuits, as well as neural circuitry more generally [60, 117]. And the ultimate task of the rod system at absolute threshold, to detect sparse signals among a convergent network of noisy units, is likewise relevant for processing elsewhere in the retina, in pathways underlying other sensory modalities, and in other areas of the nervous system generally [48, 105, 25].

3.6 Supplemental material

3.6.1 Capacitative effects

When rods were modeled with a capacitance, C_m, in parallel with the membrane resistance, capacitative effects on network voltages were found to be negligible. Considering a simple case of two such rods coupled to each other through resistance R_j, the time constant to charge C_m of one rod from a current source in the other is:

$$\tau = \frac{C_m R_m R_j}{R_m + R_j}$$

and the transfer function for voltage in one rod to voltage in the other as a function of angular frequency, s is:

$$H(s) = \frac{1}{R_j C_m s + R_j/R_m + 1} \tag{3.17}$$

In our whole cell recordings, rod capacitances ranged from 5–10 pF. Taking C_m as the upper limit of 10 pF, and assuming $R_m = 1.5$ GΩ and $R_j = 3$ GΩ (see results), gives $\tau = 10$ ms. Rod photovoltages for dim flashes are slow, with $> 99\%$ of their spectral power at or below 5 Hz. Therefore it can be seen intuitively that a membrane capacitance charging with a 10 ms time constant will have negligible effect on the photoresponse.

More rigorously, photovoltages can be fit with a standard two- or three-stage lowpass RC impulse response function [62] and the resulting fit then digitally filtered according to equation 3.17. Comparing the filtered response for $C_m = 10$ pF to the pure resistive voltage transfer with $C_m = 0$ the capacitance is found to reduce the peak response amplitude by about 0.1%. The capacitance also introduces a time delay to peak of about 5 ms, so that if the filtered and unfiltered responses are averaged together to simulate the averaging of photovoltages between neighboring rods, the additional reduction in peak amplitude is

about 0.02%. The cumulative effect of capacitance on peak response amplitude is thus a negligible 0.12%. More complicated hexagonal networks were simulated in GnuCAP, yielding maximal capacitative effects only about double those for the two rod case, i.e. still negligible. In general, the capacitative effect on voltage transfer amplitude exceeds 1% only for rods separated by 4 intervening neighbors. At this point, however, network resistances alone have attenuated transferred voltage by > 99%, so that the overall voltage transfer effect is completely dominated by resistance.

Finally, for the purposes of the psychophysical modeling, noise is assumed to be relevant only insofar as it has the same temporal characteristics as the photoresponse, so that signal and noise will in any case be affected equally by capacitative filtering.

3.6.2 Indirect current paths in paired rod recordings

When recording current passing between two neighboring rods, we generally assumed that the only current path was a junction directly between the recorded rods. In a rod network, however, current could also flow between recorded rods via indirect paths through additional intervening rods. Considering the simple case of two recorded rods connected both directly and indirectly via one intervening neighbor (figure 3.11), if one rod voltage is held and the other stepped, circuit analysis indicates that the indirect current I_i will be a fraction of the direct current I_d:

$$\frac{I_i}{I_d} = \frac{1}{2+\beta} \tag{3.18}$$

Thus, for $\beta = 2$ the indirect current is one quarter the magnitude of the direct. If we assume hexagonal rod packing, there can be at most two such indirect paths with only one intervening rod. Each will carry current according to equation 3.18, resulting in 67% of the total measured current being direct and 33% being indirect.

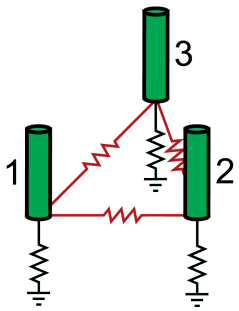

Figure 3.11: Indirect current path example
In this simple scenario, rods 1 and 2 are patch clamped. The voltage of rod 2 is held and rod 1 is stepped. The current measured at 2 is then a combination of direct flow (I_d) from 1 to 2 and indirect flow (I_i) from 1 to 2 via 3.

If we consider an infinite, fully connected hexagonal network, for any two recorded neighboring rods there are then an infinite number of indirect current paths, with varying numbers of intervening rods. It might appear that this would result in a greater proportion of the measured current being indirect rather than direct. However, in a fully connected network, the proliferation of current paths to ground makes every indirect path more leaky, such that the overall proportion of indirect current, as confirmed by GnuCAP simulation, is no greater than in the simple case of only two indirect paths each with one intervening rod.

3.6.3 Ocular point-spread function

The ocular point-spread function (PSF) describes the blurring of the external image as it passes through the eye before reaching the retina. Formally, it is the two-dimensional intensity profile of the image formed at the retina when the preretinal visual apparatus attempts to resolve an external point source of unit intensity. We assume here that the PSF is centered and radially symmetric, so that it can be described as a one-dimensional function that peaks at zero and falls off with radial distance. How quickly the PSF falls off depends on

the diameter of the viewing pupil. For very small pupils, the PSF is essentially diffraction limited, while for larger pupils the optical quality of the lens becomes the primary determining factor [24]. In practice, the PSF is difficult to obtain directly, so other measures are generally taken, such as the line-spread function or the modulation transfer transfer (MTF), from which the PSF can then be calculated. The MTF describes the preretinal eye's retention of contrast as a function of spatial frequency; it is the Fourier transform of the PSF.

For our analysis of the benefits of coupling for small spot stimuli, the PSF diameter at half-max gives us an estimate of the smallest practical retinal image. Since we are interested in the PSF for the dark-adapted human eye, we assume large pupil diameters of 6–8 mm [120]. Two studies have published analytical expressions for the human MTF at various pupil sizes [4, 57], both describing the MTF as a weighted sum of two exponentials. Given that the MTF is defined between 0 and ∞ cycles / degree, its inverse Fourier transform, i.e. the PSF, then has a direct analytical solution: a weighted sum of two Lorentzians.

Artal and Navarro [4] explicitly warn against deriving analytical PSFs from their analytical MTF expression, citing concerns that the analytical expression never reaches zero for high spatial frequencies, whereas the true MTF must eventually reach zero at the diffraction cutoff frequency. However, we find that this error is negligible for large pupil diameters. If we compute the MTF from their analytical expression for a large pupil and then set it to zero for frequencies above 50 cycles / degree, well below the true diffraction cutoff, we find that the numerically computed inverse Fourier transform is practically indistinguishable from that of the analytically calculated PSF.

Artal and Navarro [4] give MTF expressions for 6 mm and 8 mm pupils, from which we calculated PSF half-max diameters of 0.038 retinal degrees and 0.077 retinal degrees respectively. The largest pupil diameter considered by Guirao et al. [57] was 6 mm, from whose MTF we calculate a PSF half-max diameter of 0.028 retinal degrees. Thus

we conclude that for the dark-adapted human eye, the PSF ranges from about 0.03 to 0.08 degrees diameter. Interestingly, the situation in rodents appears similar. The rodent eye is of generally poorer optical quality, but the maximal pupil size is only about 2 mm, so that the dark adapted PSF has similar half-max diameter to a human's [3].

Chapter 4

General conclusions

In the preceding chapters, I have presented results on mammalian rod coupling and its effects on visual detection thresholds. In the primate retina, we showed that rods are tracer coupled, and that they share their electrical signals within small local networks. This is the first definitive evidence for rod coupling in primates, indicating that rod coupling could be relevant for understanding human vision. In the guinea pig retina, our recordings represent the first direct measurement of rod-rod coupling conductance in a mammalian retina. The rod network model I developed, by treating the voltages of coupled rods as the solution to a system of simultaneous linear equations, provides a simpler, more flexible approach than previous methods for determining the electrical behavior of these networks [126]. Many recent studies of coupled networks (e.g. [138, 63, 76, 154]) could benefit from network modeling along these lines, whether to confirm that different coupling data are mutually consistent, to extend predictions based on the existing data to situations where data are not yet available, or to enable further analysis of the greater implications of the observed coupling.

I developed a model of psychophysical detection to consider the implications of rod coupling for human vision, focusing on interactions between coupling and nonlinearities at

the rod output synapse. I also considered the total convergence of rod signals to the psychophysical detection stage, which is important for estimating sensitivity. Any subtleties of the circuitry between the rod bipolar cell layer and the ultimate psychophysical detection stage, however, were ignored in the model. This could be improved upon as our understanding of signaling between rod bipolar cells, AII amacrines, the ganglion cell layer, and the visual cortex improves. However, by focusing on the specific psychophysical task of detection of brief flashes near absolute threshold, the model is able to generate useful insights despite the missing information. It seems fair to assert that in the capacity of detection near absolute threshold, the interaction between coupling and rod output nonlinearities is most critical; effects depending on downstream circuitry would tend to be obviated by other interactions at these later stages, including convergence, AII coupling, and lateral interneuron signaling.

Given the finding that coupling can enhance detection of small spots, is there any explanation for why this would be particularly adaptive? One intriguing possibility is that the selective enhancement of small spot detection is important because it improves detection of stars. For nocturnal mammals, aerial predation risk is greatest on brightly lit nights. Therefore, many nocturnal mammals concentrate their foraging activities on the darkest nights of the lunar month, on and around new moon [26]. Aerial predation is still a major risk even under these dark conditions however [42, 68], and without the moon to provide general sky-shine, detection of predatory flyovers could depend critically on silhouetting of aerial predators against the star-field. Thus, improved detection of small points of light could be critical for visual detection of an overflying predator. Although speculative, this idea generates several intriguing hypotheses. If detection of stars is really a reason for rod coupling, for example, we would expect coupling to be more prevalent in ventral retina than dorsally. Several rodent and lagomorph retinas are known to have distinctly different complements of cones in ventral versus dorsal retina, possibly to enhance detection of objects against the

different background of the daytime sky versus the ground [150]. Primate retinas also show differences in rod densities in ventral versus dorsal areas [89, 32]. Another corollary of the star detection hypothesis is that coupling might be modulated according to lunar cycle, in addition to the previously mentioned possibility of circadian modulation. Endogenous lunar rhythms have not been much studied in mammals (but see [92]), although they are well known in other vertebrates [1].

Another suggested benefit of mammalian rod coupling is in signaling at brighter scotopic levels, when the recently discovered synapses from rods directly onto cone bipolar cells are active [130, 129]. Only about 20% of the rods appear to contact cone bipolar cells directly, so it is hypothesized that rod coupling allows the remaining majority of the rods to send indirect signals through this pathway. So far the direct rod to cone bipolar circuit has been observed only in rodents, so it would have to be established in primate before it could be offered as an explanation for the primate rod coupling demonstrated here in chapter 2. Not much is known about the relative sensitivity and dynamic range of this circuit, but the network modeling and conductance measurements presented here in chapter 3 offer a ready means to calculate the relative contribution of rod coupling to this pathway once its operating parameters are better understood.

As these alternative proposed justifications for rod coupling demonstrate, there are in fact many possible benefits and detriments for rod coupling, including electrophysiological effects at various light levels and for diverse possible stimuli, as well as non-electrical effects such as benefits of coupling for metabolic signaling or intercellular adhesion. A significant detrimental effect that is currently being explored is the possibility that photoreceptor coupling could be instrumental in the spreading degradation common in clinical cases of retinal degenerative disease [100, 33]. Clearly there is much left to learn, and many of the outstanding questions, such as potential circadian modulation of coupling or variation in coupling over different topographical areas of the retina, will probably benefit

from new high-throughput methods such as biolistic dye labeling [18], single-cell electroporation [87], and photofilling [79]. Still, it is striking that in considering only our electrophysiological data and issues of detection at absolute threshold, we can already see the possibility for a dynamic tension between coupling's putative benefits and detriments. Ultimately, while the psychophysical modeling presented in chapter 2 laid a groundwork for considering competing effects inherent to rod coupling, it was only with the additional data and refined modeling in chapter 3 that it became clear that, within the context of absolute detection threshold, the level of coupling present in mammals could effectively minimize coupling's negative consequences while maintaining and even improving on its benefits. The importance here of considering interactions between coupling and immediately downstream synaptic nonlinearities may prove instructive for understanding the role of coupling generally within convergent pathways. The work presented in this dissertation provides new insights into rod coupling in the mammalian retina, an enigma whose implications may stretch to many other areas in the neurosciences and in the study of signal processing.

Bibliography

[1] Mohamed Ather Ali. *Rhythms in Fishes: Proceedings of a NATO Advanced Study Institute on Rhythms in Fishes, Held August 4-17, 1991, in Montreal, Quebec, Canada*. Springer, 1992.

[2] A. Arman and A. P. Sampath. Contribution of rod photoresponses to the rod-cone and rod-off pathways in the mouse retina. Association for Research in Vision and Ophthalmology, 2008.

[3] P. Artal, P. Herreros de Tejada, C. Muñoz Tedó, and D. G. Green. Retinal image quality in the rodent eye. *Vis Neurosci*, 15(4):597–605, 1998.

[4] P. Artal and R. Navarro. Monochromatic modulation transfer function of the human eye for different pupil diameters: an analytical expression. *J Opt Soc Am A Opt Image Sci Vis*, 11(1):246–249, Jan 1994.

[5] D. Attwell, S. Borges, S. M. Wu, and M. Wilson. Signal clipping by the rod output synapse. *Nature*, 328(6130):522–524, August 6-12 1987.

[6] D. Attwell and M. Wilson. Behaviour of the rod network in the tiger salamander retina mediated by membrane properties of individual rods. *J Physiol*, 309:287–315, December 1980.

[7] D. Attwell, M. Wilson, and S. M. Wu. A quantitative analysis of interactions between photoreceptors in the salamander (Ambystoma) retina. *J Physiol*, 352:703–737, July 1984.

[8] D. Attwell, M. Wilson, and S. M. Wu. The effect of light on the spread of signals through the rod network of the salamander retina. *Brain Res*, 343(1):79–88, September 1985.

[9] A. Baranova, D. Ivanov, N. Petrash, A. Pestova, M. Skoblov, I. Kelmanson, D. Shagin, S. Nazarenko, E. Geraymovych, O. Litvin, A. Tiunova, T. L. Born, N. Usman, D. Staroverov, S. Lukyanov, and Y. Panchin. The mammalian pannexin family is homologous to the invertebrate innexin gap junction proteins. *Genomics*, 83(4):706–716, April 2004.

[10] H. B. Barlow. Retinal noise and absolute threshold. *J Opt Soc Am*, 46(8):634–639, August 1956.

[11] H. B. Barlow. Increment thresholds at low intensities considered as signal/noise discriminations. *J Physiol*, 136(3):469–488, May 1957.

[12] H. B. Barlow, W. R. Levick, and M. Yoon. Responses to single quanta of light in retinal ganglion cells of the cat. *Vision Res*, Suppl 3:87–101, 1971.

[13] D. A. Baylor, T. D. Lamb, and K.-W. Yau. Responses of retinal rods to single photons. *J Physiol*, 288:613–634, March 1979.

[14] D. A. Baylor, B. J. Nunn, and J. L. Schnapf. The photocurrent, noise and spectral sensitivity of rods of the monkey *Macaca fascicularis*. *J Physiol*, 357:575–607, December 1984.

[15] D. A. Baylor, B. J. Nunn, and J. L. Schnapf. Spectral sensitivity of cones of the monkey Macaca fascicularis. *J Physiol*, 390:145–160, September 1987.

[16] A. Berntson, R. G. Smith, and W. R. Taylor. Transmission of single photon signals through a binary synapse in the mammalian retina. *Vis Neurosci*, 21(5):693–702, September-October 2004.

[17] W. Bialek and W. G. Owen. Temporal filtering in retinal bipolar cells. elements of an optimal computation? *Biophys J*, 58(5):1227–1233, Nov 1990.

[18] Kevin S Bittman, Jessica A Panzer, and Rita J Balice-Gordon. Patterns of cell-cell coupling in embryonic spinal cord studied via ballistic delivery of gap-junction-permeable dyes. *J Comp Neurol*, 477(3):273–285, Sep 2004.

[19] S. A. Bloomfield and R. F. Dacheux. Rod vision: pathways and processing in the mammalian retina. *Prog Retin Eye Res*, 20(3):351–384, May 2001.

[20] S. A. Bloomfield and B. Völgyi. Function and plasticity of homologous coupling between AII amacrine cells. *Vision Res*, 44(28):3297–3306, December 2004.

[21] S. A. Bloomfield and D. Xin. A comparison of receptive-field and tracer-coupling size of amacrine and ganglion cells in the rabbit retina. *Vis Neurosci*, 14(6):1153–1165, 1997.

[22] S. A. Bloomfield, D. Xin, and S. E. Persky. A comparison of receptive field and tracer coupling size of horizontal cells in the rabbit retina. *Vis Neurosci*, 12(5):985–999, 1995.

[23] A. Borsellino and M. G. F. Fuortes. Responses to single photons in virual cells of limulus. *J Physiol*, 196(3):507–539, Jun 1968.

[24] F. W. Campbell and R. W. Gubisch. Optical quality of the human eye. *J Physiol*, 186(3):558–578, Oct 1966.

[25] P. T. Clark and M. C. W. van Rossum. The optimal synapse for sparse, binary signals in the rod pathway. *Neural Comput*, 18(1):26–44, Jan 2006.

[26] J. A. Clarke. Moonlight's influence on predator/prey interactions between short-eared owls (asio flammeus) and deermice (peromyscus maniculatus). *Behavioral Ecology and Sociobiology*, 13(3):205–209, 1983 1983.

[27] A. I. Cohen. Interphotoreceptor contacts at the inner segment level in primate retinas. *Brain Res*, 490(1):200–203, June 1989.

[28] J. D. Conner and D. I. MacLeod. Rod photoreceptors detect rapid flicker. *Science*, 195(4279):698–699, Feb 1977.

[29] J. E. Cook and D. L. Becker. Gap junctions in the vertebrate retina. *Microsc Res Tech*, 31(5):408–419, August 1995.

[30] N. Cuenca, G. C. Martínez-Navarrete, J. Esteve-Rudd, A. Angulo, I. Pinilla, and J. Martín-Nieto. Connexin 36 distribution pattern in the vertebrate retina: Impaired expression in retinitis pigmentosa rodent models. Association for Research in Vision and Ophthalmology, 2007.

[31] C. A. Curcio and K. A. Allen. Topography of ganglion cells in human retina. *J Comp Neurol*, 300(1):5–25, Oct 1990.

[32] C. A. Curcio, K. R. Sloan, R. E. Kalina, and A. E. Hendrickson. Human photoreceptor topography. *J Comp Neurol*, 292(4):497–523, Feb 1990.

[33] K. Cusato, A. Bosco, R. Rozental, CA. Guimarães, BE. Reese, R. Linden, and DC. Spray. Gap junctions mediate bystander cell death in developing retina. *J Neurosci*, 23(16):6413–6422, July 2003.

[34] N. V. Custer. Structurally specialized contacts between the photoreceptors of the retina of the axolotl. *J Comp Neurol*, 151(1):35–56, September 1973.

[35] L. Dang, S. Pulukuri, A. J. Mears, A. Swaroop, B. E. Reese, and A. Sitaramayya. Connexin 36 in photoreceptor cells: studies on transgenic rod-less and cone-less mouse retinas. *Mol Vis*, 10:323–327, May 2004.

[36] H. L. de Vries. The quantum character of light and its bearing upon threshold of vision, the differential sensitivity and visual acuity of the eye. *Physica*, 10(7):553–564, July 1943.

[37] M. R. Deans, B. Völgyi, D. A. Goodenough, S. A. Bloomfield, and D. L. Paul. Connexin36 is essential for transmission of rod-mediated visual signals in the mammalian retina. *Neuron*, 36(4):703–712, November 2002.

[38] G. C. Demontis, B. Longoni, U. Barcaro, and L. Cervetto. Properties and functional roles of hyperpolarization-gated currents in guinea-pig retinal rods. *J Physiol*, 515 (Pt 3):813–828, March 1999.

[39] P. B. Detwiler, A. L. Hodgkin, and P. A. McNaughton. A surprising property of electrical spread in the network of rods in the turtle's retina. *Nature*, 274(5671):562–565, August 1978.

[40] S. H. DeVries and D. A. Baylor. An alternative pathway for signal flow from rod photoreceptors to ganglion cells in mammalian retina. *Proc Natl Acad Sci U S A*, 92(23):10658–10662, November 1995.

[41] S. H. DeVries, X. Qi, R. Smith, W. Makous, and P. Sterling. Electrical coupling between mammalian cones. *Curr Biol*, 12(22):1900–1907, November 2002.

[42] L. R. Dice. Minimum intensities of illumination under which owls can find dead prey by sight. *The American Naturalist*, 79(784):385–416, Sep. - Oct. 1945.

[43] G. Dvoriantchikova, D. Ivanov, Y. Panchin, and V. I. Shestopalov. Expression of pannexin family of proteins in the retina. *FEBS Lett*, Mar 2006.

[44] V. I Esipenko and O. B Shchuko. Probability density of the sum of random variables with random coefficients. *Radiophysics and Quantum Electronics*, 38(6):390–394, 1995.

[45] W. H. Evans and P. E. Martin. Gap junctions: structure and function (Review). *Mol Membr Biol*, 19(2):121–136, April–June 2002.

[46] G. L. Fain. Quantum sensitivity of rods in the toad retina. *Science*, 187(4179):838–841, March 1975.

[47] G. D. Field and E. J. Chichilnisky. Information processing in the primate retina: circuitry and coding. *Annu Rev Neurosci*, 30:1–30, 2007.

[48] G. D. Field and F. Rieke. Nonlinear signal transfer from mouse rods to bipolar cells and implications for visual sensitivity. *Neuron*, 34(5):773–785, May 2002.

[49] J. L. Flagg-Newton and W. R. Loewenstein. Asymmetrically permeable membrane channels in cell junction. *Science*, 207(4432):771–773, February 1980.

[50] M. G. F. Fuortes and S. Yeandle. Probability of occurrence of discrete potential waves in the eye of limulus. *J Gen Physiol*, 47:443–463, Jan 1964.

[51] J.-L. Giavitto, G. Malcolm, and O. Michel. Rewriting systems and the modelling of biological systems. *Comparative and Functional Genomics*, 5:95–99, 2004.

[52] G. H. Gold and J. E. Dowling. Photoreceptor coupling in retina of the toad, Bufo marinus. I. Anatomy. *J Neurophysiol*, 42(1 Pt 1):292–310, January 1979.

[53] C. H. Graham and N. R. Bartlett. The relation of size of stimulus and intensity in the human eye: I. intensity thresholds for white light. *J Exp Psychol*, 24:555–573, 1939.

[54] C. H. Graham and N. R. Bartlett. The relation of size of stimulus and intensity in the human eye: II. intensity thresholds for red and violet light. *J Exp Psychol*, 24:574–587, 1939.

[55] D. M. Green and J. A. Swets. *Signal detection theory and psychophysics*. Wiley, New York, 1966.

[56] U. Grünert. Anatomical evidence for rod input to the parvocellular pathway in the visual system of the primate. *Eur J Neurosci*, 9(3):617–621, Mar 1997.

[57] A. Guirao, C. González, M. Redondo, E. Geraghty, S. Norrby, and P. Artal. Average optical performance of the human eye as a function of age in a normal population. *Invest Ophthalmol Vis Sci*, 40(1):203–213, Jan 1999.

[58] S. Hecht, S. Shlaer, and M. H. Pirenne. Energy, quanta, and vision. *The Journal of General Physiology*, 25(6):819–840, 1942.

[59] S. H. Hendry and R. C. Reid. The koniocellular pathway in primate vision. *Annu Rev Neurosci*, 23:127–153, 2000.

[60] S. G. Hormuzdi, M. A. Filippov, G. Mitropoulou, H. Monyer, and R. Bruzzone. Electrical synapses: a dynamic signaling system that shapes the activity of neuronal networks. *Biochim Biophys Acta*, 1662(1-2):113–137, March 2004.

[61] R. Horn and A. Marty. Muscarinic activation of ionic currents measured by a new whole-cell recording method. *J Gen Physiol*, 92(2):145–159, Aug 1988.

[62] E. P. Hornstein, J. Verweij, P. H. Li, and J. L. Schnapf. Gap-junctional coupling and absolute sensitivity of photoreceptors in macaque retina. *Journal of Neuroscience*, 25(48):11201–11209, November 2005.

[63] E. P. Hornstein, J. Verweij, and J. L. Schnapf. Electrical coupling between red and green cones in primate retina. *Nat Neurosci*, 7(7):745–750, July 2004.

[64] G. H. Jacobs and J. F. Deegan. Spectral sensitivity, photopigments, and color vision in the guinea pig (Cavia porcellus). *Behav Neurosci*, 108(5):993–1004, October 1994.

[65] R. A. Jacoby and D. W. Marshak. Synaptic connections of db3 diffuse bipolar cell axons in macaque retina. *J Comp Neurol*, 416(1):19–29, Jan 2000.

[66] M. Kameyama. Electrical coupling between ventricular paired cells isolated from guinea-pig heart. *J Physiol*, 336:345–357, Mar 1983.

[67] H. Kolb, R. Nelson, and A. Mariani. Amacrine cells, bipolar cells and ganglion cells of the cat retina: a golgi study. *Vision Res*, 21(7):1081–1114, 1981.

[68] B. P. Kotler, J. S. Brown, and O. Hasson. Factors affecting gerbil foraging behavior and rates of owl predation. *Ecology*, 72(6):2249–2260, Dec. 1991.

[69] T. W. Kraft, D. M. Schneeweis, and J. L. Schnapf. Visual transduction in human rod photoreceptors. *J Physiol*, 464:747–765, May 1993.

[70] D. Krizaj, R. Gábriel, W. G. Owen, and P. Witkovsky. Dopamine D2 receptor-mediated modulation of rod-cone coupling in the Xenopus retina. *J Comp Neurol*, 398(4):529–538, September 1998.

[71] N. M. Kumar and N. B. Gilula. The gap junction communication channel. *Cell*, 84(3):381–388, Feb 1996.

[72] T. D. Lamb and E. J. Simon. The relation between intercellular coupling and electrical noise in turtle photoreceptors. *J Physiol*, 263(2):257–286, December 1976.

[73] B. B. Lee, V. C. Smith, J. Pokorny, and J. Kremers. Rod inputs to macaque ganglion cells. *Vision Res*, 37(20):2813–2828, Oct 1997.

[74] E. J. Lee, J. W. Han, H. J. Kim, I. B. Kim, M. Y. Lee, S. J. Oh, J. W. Chung, and M. H. Chun. The immunocytochemical localization of connexin 36 at rod and cone gap junctions in the guinea pig retina. *Eur J Neurosci*, 18(11):2925–2934, December 2003.

[75] P. Lennie and M. D. Fairchild. Ganglion cell pathways for rod vision. *Vision Res*, 34(4):477–482, Feb 1994.

[76] W. Li and S. H. DeVries. Separate blue and green cone networks in the mammalian retina. *Nat Neurosci*, 7(7):751–756, July 2004.

[77] A. Lindenmayer. Mathematical models for cellular interactions in development. i. filaments with one-sided inputs. *J Theor Biol*, 18(3):280–299, Mar 1968.

[78] C. Lu and D. G. McMahon. Gap junction channel gating at bass retinal electrical synapses. *Vis Neurosci*, 13(6):1049–1057, November-December 1996.

[79] M. A. MacNeil, J. K. Heussy, R. F. Dacheux, E. Raviola, and R. H. Masland. The shapes and numbers of amacrine cells: matching of photofilled with Golgi-stained cells in the rabbit retina and comparison with other mammalian species. *J Comp Neurol*, 413(2):305–326, October 1999.

[80] R. H. Masland. The fundamental plan of the retina. *Nat Neurosci*, 4(9):877–886, September 2001.

[81] S. C. Massey and S. L. Mills. A calbindin-immunoreactive cone bipolar cell type in the rabbit retina. *J Comp Neurol*, 366(1):15–33, Feb 1996.

[82] S. C. Massey, J. J. O'Brien, E. B. Trexler, W. Li, J. W. Keung, S. L. Mills, and J. O'Brien. Multiple neuronal connexins in the Mammalian retina. *Cell Commun Adhes*, 10(4-6):425–430, July-December 2003.

[83] A. Merighi, E. Raviola, and R. F. Dacheux. Connections of two types of flat cone bipolars in the rabbit retina. *J Comp Neurol*, 371(1):164–178, July 1996.

[84] S. L. Mills and S. C. Massey. Aii amacrine cells limit scotopic acuity in central macaque retina: A confocal analysis of calretinin labeling. *J Comp Neurol*, 411(1):19–34, Aug 1999.

[85] Gabe J Murphy and Fred Rieke. Signals and noise in an inhibitory interneuron diverge to control activity in nearby retinal ganglion cells. *Nat Neurosci*, 11(3):318–326, Mar 2008.

[86] R. Nelson. Cat cones have rod input: a comparison of the response properties of cones and horizontal cell bodies in the retina of the cat. *J Comp Neurol*, 172(1):109–135, March 1977.

[87] J. Olofsson, K. Nolkrantz, F. Ryttsén, B. A. Lambie, S. G. Weber, and O. Orwar. Single-cell electroporation. *Curr Opin Biotechnol*, 14(1):29–34, February 2003.

[88] W. G. Owen. Chemical and electrical synapses between photoreceptors in the retina of the turtle, chelydra serpentina. *J Comp Neurol*, 240(4):423–433, Oct 1985.

[89] O. Packer, A. E. Hendrickson, and C. A. Curcio. Photoreceptor topography of the retina in the adult pigtail macaque (macaca nemestrina). *J Comp Neurol*, 288(1):165–183, Oct 1989.

[90] J. W. Parry and J. K. Bowmaker. Visual pigment coexpression in Guinea pig cones: a microspectrophotometric study. *Invest Ophthalmol Vis Sci*, 43(5):1662–1665, May 2002.

[91] P. Phelan and T. A. Starich. Innexins get into the gap. *Bioessays*, 23(5):388–396, May 2001.

[92] Giuseppe Piccione and Giovanni Caola. Biological rhythm in livestock. *J Vet Sci*, 3(3):145–157, Sep 2002.

[93] W. H. Press, S. A. Teukolsky, W. T. Vetterling, and B. P. Flannery. *Numerical recipes in C, the art of scientific computing*. Cambridge University Press, Cambridge, Cambridgeshire, UK, 2nd edition, 1992.

[94] H. Qian, R. P. Malchow, and H. Ripps. Gap-junctional properties of electrically coupled skate horizontal cells in culture. *Vis Neurosci*, 10(2):287–295, March-April 1993.

[95] E. Raviola and N. B. Gilula. Gap junctions between photoreceptor cells in the vertebrate retina. *Proc Natl Acad Sci U S A*, 70(6):1677–1681, June 1973.

[96] A. Ray, G. Zoidl, S. Weickert, P. Wahle, and R. Dermietzel. Site-specific and developmental expression of pannexin1 in the mouse nervous system. *Eur J Neurosci*, 21(12):3277–3290, June 2005.

[97] C. Ribelayga, Y. Cao, and S. C. Mangel. The circadian clock in the retina controls rod-cone coupling. *Neuron*, 59:790–801, September 2008.

[98] A. Ricco. Relazioni fra il minimo angolo visuale e l'intensià luminosa. *Ann. Ottol.*, 6:373–479, 1877.

[99] F. Rieke and D. A. Baylor. Origin of reproducibility in the responses of retinal rods to single photons. *Biophys J*, 75(4):1836–1857, October 1998.

[100] H. Ripps. Cell death in retinitis pigmentosa: gap junctions and the 'bystander' effect. *Exp Eye Res*, 74(3):327–336, March 2002.

[101] S. R. Robinson, E. C. Hampson, M. N. Munro, and D. I. Vaney. Unidirectional coupling of gap junctions between neuroglia. *Science*, 262(5136):1072–1074, November 1993.

[102] J. G. Robson and L. J. Frishman. Response linearity and kinetics of the cat retina: the bipolar cell component of the dark-adapted electroretinogram. *Vis Neurosci*, 12(5):837–850, 1995.

[103] J. G. Robson, H. Maeda, S. M. Saszik, and L. J. Frishman. In vivo studies of signaling in rod pathways of the mouse using the electroretinogram. *Vision Res*, 44(28):3253–3268, December 2004.

[104] A. Rose. The sensitivity performance of the human eye on an absolute scale. *Journal of the Optical Society of America*, 38:196–208, 1948.

[105] AP. Sampath and F. Rieke. Selective transmission of single photon responses by saturation at the rod-to-rod bipolar synapse. *Neuron*, 41(3):431–443, February 2004.

[106] J. L. Schnapf and D. R. Copenhagen. Differences in the kinetics of rod and cone synaptic transmission. *Nature*, 296(5860):862–864, April 1982.

[107] J. L. Schnapf, B. J. Nunn, M. Meister, and D. A. Baylor. Visual transduction in cones of the monkey *Macaca fascicularis*. *J Physiol*, 427:681–713, August 1990.

[108] D. M. Schneeweis and J. L. Schnapf. Photovoltage of rods and cones in the macaque retina. *Science*, 268(5213):1053–1056, May 1995.

[109] D. M. Schneeweis and J. L. Schnapf. The photovoltage of macaque cone photoreceptors: adaptation, noise, and kinetics. *J Neurosci*, 19(4):1203–1216, February 1999.

[110] D. M. Schneeweis and J. L. Schnapf. Noise and light adaptation in rods of the macaque monkey. *Vis Neurosci*, 17(5):659–666, September-October 2000.

[111] A. M. Scholtes and M. A. Bouman. Psychophysical experiments on spatial summation at threshold level of the human peripheral retina. *Vision Res*, 17(7):867–873, 1977.

[112] E. A. Schwartz. Rod-rod interaction in the retina of the turtle. *J Physiol*, 246(3):617–638, Apr 1975.

[113] L. T. Sharpe. The light-adaptation of the human rod visual system. In R. F. Hess, L. T. Sharpe, and Knut Nordby, editors, *Night Vision: Basic, Clinical and Applied Aspects*, pages 49–124. Cambridge University Press, 1990.

[114] L. T. Sharpe, C. Fach, K. Nordby, and A. Stockman. The incremental threshold of the rod visual system and weber's law. *Science*, 244(4902):354–356, Apr 1989.

[115] L. T. Sharpe, A. Stockman, and D. I. MacLeod. Rod flicker perception: scotopic duality, phase lags and destructive interference. *Vision Res*, 29(11):1539–1559, 1989.

[116] R. G. Smith, M. A. Freed, and P. Sterling. Microcircuitry of the dark-adapted cat retina: functional architecture of the rod-cone network. *J Neurosci*, 6(12):3505–3517, December 1986.

[117] G. Söhl, S. Maxeiner, and K. Willecke. Expression and functions of neuronal gap junctions. *Nat Rev Neurosci*, 6(3):191–200, March 2005.

[118] E. Soucy, Y. Wang, S. Nirenberg, J. Nathans, and M. Meister. A novel signaling pathway from rod photoreceptors to ganglion cells in mammalian retina. *Neuron*, 21(3):481–493, September 1998.

[119] D. C. Spray, A. L. Harris, and M. V. Bennett. Equilibrium properties of a voltage-dependent junctional conductance. *J Gen Physiol*, 77(1):77–93, January 1981.

[120] K. H. Spring and W. S. Stiles. Variation of pupil size with change in the angle at which the light stiumulus strikes the retina. *Br J Ophthalmol*, 32(6):340–346, Jun 1948.

[121] M. Srinivas, R. Rozental, T. Kojima, R. Dermietzel, M. Mehler, D. F. Condorelli, J. A. Kessler, and D. C. Spray. Functional properties of channels formed by the neuronal gap junction protein connexin36. *J Neurosci*, 19(22):9848–9855, November 1999.

[122] P. Sterling. How retinal circuits optimize the transfer of visual information. In L. M. Chalupa and J. S. Warner, editors, *The Visual Neurosciences*, chapter 17, pages 234–259. MIT Press, Cambridge, Massachusettes, 2004.

[123] P. Sterling, M. A. Freed, and R. G. Smith. Architecture of rod and cone circuits to the on-beta ganglion cell. *J Neurosci*, 8(2):623–642, February 1988.

[124] A. Stockman, L. T. Sharpe, E. Zrenner, and K. Nordby. Slow and fast pathways in the human rod visual system: electrophysiology and psychophysics. *J Opt Soc Am A*, 8(10):1657–1665, October 1991.

[125] E. Strettoi, E. Raviola, and R. F. Dacheux. Synaptic connections of the narrow-field, bistratified rod amacrine cell (AII) in the rabbit retina. *J Comp Neurol*, 325(2):152–168, November 1992.

[126] M. Tessier-Lavigne and D. Attwell. The effect of photoreceptor coupling and synapse nonlinearity on signal:noise ratio in early visual processing. *Proc R Soc Lond B Biol Sci*, 234(1275):171–197, July 1988.

[127] V. Torre and W. G. Owen. High-pass filtering of small signals by the rod network in the retina of the toad, bufo marinus. *Biophys J*, 41(3):305–324, Mar 1983.

[128] Y. Tsukamoto, P. Masarachia, S. J. Schein, and P. Sterling. Gap junctions between the pedicles of macaque foveal cones. *Vision Res*, 32(10):1809–1815, October 1992.

[129] Y. Tsukamoto, K. Morigiwa, M. Ishii, M. Takao, K. Iwatsuki, S. Nakanishi, and Y. Fukuda. A novel connection between rods and on cone bipolar cells revealed by ectopic metabotropic glutamate receptor 7 (mglur7) in mglur6-deficient mouse retinas. *J Neurosci*, 27(23):6261–6267, Jun 2007.

[130] Y. Tsukamoto, K. Morigiwa, M. Ueda, and P. Sterling. Microcircuits for night vision in mouse retina. *J Neurosci*, 21(21):8616–8623, November 2001.

[131] D. L. Turner and C. L. Cepko. A common progenitor for neurons and glia persists in rat retina late in development. *Nature*, 328(6126):131–136, July 9-15 1987.

[132] S. Uga, F. Nakao, M. Mimura, and H. Ikui. Some new findings on the fine structure of the human photoreceptor cells. *J Electron Microsc (Tokyo)*, 19(1):71–84, 1970.

[133] H. V. M. van Rijen, R. Wilders, A. C. G. van Ginneken, and H. J. Jongsma. Quantitative analysis of dual whole-cell voltage-clamp determination of gap junctional conductance. *Pflugers Arch*, 436(1):141–151, June 1998.

[134] M. C. van Rossum and R. G. Smith. Noise removal at the rod synapse of mammalian retina. *Vis Neurosci*, 15(5):809–821, September-October 1998.

[135] D. I. Vaney. Patterns of neuronal coupling in the retina. *Progress in Retinal and Eye Research*, 13:301–355, 1994.

[136] D. I. Vaney. Neuronal coupling in the central nervous system: lessons from the retina. *Novartis Found Symp*, 219:113–125, 1999.

[137] R. D. Veenstra. Voltage clamp limitations of dual whole-cell gap junction current and voltage recordings. i. conductance measurements. *Biophys J*, 80(5):2231–2247, May 2001.

[138] M. L. Veruki and E. Hartveit. AII (Rod) amacrine cells form a network of electrically coupled interneurons in the mammalian retina. *Neuron*, 33(6):935–946, March 2002.

[139] M. L. Veruki and E. Hartveit. Electrical synapses mediate signal transmission in the rod pathway of the mammalian retina. *J Neurosci*, 22(24):10558–10566, December 2002.

[140] J. Verweij, E. P. Hornstein, and J. L. Schnapf. Surround antagonism in macaque cone photoreceptors. *J Neurosci*, 23(32):10249–10257, November 2003.

[141] J. Verweij, P. H. Li, O. Packer, D. M. Dacey, and J. L. Schnapf. Primate blue cones receive rod input. 2008.

[142] J. P. Vessey, M. R. Lalonde, H. A. Mizan, N. C. Welch, M. E. Kelly, and S. Barnes. Carbenoxolone inhibition of voltage-gated Ca channels and synaptic transmission in the retina. *J Neurophysiol*, 92(2):1252–1256, August 2004.

[143] B. Völgyi, M. R. Deans, D. L. Paul, and S. A. Bloomfield. Convergence and segregation of the multiple rod pathways in mammalian retina. *J Neurosci*, 24(49):11182–11192, December 2004.

[144] Y. Wen and S. C. Mangel. A circadian clock in the fish retina regulates rod-cone coupling. Association for Research in Vision and Ophthalmology, 2005.

[145] F. S. Werblin. Transmission along and between rods in the tiger salamander retina. *J Physiol*, 280:449–470, Jul 1978.

[146] G. G. Whitlock and T. D. Lamb. Variability in the time course of single photon responses from toad rods: termination of rhodopsin's activity. *Neuron*, 23(2):337–351, Jun 1999.

[147] G. Wyszecki and W. S Stiles. *Color science: concepts and methods, quantitative data and formulae*. Wiley, New York, 1982.

[148] Y. Xia and S. Nawy. The gap junction blockers carbenoxolone and 18beta-glycyrrhetinic acid antagonize cone-driven light responses in the mouse retina. *Vis Neurosci*, 20(4):429–435, July-August 2003.

[149] X. L. Yang and S. M. Wu. Modulation of rod-cone coupling by light. *Science*, 244(4902):352–354, April 1989.

[150] L. Yin, R. G. Smith, P. Sterling, and D. H. Brainard. Chromatic properties of horizontal and ganglion cell responses follow a dual gradient in cone opsin expression. *J Neurosci*, 26(47):12351–12361, Nov 2006.

[151] K. R. Zahs and E. A. Newman. Asymmetric gap junctional coupling between glial cells in the rat retina. *Glia*, 20(1):10–22, May 1997.

[152] J. H. Zar. *Biostatistical analysis*. Prentice Hall Upper Saddle River, New Jersey, 1999.

[153] J. Zhang and S. M. Wu. Connexin35/36 gap junction proteins are expressed in photoreceptors of the tiger salamander retina. *J Comp Neurol*, 470(1):1–12, February 2004.

[154] J. Zhang and S. M. Wu. Physiological Properties of Rod Photoreceptor Electrical Coupling in the Tiger Salamander Retina. *J Physiol*, March 2005.

[155] P. Zuidema, H. Verschuure, M. A. Bouman, and J. J. Koenderink. Spatial and temporal summation in the human dark-adapted retina. *J Opt Soc Am*, 71(12):1472–1480, December 1981.

Appendix A

Code listings

A.1 cellnet.m

```
function W = cellnet(C, beta)
%CELLNET
%   W = cellnet(C, beta)
%   Solves for the normalized voltage transfer matrix for a network of N
%   cells.  Each cell has a membrane resistance to ground Rm and a
%   resistance to neighboring cells Rj.  These parameters are captured in
%   the function parameter BETA = Rj / Rm.  The connectivity of the
%   network is captured in the connectivity matrix C, which is an NxN
%   symmetric matrix with ones where cells are connected and zeroes where
%   they aren't. C should be specified with zeros on the diagonal; a cell
%   is not considered to be connected to itself.
%
%   For example, a four cell cycle:
%       1-2
%       | |
%       3-4
%   would be represented with connectivity matrix:
%       [0 1 1 0
%        1 0 0 1
%        1 0 0 1
%        0 1 1 0]

error(nargchk(2, 2, nargin));

if(numel(size(C)) ~=2 || size(C, 1) ~= size(C, 2) || ...
        ~all(all(C == C')) || any(diag(C)))
   error(['C should be a symmetric square matrix with zeros' ...
          ' along the diagonal']);
end

% Calculate the number of other cells each cell is connected to
NumC = sum(C);

% Form matrices for system of equations
D = diag(-(NumC + beta));
S = C + D;

% We want to solve the system of equations defined by S * w = B with a
% series of different answer column vectors, B.  So instead make B a
% matrix of all the answer columns lined up.
B = diag(ones(1, size(C, 1)) .* -beta);

W = S \ B;
```

A.2 hexconnect.m

```
function C = hexconnect(l)
%HEXCONNECT
%   C = hexconnect(l)
%   Generates a connectivity matrix representing a hexagonal network of
%   connected nodes with L surrounding layers.  A network L = 1 has 7
%   nodes, one in the center and 6 surrounding it.  For a network with N
%   nodes, C will be an NxN symmetric square matrix with ones to indicate
%   where two nodes are connected and zeros everywhere else.
%
%   HEXCONNECT generates networks with full hexagonal connectivity, but
%   note that it would be trivial to include stochasticity into the
%   connection forming step to represent a stochastically connected,
%   hexagonally packed array of nodes.

error(nargchk(1, 1, nargin));

if l < 0
    error('L must be >= 0');
end

% Calculate the number of nodes in a hexagonal network of L layers
% Each layer X has X * 6 nodes, except for layer 0 which has 1 node.
% We can calculate N using the triangular number formula.
n = 1 + 6 * l/2 * (l + 1);

% Initiate the connectivity matrix as an NxN sparse matrix of zeros
C = sparse(n, n);

% Now iteratively go through the layers, adding ones to the connectivity
% matrix to indicate connections between nodes.
prevL = [1]; % Start with layer 0, containing only node 1.
for i = 1:l,
    % Sanity check
    if(numel(size(C)) ~=2 || size(C, 1) ~= size(C, 2) || ...
        ~all(all(C == C')) || any(diag(C)))
       error(['C should be a symmetric square matrix with zeros' ...
               ' along the diagonal']);
    end

    numconnections = sum(C); % Num connections for each node so far
    numnewL = i*6;           % Num nodes in the new layer

    % For each node in the previous outer layer, connect to appropriate
    % nodes in the new outer layer.
    lastnewnode = 1;
    for j = prevL,
        % How many new nodes must be connected to this previous layer node
        % to bring the previous layer node to 6 connections total?
        newconnections = 6 - numconnections(j);

        % Name the new layer nodes attached to this previous layer node
        % This should be a sequence of node numbers e.g. [1 2 3].  If the
        % last node was connected to nodes [1 2 3] then this node should be
        % connected to nodes [3 4 5]; i.e. there is 1 node overlap in new
        % layer nodes connecting to previous layer nodes.
        newnodes = lastnewnode:newconnections+lastnewnode-1;
        lastnewnode = newnodes(end);

        % Wrap around the new node numbers; if there are 12 nodes in the
        % new layer, then node 13 is really node 1.
        newnodes = mod(newnodes-1, numnewL)+1;

        % Add the connections to the connectivity matrix.  The new node
        % numbers are relative to their own new layer, e.g. 1:12.  We must
        % step them up by PREVL(END) to get their numbering in agreement
```

```
        % with the numbering for the whole network as used in C.
        for k = newnodes + prevL(end),
            C(j,k) = 1;
            C(k,j) = 1;
        end
    end

    % For each new node, connect it to its neighbors in the new outer layer
    newL = (1:numnewL) + prevL(end);
    for j = newL(1:end-1),
        k = j + 1;
        C(j,k) = 1;
        C(k,j) = 1;
    end
    C(newL(end), newL(1)) = 1;
    C(newL(1), newL(end)) = 1;

    prevL = newL;
end
```

Publishing Agreement

It is the policy of the University to encourage the distribution of all theses, dissertations, and manuscripts. Copies of all UCSF theses, dissertations, and manuscripts will be routed to the library via the Graduate Division. The library will make all theses, dissertations, and manuscripts accessible to the public and will preserve these to the best of their abilities, in perpetuity.

Please sign the following statement:

I hereby grant permission to the Graduate Division of the University of California, San Francisco to release copies of my thesis, dissertation, or manuscript to the Campus Library to provide access and preservation, in whole or in part, in perpetuity.

Author Signature

12/17/2008

Date